

An investigation into
chalcopyrite and dolerite dykes at the
George Fisher Pb-Zn-(Ag) Mine,
NW Queensland, Australia

Jacob Hendrikus Kuys
a1705167

Main text word count: 7,388
Number of figures: 18
Number of tables: 3

An investigation into
chalcopyrite and dolerite dykes at the
George Fisher Pb-Zn-(Ag) Mine,
NW Queensland, Australia

Thesis submitted in accordance with the requirements of the University of
Adelaide for an Honours Degree in Geology

Jacob Hendrikus Kuys

November 2019



THE UNIVERSITY
of ADELAIDE

**TITLE: AN INVESTIGATION INTO CU DISTRIBUTION AND DOLERITE DYKES
AT THE GEORGE FISHER Pb-Zn-(Ag) MINE, NW QUEENSLAND, AUSTRALIA**

RUNNING TITLE: GEORGE FISHER MINE CU AND DOLERITE DYKES

ABSTRACT

The George Fisher mine is situated in the Western Fold Belt of the Mount Isa Inlier, NW Queensland, and comprises two separate ore deposits of stratiform and breccia-hosted Pb-Zn-(Ag) mineralisation; Hilton and George Fisher. Both deposits are hosted within the Proterozoic Urquhart Shale and contain anomalous, and potentially economic Cu mineralisation. Chalcopyrite (CuFeS_2) is spatially associated with galena (PbS) and sphalerite (ZnS), and gangue Fe-sulphides pyrite and pyrrhotite. The genesis of these deposits has previously been compared to that of the giant Mount Isa Cu-Pb-Zn-(Ag) deposit located 22km to the south, along strike. Two metallogenic models are proposed for ore genesis at George Fisher: syngenetic Pb-Zn ('SEDEX') overprinted by epigenetic Cu; or epigenetic Cu-Pb-Zn mineralisation.

This study investigates the mineralogy, textures and association of Cu with the Pb-Zn-(Ag) system and concludes that chalcopyrite is texturally coeval with the main galena and sphalerite mineralisation stage, favouring a co-genetic Cu-Pb-Zn model. Chalcopyrite (Cd:Zn) geothermometry estimates an emplacement temperature of 280—350°C, with a temperature gradient decreasing to the north. Additional Cu is unlikely to be present north of George Fisher however, potential remains for additional (deep) structurally controlled Cu mineralisation at Hilton and south along strike towards the Mount Isa deposit.

This study also investigates the presence and geochemistry of the dolerite dykes within the George Fisher and Hilton deposits. The dolerites are sheared and strongly altered by pre-mineralisation hydrothermal activity and host minor Pb-Zn and Cu mineralisation providing evidence for their emplacement prior to ore mineralisation. Low Ti and overlapping Y/Nb-Zr/Nb and REE fields infer the dolerites share the same mantle source as the Eastern Creek Volcanics (ca. 1779 Ma) but have been produced by a later stage of tectonically-induced melting, most likely associated with deformation during the D₂ stage of the Isan Orogeny (~1575 Ma). The presence of pre-ore hydrothermally altered and sheared dykes provides considerable field evidence for epigenetic Cu-Pb-Zn ore genesis, concurring with recent studies of the Mount Isa deposit.

KEYWORDS

SEDEX, Ore Genesis, Chalcopyrite, Geochemistry, Dolerite, Proterozoic Pb-Zn deposit, Mount Isa

TABLE OF CONTENTS

Abstract.....	i
Keywords.....	i
List of Figures.....	3
List of Tables.....	3
1. Introduction.....	4
2. Geological Setting.....	7
2.1 Regional Geology.....	7
2.2 Local Geology & Ore Genesis.....	9
2.3 Dolerite Dykes.....	14
3. Methods.....	16
3.1 Sampling & Preparation.....	16
3.2 Scanning Electron Microscope-Mineral Liberation Analysis.....	18
3.3 Laser Ablation-Induced Coupled Plasma-Mass Spectrometry.....	19
3.4 Dolerite Dyke Trace Element & Whole Rock Geochemistry.....	21
4. Observations & Results.....	22
4.1 Chalcopyrite Petrology.....	22
4.2 Chalcopyrite SEM/MLA Observations.....	26
4.3 Chalcopyrite Geochemistry.....	28
4.31 Trace Element Distribution.....	28
4.32 Trace Element Correlations.....	33
4.4 Dolerite Dyke Petrology.....	35
4.5 Structural Setting of Dolerite Dykes.....	35
4.6 Dolerite Dyke Geochemistry.....	38
4.61 Element Mobility.....	41
5. Discussion.....	44
5.1 Chalcopyrite Petrology.....	44
5.2 Chalcopyrite Geochemistry.....	46
5.21 Deposit Geothermometry.....	48
5.3 Dolerite Dyke Petrology.....	51
5.4 Dolerite Dyke Geochemistry.....	51
5.5 Relationship between Cu and Dolerite Dyke distribution.....	58
5.6 Interpreted Timeline of Events.....	58
6. Conclusions.....	59

Acknowledgments	61
References	62
Appendix A: Host Lithology Descriptions.....	66
Appendix B: Pb-Zn Mineralisation Style Descriptions.....	69
Appendix C: List of Drill holes	70
Appendix D: Sample Descriptions	71
Appendix E: MLA Maps	93
Appendix F: Element Correlation Tables.....	96
Appendix G: Extended Chalcopyrite Boxplots	98
Appendix H: Additional Geochemical Plots	101
Appendix I: Dolerite Dyke Whole Rock and Trace Element Data	102
Appendix J: Chalcopyrite Geochemical Data	104

LIST OF FIGURES

Figure 1: Geological map of the George Fisher area	7
Figure 2: West-East cross-sections of Hilton and George Fisher.....	13
Figure 3: Example of a Cu-bearing sample	17
Figure 4: Reflected light images of Cu.....	25
Figure 5: SEM images and MLA map cut-outs.....	27
Figure 6: Log boxplots of selected chalcopyrite trace elements	30
Figure 7: ICP-MS spot data	31
Figure 8: Scatterplot displaying the lateral distribution	32
Figure 9: Scatterplots of chalcopyrite trace element correlations	34
Figure 10: Images of dolerite dyke samples.....	37
Figure 11: TAS classification of dolerite dykes	39
Figure 12: AFM classification of dolerite dykes	40
Figure 13: Scatterplots displaying Zircon (Zr) and major elements.....	42
Figure 14: Scatterplots displaying Zircon (Zr) and trace elements	43
Figure 15: Cd/Zn against inferred chalcopyrite crystallisation temperatures.....	50
Figure 16: Ti-V discrimination diagram.....	54
Figure 17: Y/Nb-Zr/Nb scatterplot	55
Figure 18: N-MORB normalised multi-element plot	57

LIST OF TABLES

Table 1: Characteristics of Western Succession dolerite dykes	15
Table 2: Overview of LA-ICP-MS parameters.	20
Table 3: Cu mineralisation samples.....	23

1. INTRODUCTION

George Fisher is a world-class Pb-Zn-(Ag) mine located approximately 22 km north along-strike of Mount Isa, Northwest Queensland within the Proterozoic Mount Isa Inlier. The George Fisher mine consists of two discrete deposits: (1) George Fisher (termed L72); and (2) Hilton (termed P49), which are separated by approximately 2 km of barren shale (Figure 1). Both deposits are hosted in the Proterozoic Urquhart Shale, which is composed of interbedded, fine-grained pyritic and carbonaceous siltstones and mudstones. Economic Pb-Zn-(Ag) and sub-economic Cu mineralisation is comprised of a series of stacked strata-bound ore horizons, lenses and breccias which share a similar host lithology and ore textures to the giant Mount Isa Cu-Pb-Zn-(Ag) deposit.

The George Fisher (L72) deposit has a total resource estimate of 138 Mt @ 7.8% Zn, 3.1% Pb and 52g/t Ag, while the Hilton (P49) deposit has a resource estimate of 46 Mt @ 7.8% Zn, 4.9% Pb and 100g/t Ag (Glencore, 2014).

Both the George Fisher and Hilton deposits have predominantly been attributed to the syngenetic, sedimentary-hosted Pb-Zn-(Ag) sedimentary exhalative or 'SEDEX' deposit style similar to other important deposits in the Mount Isa Inlier region (including Mount Isa, Lady Loretta, Century and McArthur River (Broadbent, Myers, & Wright, 1998; Cox & Curtis, 1977; Perkins & Bell, 1998; Williams, 1998). The two major studies on the geology of the George Fisher deposit resulted in significantly different interpretations regarding the formation model. Chapman's (1999) syngenetic model proposed mineralisation over nine separate stages with two major processes of ore formation. Firstly, the syngenetic (sea-floor related) mineralisation of the host shale

sequence formed the majority of the ore deposit and secondly, the re-mobilization of ore with the addition of minor galena, sphalerite and chalcopyrite. However, Murphy's (2004) study proposed epigenetic Pb-Zn-Cu mineralisation was produced by magmatic-derived fluids feeding the system via fault structures and deposited during a major post-diagenetic deformation event. Current research efforts aim to clarify the syngenetic or epigenetic origin of the mineralisation, and whether the George Fisher and Hilton deposits share a comparable mode of origin to the nearby Mount Isa deposit.

This study will investigate the mineralogy, textural relationships and geochemistry of Cu mineralisation present at both the Hilton and George Fisher deposits. This will aid in the understanding of the continuity between deposits, distribution patterns, mineralisation styles and association with the Pb-Zn-(Ag) ore minerals. These findings will then be compared to the Mount Isa Cu-Pb-Zn-(Ag) deposit which share host lithology and a comparable structural evolution with the George Fisher Pb-Zn-(Ag) deposits (Murphy, 2004).

Host lithology of the George Fisher and Hilton deposits is also intruded and cut by unconformable units traditionally identified as dolerite dykes by mine geologists. The dolerite dykes have been recorded within the core logging profile at both deposits, however considerable uncertainty remains as to their relationship with the Pb-Zn-(Ag) mineralisation. The dolerite dykes are associated with, and oriented along major fault structures throughout the Pb-Zn orebodies (Figure 2). Further research into the dyke's geochemistry and alteration history will assist with understanding their spatial and temporal relationships within the ore system.

Four key research questions have been identified:

- Is chalcopyrite mineralisation associated with the introduction of the main Pb-Zn-(Ag) ore stage at the George Fisher and Hilton deposits? If so, is this comparable with Cu mineralisation at the nearby Mount Isa deposit?
- Is there a difference in trace element geochemistry of chalcopyrite from the George Fisher, Hilton and Mount Isa deposits?
- What is the geochemistry of the dolerite dykes and how do they compare to other volcanic units in the area?
- What is the relative timing of intrusion of the dolerite dykes and where do they fit into the evolution of the George Fisher and Hilton deposits?

2. GEOLOGICAL SETTING

2.1 Regional Geology

The Proterozoic Mount Isa Inlier hosts the world-class deposits of Mount Isa (Cu-Pb-Zn), George Fisher (Pb-Zn-(Ag)), Hilton (Pb-Zn-(Ag)), Lady Loretta (Pb-Zn-(Ag)) and Century (Pb-Zn-(Ag)) in northwest Queensland, Australia. This world renowned metallogenic province is the remnants of an intra-continental extensional basin system sub-divided into three major structural belts; Western Fold Belt (WFB), central Kalkadoon-Leichardt Fold Belt (KLFB) and the Eastern Fold Belt (EFB) (Blake & Stewart, 1992; O'Dea, 1997). Development of the Mount Isa Inlier began around 1870 Ma years ago with the deformation and metamorphism of the basement gneissic rocks during the Barramundi orogeny (Scott et al., 2000).

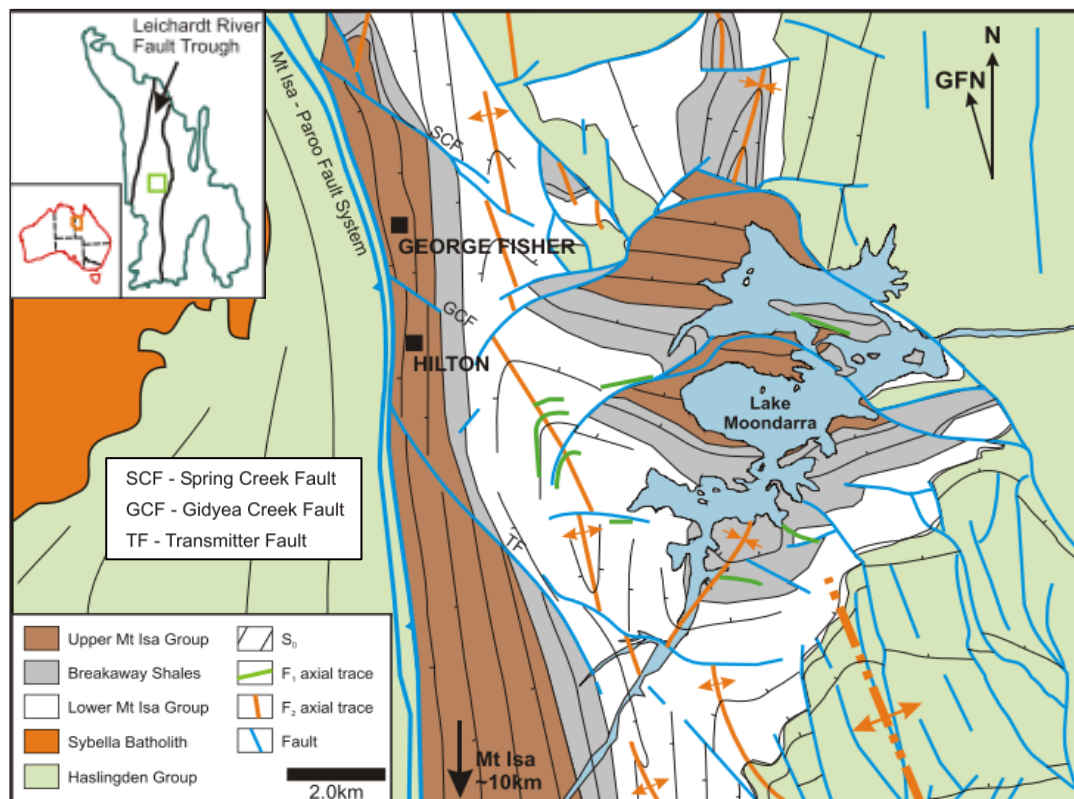


Figure 1: Geological map of the George Fisher area illustrating location of George Fisher and Hilton deposits, key geological units of the Mount Isa Inlier, major localized fault structures, bedding orientation and axial traces of folded deformation. The Spring Creek Fault (SCF) to the north, Transmitter Fault (TF) to the south and Gidyea Creek Fault (GCF) in between the George Fisher deposits are oriented NW-SE splaying off the major Mount Isa – Paroo Fault system, creating sinistral movement of the Upper Mt. Isa Group and the Breakaway Shales unit. F₂ folding to the east of the deposits dominates the structural orientation of the Leichardt River fault trough (Murphy, 2004).

The major tectonic belt zones were active between 1800 Ma and 1600 Ma ago (Blake, 1987; Etheridge & Wall, 1994; Scott et al., 2000), during which discrete episodes of volcanism, rifting and post-rift subsidence created four unconformable cover sequences within the Western Fold Belt (Blake, 1987; O'Dea, 1997). Deposition of these cover sequences occurred between 1870 Ma and 1590 Ma ago with the majority of the mineralisation hosted within the Mount Isa Group of the Leichardt River Fault Trough in cover sequence four (Figure 1) (Chapman, 2004). The Mount Isa Group is composed of fine-grained siliclastic and carbonate sediment (Conaghan, Hannan, & Tolman, 2003; Large, McGoldrick, Bull, & Cooke, 2004; Neudert, 1983). U-Pb SHRIMP zircon dating of tuff marker beds (TMBs) in the Urquhart Shale from both the Hilton and George Fisher deposits gave a date of 1654 ± 5 Ma (Chapman, 1999; Forrestal, 1990; Perkins & Bell, 1998; Williams, 1998). The Isan Orogeny initiated between 1610—1590 Ma, during which the WFB experienced sub-horizontal north-south shortening (D_1) with consecutive periods of sub-vertical east-west shortening (D_2 & D_3) (Bell & Hickey, 1998; O'Dea, 1997; Page & Bell, 1986). D_2 , the main deformation phase, represents peak metamorphism and also formed tight, upright folds with steeply dipping N—S axial planes ~1575 Ma defined by the seaming of carbonate material (Bell & Hickey, 1998; Chapman, 2004). D_3 was the continuous development of fold structures at ~1530 Ma, creating gently plunging axes trending NW—SE and associated with planar schistose features (Bell & Hickey, 1998; Davis, 2004). A later deformation event (D_4) has also be interpreted for George Fisher involving small-scale NW—SE trending folding developing upright folds equivalent to the regional D_3 event (Valenta, 1994).

2.2 Local Geology & Ore Genesis

Economic mineralisation is composed of galena (PbS) and sphalerite ((Zn,Fe)S) and is hosted within the 350 m thick westerly-dipping stratigraphic beds of the Urquhart Shale striking N—S of 1.2 km, reaching depths of at least 1 km (Chapman, 2004). The George Fisher and Hilton deposits are positioned in a structurally complex zone and are surrounded by four major faults that displace the Upper Mount Isa Group (including the Urquhart Shale) and Breakaway Shales in a sinistral motion (Murphy, 2004). At depth to the west, the deposits are truncated by the Hanging Wall Fault with the main lithological difference between deposits being the interbedded presence of black shale towards the base of Hilton's ore zone (Chapman, 2004). NE—SW trending dextral faults splaying from the major Mount Isa-Paroo Fault to the west are present throughout the Hilton and George Fisher deposits, and predate mineralisation (Murphy, 2004) (Figure 2).

A 2km long sequence of barren Eastern Creek Volcanics (ECVs), metabasalts and metasedimentary rocks, separate the George Fisher and Hilton deposits (Hannan, Golding, Herbert, & Krouse, 1993). The ECVs host a sequence of sub-alkaline members; the lowermost Cromwell Metabasalt, an interbedded Lena Quartzite and the uppermost Pickwick Metabasalt; which are interpreted to have formed in an intracratonic rift setting (Gregory et al., 2005; Wilson, Derrick, & Perkin, 1985).

Deformation and greenschist facies metamorphism during the Isan Orogeny has affected all three members (Wilson et al., 1985). The ECVs have been observed to contain trace to minor copper sulphide mineralisation (predominantly as chalcopyrite) and have been proposed as a potential source for the Cu within the Pb-Zn-(Ag) ore systems (Gregory

et al., 2005; Gulson, Perkins, & Mizon, 1983). NE—SW trending faults also bound the ECV complex to the north and south creating uncertainty regarding whether Hilton and George Fisher deposits are a continuous mineralised system.

The mineralised units are stacked, strata-bound lenses hosted within laminated fine-grained, pyrite-rich carbonaceous siltstones and separated by unmineralized mudstone beds and TMBs characterised by their thickness, mineralogy and structural features. Stratigraphic identification of these mineralized units allows for a correlation between stratigraphic units throughout the George Fisher and Hilton deposits (Chapman, 2004) (Figure 2). Descriptions of host lithologies can be found in Appendix A.

George Fisher is composed of 11 economically mineralized stratigraphic units. Four styles of Pb-Zn mineralisation are present within each mineralised unit: (1) layer-parallel disseminated sphalerite; (2) layer-parallel vein-hosted sphalerite; (3) breccia-hosted sphalerite; and (4) vein- and breccia-hosted galena (Descriptions in Appendix B).

Pb-Zn-(Ag) and Cu ore genesis of Mount Isa deposits (Mount Isa, George Fisher & Hilton) has been classified into three concepts of origin;

- 1) Syngenetic Pb-Zn within a SEDEX-style environment (ca. 1650 Ma) with overprinting and remobilization by epigenetic Cu during metamorphism and D₂-D₃ deformation (ca. 1575—1530 Ma) has been the most widely accepted model (Gulson et al., 1983; Large, McGoldrick, Bull, & Cooke, 2004; Smith, Burns, & Croxford, 1978; Stanton, 1963).

- 2) Syngenetic Pb-Zn and Cu both forming in a SEDEX-style environment was a geometric model produced by Finlow-Bates and Stumpfl (1980). The model argues early ore-bearing hydrothermal fluid infiltrating stratigraphy causing brecciation of silica-dolomite lithology. Precipitation of Cu within stockwork and precipitation of Pb-Zn across the sea floor resulted from the cooling of hydrothermal ore fluid. Deposit-scale zonation of Cu => Pb => Zn was inferred to be created by the changes in temperature during seawater mixing, remaining consistent with metal solubility (Finlow-Bates & Stumpfl, 1980; McGoldrick & Keays, 1990). Post-ore fluids channelling through the Paroo Fault are responsible for the redistribution of strata-bound Cu (McGoldrick & Keays, 1990).
- 3) Coeval and epigenetic Cu and Pb-Zn mineralisation was proposed by Grondijs and Schouten (1937) and further supported by Perkins (1997) and Davis (2004). Based on petrology, Cu and Pb-Zn ores are responsible for the brecciation and replacement of carbonate with further replacement of deformed and fine-grained pyrite-rich shale by stratiform Pb-Zn mineralisation (Grondijs & Schouten, 1937). Microstructural and textural evidence of Pb-Zn ore proposed the input of a single, juvenile magmatic source synchronous with D₃ (ca. 1530—1510 Ma) deformation developing Cu-Pb-Zn zonation because of different precipitation temperatures, consistent with previous models (Davis, 2004; Perkins, 1997).

Understanding proposed ore genesis models for deposits within the Mount Isa Inlier will help to interpret the paragenesis of Cu mineralisation at George Fisher. According to Chapman (1999), the George Fisher deposit resembles syngenetic Pb-Zn-(Ag) mineralisation with the host ~1653 Ma Urquhart Shale sequence followed by significant

re-mobilization and addition of minor galena, sphalerite and chalcopyrite. Infiltration of warm, basin-derived fluids created the chemical zonation of carbonate allowing for the emplacement of Zn-Pb-(Ag)-bearing fluid. Pb isotope modelling displayed an age of ~1653 Ma reflecting the date of Zn-Pb-(Ag) mineralisation. According to Murphy (2004), George Fisher hosts epigenetic Pb-Zn-Cu mineralisation fed by the influx of hydrothermal fluids via fault structures and deposited into host rock that has experienced diagenetic deformation. Vein-hosted sphalerite and breccia galena are observed as the major ore-bearing textures displaying cross-cutting relationships post-dating D₂.

It should also be noted that silica-dolomite alteration, the main host and important rheological control to the distribution of the Mount Isa copper ore bodies (Perkins, 1997) is rarely observed at the current mining levels of the Hilton and George Fisher deposits. Cu distribution at Hilton and George Fisher is mainly associated with the Hangingwall Fault, close to the main fluid ingress point being the hottest part of the system (Valenta, 1994).

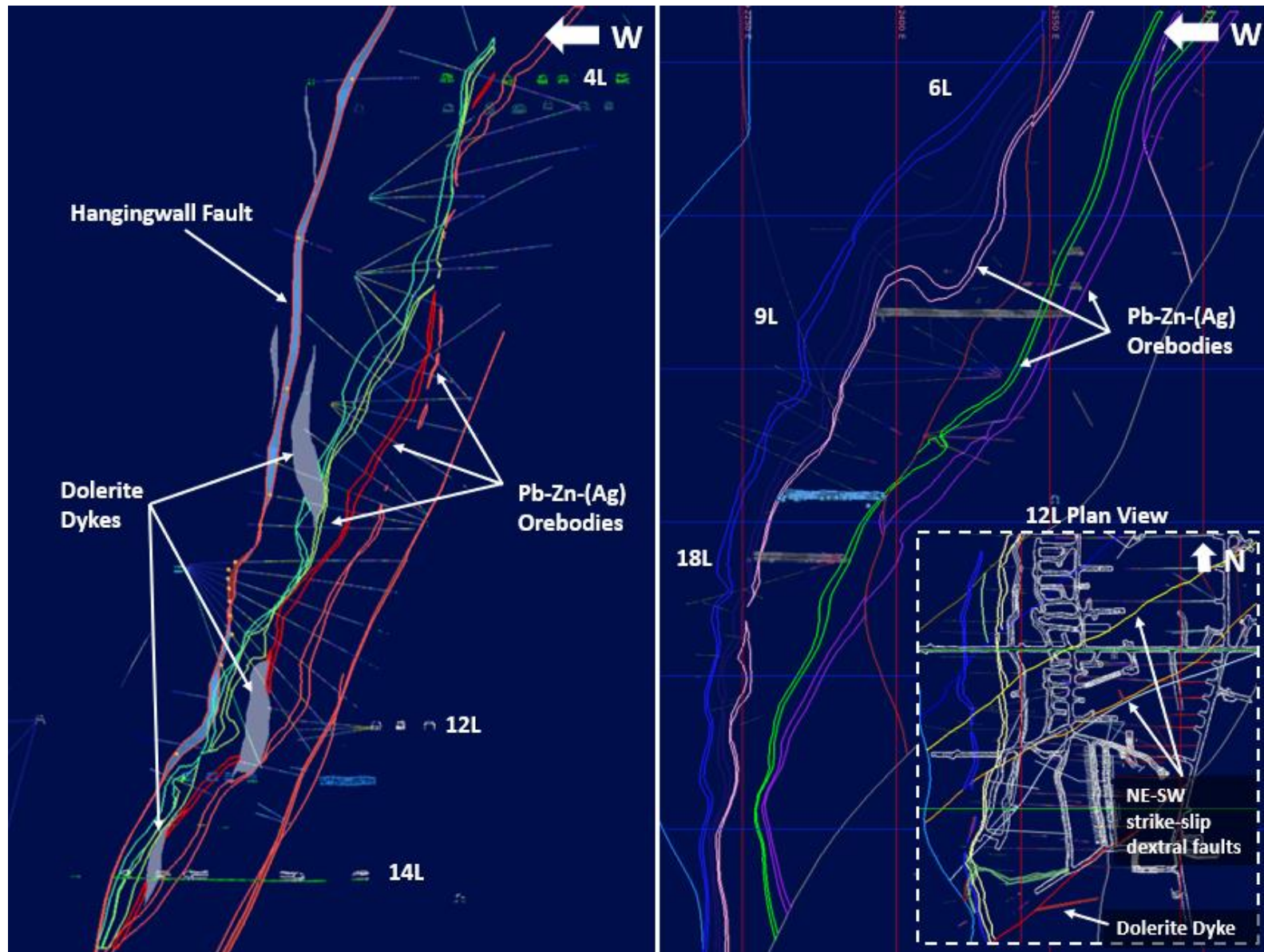


Figure 2: West-east cross-sections of Hilton (Left) and George Fisher (Right) displaying the location of dolerite dykes, major fault structures and Pb-Zn ore lenses. Dolerite dyke at George Fisher appears to splay out from one of the several strike-slip dextral faults cutting through the deposit. Cross-sections provided by Vincent Wai, George Fisher Mine Senior Geologist.

2.3 Dolerite Dykes

Hilton (P49) has been recorded to contain dolerite dyke lithologies interpreted to have intruded the Zn-Pb-(Ag) systems during D₂ regional deformation (Chapman, 1999; Valenta, 1988). Dolerite dykes host pervasive carbonate veining, Zn-Pb-Cu sulphide mineralisation and have been influenced by stages of syn-deformational epidote, rutile, biotite and chlorite alteration indicating early intrusion prior to peak metamorphism (D₂) (Hannan, Golding, Herbert, & Krouse, 1993; Valenta, 1994). Hannan et al. (1993) investigated minimally deformed metabasalt and metadolerites of the ECVs located between the Mount Isa and Paroo faults. ECV samples were heavily deformed and experienced albite-carbonate alteration followed by overprinting of biotite-chlorite alteration (Hannan et al., 1993).

Furthermore, Ellis & Wyborn (1984) investigated the petrology and geochemistry of cross-cutting Proterozoic dolerites from the Mount Isa Inlier. In their study they classified three groups of dolerite intrusion within the Western Succession; W1 & W2, which intruded prior to regional metamorphism, and W3, a relatively younger and unmetamorphosed group. Characteristics of each group can help classify dolerite dyke lithologies observed at Hilton and George Fisher (Table 1) (Ellis & Wyborn, 1984).

Table 1: Characteristics of three dolerite intrusion groups within the western succession compared with dolerite dyke samples from Hilton and George Fisher indicating their location, timing, mineral assemblage, textures and selected major element geochemistry implemented from Ellis & Wyborn (1984) and Blake, Page, Wyborn, & Etheridge, (1984).

	W1 dykes & sills	W2 dolerites	W3 dykes	Hilton & George Fisher dolerite dykes
Location	Intrude Mount Guide Quartzite, ECVs and Myally Subgroup	Intrude Sybella Granite	Cross-cut W1 dykes	Intruding Mount Isa Group
Timing	Pre-metamorphism (>1610 ± 3 Ma)	Pre-metamorphism (≤1671 ± 8 Ma)	Post-metamorphism (<1480 Ma)	Pre-metamorphism (<1650 Ma)
Mineral Assemblages	Lower greenschist grade to amphibolite facies. Tremolite/actinolite and hornblende with chlorite, epidote, titanite and magnetite. Preserved quartz and feldspars in groundmass.	Plagioclase, orthopyroxene, clinopyroxene, biotite and minor actinolite, magnetite, pyrite, ilmenite and chalcopyrite. Quartz restricted to groundmass. Accessory apatite.	Clinopyroxene, plagioclase, minor orthopyroxene and magnetite with traces of biotite, hornblende quartz and albite.	Significant carbonate, biotite and chlorite alteration. Calcite and quartz dominates groundmass. Hosts sphalerite, galena, pyrite, pyrrhotite, chalcopyrite and minor apatite.
Textures	Greenschist grade has well preserved igneous textures. Amphibolite facies has medium-grained equigranular rocks with granoblastic textures.	Medium to coarse-grained ophitic to sub-ophitic textures. Textural gradation from biotite and amphibole-poor dolerite to granodiorite.	Coarse-grained ophitic texture with clinopyroxene clearly visible in hand sample.	Fine to coarse grains with typical porphyritic texture. Heavily deformed and very-fine grained groundmass.
Chemistry	TiO ₂ wt% (0.86-2.56) SiO ₂ wt% (48.05-51.34)	TiO ₂ wt% (0.85-1.98) SiO ₂ wt% (48.75-65.10)	TiO ₂ wt% (0.94-3.29) SiO ₂ wt% (47.91-55.52)	TiO ₂ wt% (2.31-3.12) SiO ₂ wt% (39.8-50.6)

3. METHODS

3.1 Sampling & Preparation

Fieldwork was completed at George Fisher mine during March 2019. Core samples were selected from 11 drill cores from both George Fisher and Hilton deposits (Full list in Appendix C). The drill holes were selected with assistance from George Fisher senior geologists after reviewing mine assay data and the 3D deposit model to target zones of Cu mineralisation.

Samples were sent to Adelaide Petrographic to be made into polished thin-sections. Polished resin blocks were also made from selected samples for analysis by laser ablation (Figure 3).

Petrography of thin-section samples were examined under the Olympus BX51 optical microscope. Polished resin blocks of copper samples were analysed with the FEI Quanta 600 and a Philips XL30 FEG Scanning Electron Microscope (SEM) supported with Energy-Dispersive X-ray Spectroscopy (EDS).

L72-201.4

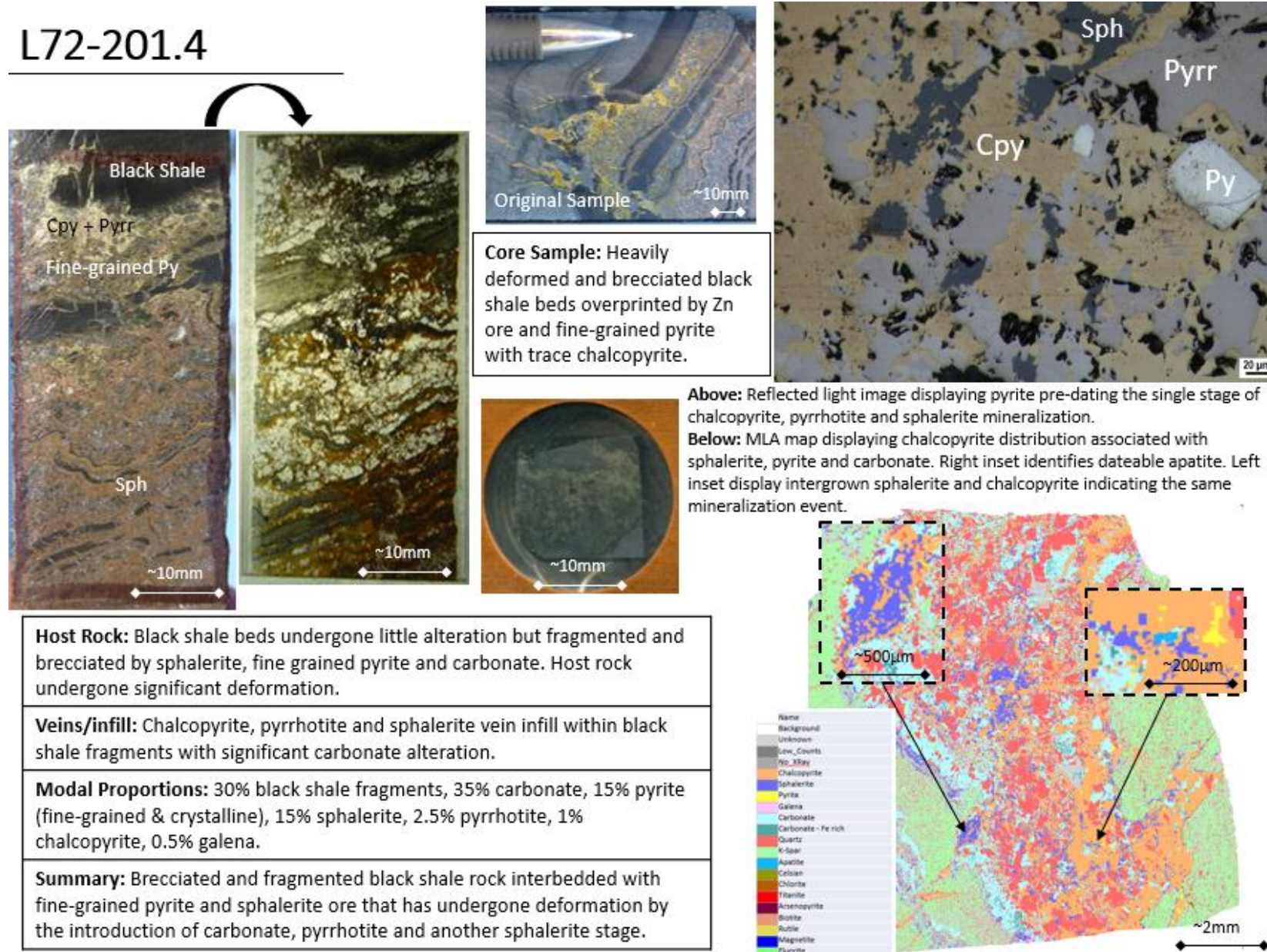


Figure 3: Example of a Cu-bearing sample with description, thin-section, polished resin block sample, reflected light image and MLA map.

3.2 Scanning Electron Microscope-Mineral Liberation Analysis (SEM-MLA)

The FEI Quanta 600 was primarily used to identify sulphide minerals and any other minerals associated with the ore system. Fitted with a tungsten filament electron source and Energy Dispersive X-Ray Spectroscopy (EDS) system, the samples were able to be imaged from secondary electrons creating an x-ray image and backscatter electrons (BSE) used to image the contrast of mean atomic numbers displaying elemental distribution on the surface.

The SEM generated high-quality grey-scale images using backscattered electron (BSE) mode to identify mineral relationships of chalcopyrite with the primary ore-bearing minerals, sphalerite and galena.

The MLA software used elemental composition differences to generate a colour-coded mineral map for three of the resin-set blocks; L72-201.4m, L72-431.5m and P49-17.4m. Each MLA map was used to observe distribution of chalcopyrite and to interpret mineral relationships within the Hilton and George Fisher deposits. All MLA maps can be viewed in Appendix E.

High-resolution images were captured by the XL30 SEM to identify chalcopyrite grains and surrounding minerals in BSE mode with an acceleration voltage ranging from 20-30 kV. The EDS system was used to identify the different sulphide minerals and validate the chalcopyrite grains from the pyrite and sphalerite grains.

3.3 Laser Ablation-Induced Coupled Plasma-Mass Spectrometry (LA-ICP-MS)

ICP-MS analysis was used to obtain quantitative geochemical data for chalcopyrite to investigate whether there are similarities and/or difference between George Fisher, Hilton and Mount Isa's deposits.

A selection of elements (Table 2) were analysed however priority elements (Cu, Pb, Zn, Fe, S, Ag) were set with longer acquisition time to ensure sufficient collection of data. Spot size (29 & 51µm diameter) was used dependent on the size of the chalcopyrite grain, to avoid analysis of neighbouring minerals and pitted polishing imperfections which may contaminate the representative chalcopyrite chemistry. Quantitative analysis of ~350 spots was collected from nine resin block-set samples hosting various chalcopyrite mineralisation styles; vein-infill, disseminated and strata-bound.

Two standards were used during ICP-MS analysis: STDGL3 (Fe-Zn-rich sulphide glass); and GSD-1G (Fe-Al-Si basaltic-like glass). Standards were analysed after every twenty sample analyses to correct for instrumental drift.

Trace element compositions of chalcopyrite is calculated using the Iolite Trace Element_IS data reduction scheme (DRS) (Paton, Hellstrom, Paul, Woodhead, & Hergt, 2011). Mass spectrometer results were further processed using Excel to assess and remove data below the detection limit of the ICP-MS.

Table 2: Overview of LA-ICP-MS parameters, data acquisition and standards used to obtain geochemistry of chalcopyrite. Iolite (Paton, Hellstrom, Paul, Woodhead, & Hergt, 2011)

LA-ICP-MS Parameters	
	<i>Chalcopyrite (Sulphide)</i>
<i>Instruments (Brand and Model)</i>	<i>RESolution 193nm excimer laser with an Agilent 7900 ICP-MS</i>
<i>Internal Standard</i>	<i>Fe</i>
<i>Spot Size</i>	<i>29 & 51 μm</i>
<i>Laser Fluence</i>	<i>$\sim 3 \text{ J/cm}^3$</i>
<i>Laser Warm Up (background collection)</i>	<i>30 s</i>
Data Acquisition Parameters	
<i>Data Acquisition Protocol</i>	<i>Time-resolved analysis</i>
<i>Cleaning Method</i>	<i>Firing 5 pulses followed by washout</i>
<i>Scanned Masses</i>	<i>Al27, Si29, S34, Mn55, Fe57, Co59, Ni60, Cu65, Zn66, Ga69, Ga71, As75, Se77, Mo95, Pd106, Ag107, Cd111, Ln115, Sn118, Sb121, Te125, Ba137, W182, Pt195, Au197, Hg201, Ti205, Pb206, Pb207, Pb208, Bi209</i>
<i>Background Collection</i>	<i>30 s</i>
<i>Ablation Time</i>	<i>50 s</i>
<i>Washout</i>	<i>20 s</i>
Standardisation and Data Reduction	
<i>Primary Standard</i>	<i>STDGL3</i>
<i>Secondary Standard</i>	<i>GSD-1G (USGS)</i>
<i>Data reduction Software</i>	<i>Iolite</i>

3.4 Dolerite Dyke Trace Element & Whole Rock Geochemistry

Eleven dolerite dyke samples were cut with a diamond saw to remove carbonate veins before being sent to ALS Limited (South Australia) for whole rock and trace element geochemical analysis. Crushing (ALS code: CRU-21) involved the coarse crushing of the drill samples to 70% passing 6mm. Samples were then further crushed to 70% less than 2mm, riffle split off 250g and pulverize split to better than 85% passing 75 microns (ALS code: PREP-31). Whole rock analysis (ALS code: ME-ICP06) was conducted using Inductively Coupled Plasma Atomic Emission Spectroscopy (ICP-AES) on an acid digested, fused bead. Processing of samples for trace element analysis (ALS code: ME-MS81) by lithium borate fusion and acid dissolution was implemented before Inductively Coupled Plasma Spectrometry (ICP-MS). Four-acid digestion and ICP-AES was further utilized to collect supplementary trace element data (ALS code: ME-4ACD81).

4. OBSERVATIONS & RESULTS

4.1 Chalcopyrite Petrology

Hilton (P49) and George Fisher (L72) samples host varying Cu mineralisation textures within a variety of lithologies including carbonaceous shale and pyritic shale. Lithology was not observed to influence the presence or absence of chalcopyrite. Three basic Cu mineralisation textures were observed during initial sample collection: (1) vein-infill chalcopyrite; (2) disseminated chalcopyrite; and (3) strata-bound chalcopyrite.

Vein-infill style mineralisation has been characterized as the crystallisation of fine-coarse-grained quartz and calcite hosting chalcopyrite \pm sphalerite \pm galena \pm pyrrhotite \pm pyrite typically crosscut host rock bedding. Disseminated style mineralisation is identified by the scattering of fine-grained chalcopyrite throughout areas of high-grade sphalerite and galena ore. This style of mineralisation tends to replace carbonate minerals along with all sulphides. Strata-bound mineralisation is distinctly characterized by its conformable orientation and confinement to a single stratigraphic unit either between host rock beds or mineralised zones. Table 2 displays sample ID, interpreted style of Cu mineralisation, recorded host lithology and ore domain. From collating sample characteristics and analysing thin-sections in more detail, the observed Cu mineralisation style has no association with ore domain or host lithology.

Table 3: Cu mineralisation samples, their mineralisation styles present, lithology and ore domain recorded at GFM. Interpretation of mineralisation style depends on prominence within hand sample observed with the naked-eye (thin-sections and polished resin blocks). FGP = Fine-grained pyrite, Gal=Galena, Pyrr=Pyrrhotite, Sph=Sphalerite.

Sample ID	Style	Lithology Comments	Ore Domain	Sample ID	Style	Lithology Comments	Ore Domain
<i>P49-125.6m</i> DH: 12L_H558_09	Vein-infill	FGP and black shale beds	3a	<i>L72-264m</i> DH: 16C_I696_04	Vein-infill	Massive interbedded FGP and black shale	hw1
<i>P49-177m</i> DH: 12L_H558_08	Disseminated	Massive Sph ore and 'buff' altered shale beds	4cm	<i>L72-395.8m</i> DH: 201406212	Disseminated	Massive Gal, chloritized and remnant shale	a2m
<i>P49-17.4m</i> DH: 5L_K579_03	Strata-bound	Massive FGP and minor black shale bed	1m	<i>L72-149m</i> DH: 201504162	Vein-infill & strata-bound	'Buff' altered mudstone bed with massive Sph ore	b3m
<i>P49-154.3m</i> DH: 12L_H558_09	Disseminated	Sph+Gal with remnant black shale fragments	4fm	<i>L72-431.5m</i> DH: 12L_K796_01	Disseminated & vein-infill	Massive Gal, black shale beds and remnants	a3
<i>P49-213.7m</i> DH: 14L_J558_01	Vein-infill	Massive Sph, carbonate veining and black shale	3cm	<i>L72-230.3m</i> DH: 16C_I696_04	Disseminated & vein-infill	Massive FGP +Sph+Pyrr	hw1
<i>P49-194.2m</i> DH: 14L_J573_03	Disseminated	Massive Pyrr and black shale brecciation	3cm	<i>L72-293.5m</i> DH: 16C_I696_04	Vein-infill	Coarse quartz and calcite with Gal	hw1
<i>L72-201.4m</i> DH: 201504162	Vein-infill	Massive FGP +Sph and black shale beds	a2m	<i>L72-456.6m</i> DH: 201406212	Vein-infill & strata-bound	Chloritized shale beds with massive Sph + Gal	a2m

Reflected light images clearly display the key relationships observed between chalcopyrite and the associated sulphide minerals including pyrite, sphalerite, galena and pyrrhotite.

Initial observations indicate an intergrown nature of chalcopyrite with main Zn-Pb ore-bearing sphalerite (Figure 4f) and galena (Figure 4c & 4g) as part of a major infill zone supported by Taylor's (2019) observations. Intergrown Cu-Zn-Pb are observed within both vein-infill (Figure 4d & 4e) and disseminated (Figure 4h) mineralisation textures. Replacement and overprinting of sphalerite by chalcopyrite is observed within George Fisher (Figure 4h) and Hilton samples (Taylor, 2019). Pyrrhotite (Figure 4a & 4f) and pyrite (Figure 4b) are observed as vug infill with overprinting chalcopyrite for George Fisher samples and are supported by Taylor's (2019) Hilton observations. Vein-infill

chalcopyrite lacking Zn-Pb ore-bearing mineralisation and cross-cutting fine-grained pyrite was observed (Figure 4i).

Paragenesis of the Hilton deposit by Taylor (2019) identifies an early stage of replacive sphalerite followed by a later 'main' hydrothermal event of galena, chalcopyrite and a secondary sphalerite. The presence of high temperature minerals (i.e. magnetite, feldspar and biotite) were observed within Cu-rich zones by Taylor (2019) resembling potassic alteration within magmatic related rock which is unusual for Hilton, however, indicate an early 'hot' mineralisation event pre-dating ore.

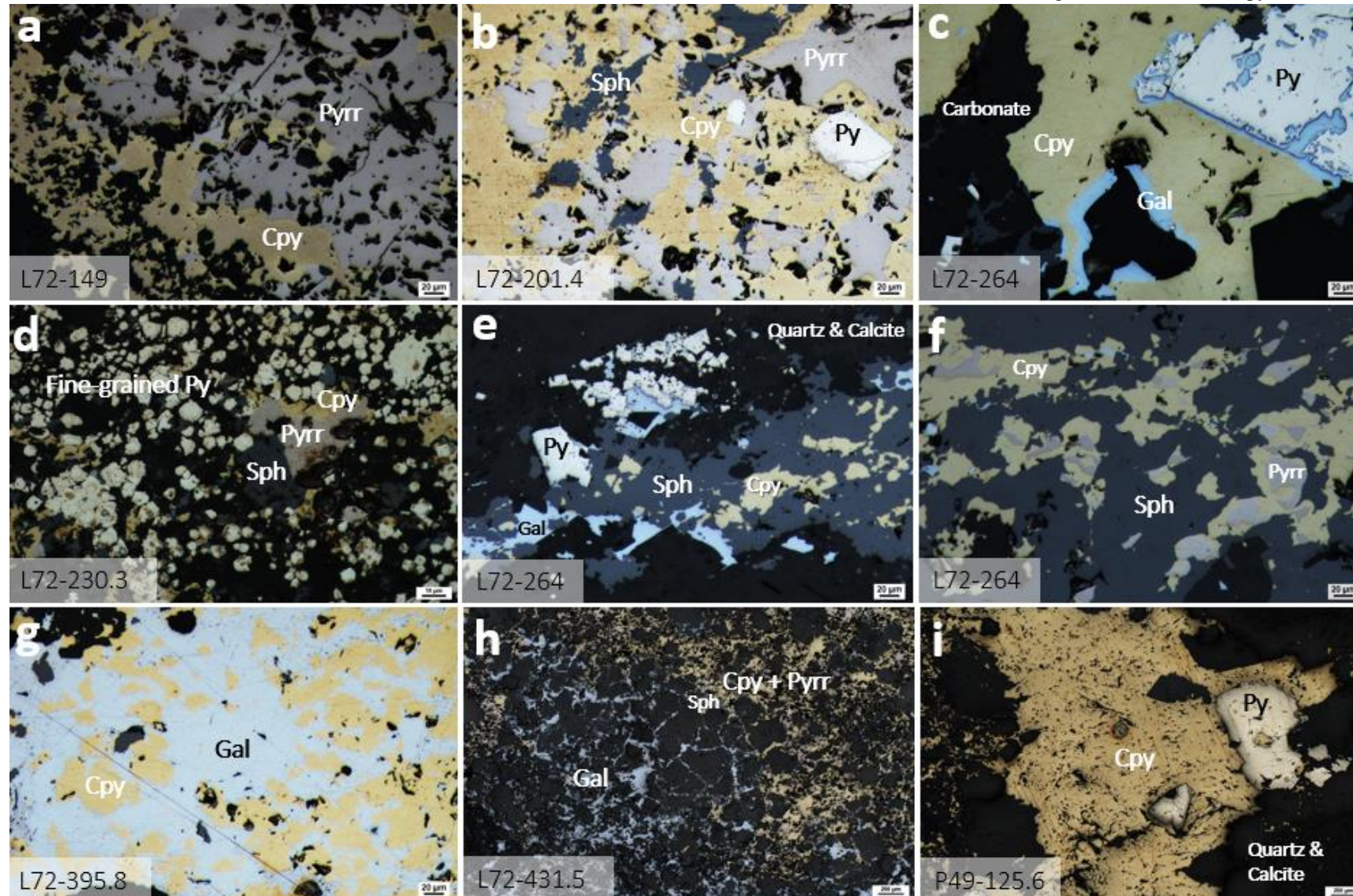


Figure 4: Reflected light images displaying key relationships between Cu and Pb-Zn ore-bearing minerals. a) Intergrown chalcopyrite (yellow) and pyrrhotite (light pale brown) with remnant carbonaceous rock (black), b) Intergrown chalcopyrite, pyrrhotite and sphalerite (dark grey) with minor euhedral pyrite (white), c) Galena (light blue/grey) rimming pyrite crystal and carbonate fragments both surrounded by chalcopyrite, indicating relatively early galena precipitation, d) Chalcopyrite, pyrrhotite and sphalerite veining and replacing fine-grained pyrite, e) Vein-infill of sphalerite, chalcopyrite, galena and pyrite within quartz and calcite, f) Sphalerite with disseminated chalcopyrite and intergrown pyrrhotite, g) Galena with coeval 25 chalcopyrite, h) Crackle-breccia infill of chalcopyrite and pyrrhotite to the right with galena and sphalerite to the left. Note angular clasts with limited alteration in centre-left of image, with increasing alteration of clasts to the right of the image, i) Vein-infill of chalcopyrite with coarse paragenetically earlier crystalline pyrite within quartz and calcite. All textures and mineral relationships are observed within both Hilton (P49) and George Fisher (L72). Refer to Taylor (2019) for an extended paragenetic report on the Hilton (P49) system.

4.2 Chalcopyrite SEM/MLA Observations

MLA mapping of Cu-bearing samples was produced for three Cu-bearing samples; L72-201.4 (vein-infill), L72-431.5 (disseminated) and P49-17.4 (strata-bound) with SEM observations completed during the same session. Two relationships inferred from SEM observations and MLA mapping include the presence of magnetite (Figure 5a) and celsian (Ba) feldspar (Figure 5b) in high-grade Cu zones unique to the Hilton samples, and the association of chalcopyrite and pyrite mineralisation (Figure 5c). Magnetite and celsian (Ba) feldspar grains at Hilton are heavily fractured and host inclusions of sphalerite, galena, pyrrhotite and fragments of shale indicating that magnetite and celsian formation pre-date mineralisation (Figure 5a & 5b). Sphalerite, galena, chlorite veining and an unidentified Pt-Pd-rich mineral grain (Figure 5e) were observed in a Cu-bearing sample (DH 5L_K579_03 @ 17.4m) from Hilton. The Pt-Pd-rich mineral is the first ever to be observed at Hilton. During the fractional crystallisation of Cu-rich sulphide magma, elements such as Pt and Pd in the presence of As, Te, Bi and Sn typically form their own microphases (i.e. Cooperite (Pt,Pd)S) within the matrix as micro-inclusions which may be the origin of Pt-Pd mineralisation (Sinyakova, Kosyakov, Distler, & Karmanov, 2016). Presence of Pt-Pd mineralisation also indicates a mafic influence on the source of metals providing evidence for Eastern Creek Volcanics as a plausible metal source. Full-page MLA maps can be viewed in Appendix E.

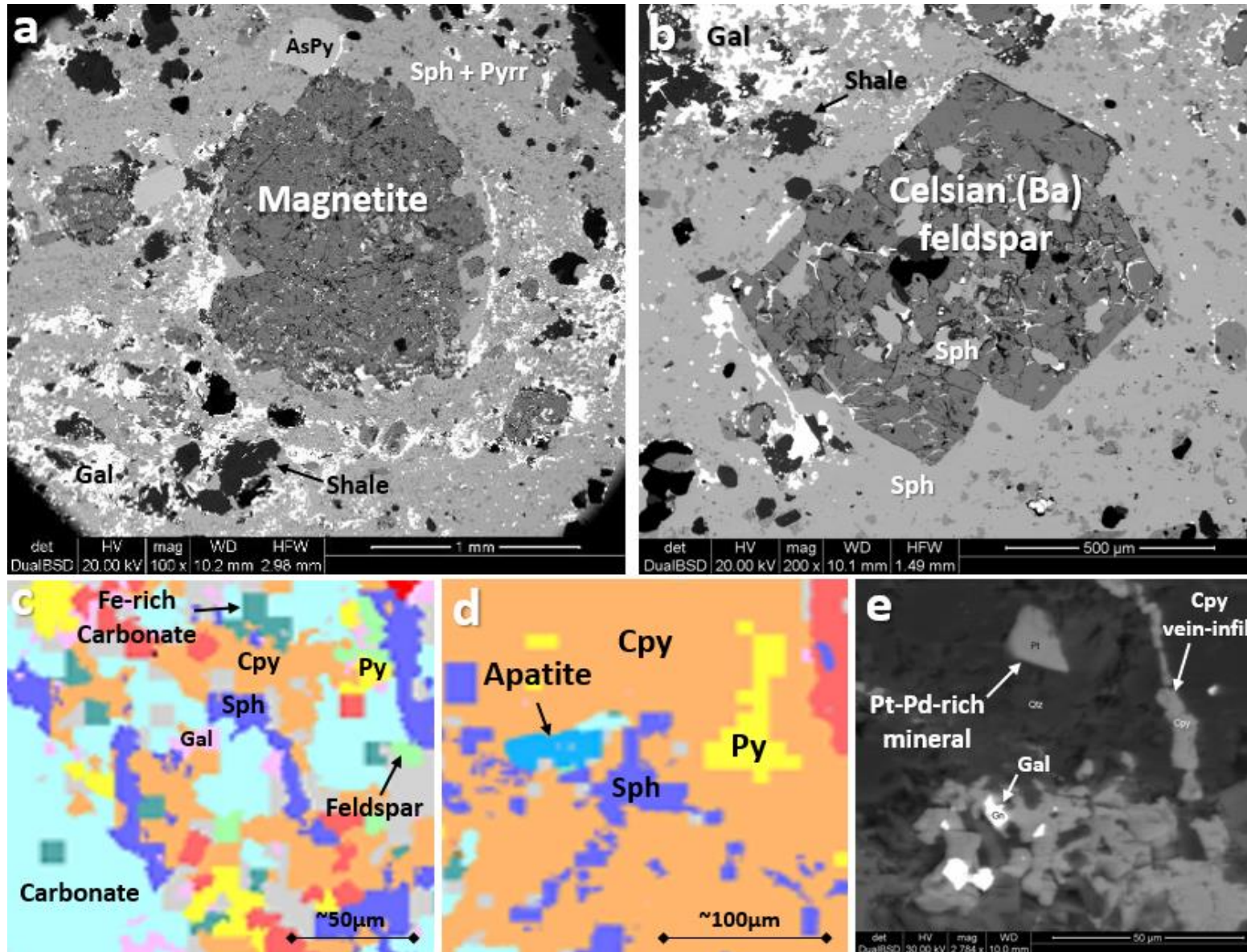


Figure 5: SEM images and MLA map cut-outs displaying unique mineralogy and mineral associations within high-grade Cu zones of Hilton and George Fisher. Images and their sample descriptions can be found in Appendix D. SEM images A and B provided by R. Lilly.

4.3 Chalcopyrite Geochemistry

Trace element concentrations for Hilton (P49) and George Fisher (L72) samples were collected using LA-ICP-MS spot analysis. Raw chalcopyrite geochemical data located in Appendix J. Using unpublished trace element data of Mount Isa chalcopyrite (Cave, Lilly, & Bavorich, 2019), comparisons can be made to further understand both deposits, origin of chalcopyrite and investigate the continuity of the system.

4.31 TRACE ELEMENT DISTRIBUTION

Measurable concentrations of ^{27}Al , ^{55}Mn , ^{59}Co , ^{60}Ni , ^{66}Zn , ^{71}Ga , ^{75}As , ^{77}Se , ^{107}Ag , ^{111}Cd , ^{115}Ln , ^{118}Sn , ^{121}Sb , ^{125}Te , ^{205}Tl , ^{208}Pb and ^{209}Bi are hosted within chalcopyrite.

Boxplots display log concentrations of elements within chalcopyrite of Mount Isa, Hilton and George Fisher. ^{27}Al , ^{55}Mn , ^{59}Co , ^{66}Zn and ^{111}Cd concentrations within chalcopyrite at Hilton and George Fisher display similar abundances to those observed at Mount Isa. ^{57}Fe , ^{71}Ga , ^{205}Tl and ^{208}Pb concentrations progressively increase from Mount Isa to Hilton and George Fisher demonstrating increasing abundances to the north and distal to the Mount Isa deposit. ^{77}Se , ^{125}Te and ^{209}Bi concentrations progressively decrease from Mount Isa to Hilton to George Fisher.

^{60}Ni and ^{107}Ag concentrations display multiple clusters of data with some correlating with Mount Isa and some unique to Hilton and George Fisher (Figure 6). Chalcopyrite geochemistry displaying different concentrations of trace elements identifies different precipitation conditions. ^{60}Ni displays two clusters of geochemical data; one correlating with both the Mount Isa and Hilton deposits, and one unique to George Fisher ranging

from ~4—7ppm (Figure 6). ^{107}Ag displays three clusters; two correlating between all three deposits, and one weak cluster correlating between Hilton and George Fisher ranging from ~1000—3000ppm (Figure 6). Clustering of trace elements comparable with Mount Isa indicates an evolved hydrothermal system.

Mean concentrations of Bi in chalcopyrite progressively decrease from Mount Isa (2.41 ppm) to Hilton (0.027 ppm) to George Fisher (0.024 ppm) (Figure 6). Mean concentrations of Pb in chalcopyrite progressively increase from Mount Isa (70.39 ppm) to Hilton (566 ppm) to George Fisher (710 ppm) (Figure 6). This trend in data can be used to better understand the association and crystallising style of chalcopyrite throughout Pb-Zn mineralisation.

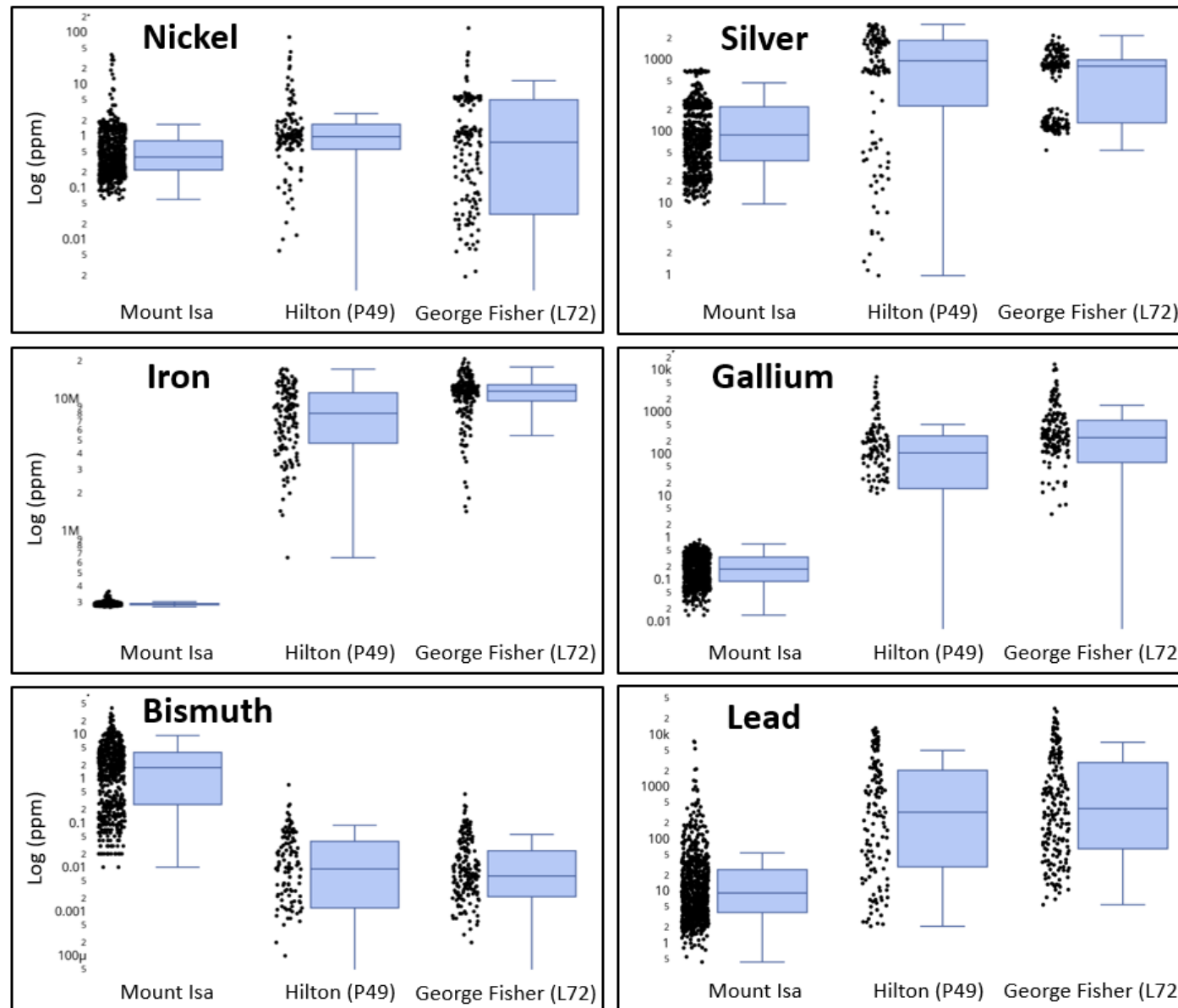


Figure 6: Log boxplots showing the distribution of chalcopyrite trace element concentrations of Mount Isa, Hilton (P49) and George Fisher (L72) deposits. Different concentrations of trace elements can be used to interpret the temperature of the system and source of hydrothermal fluid.

Representative time-resolved LA-ICP-MS depth profiles of trace elements in chalcopyrite display elements in solid solution and nano-inclusions (Figure 7). Elements in solid solution with ^{65}Cu include ^{57}Fe , ^{34}S , ^{107}Ag , ^{121}Sb , ^{205}Tl , ^{66}Zn and ^{208}Pb . Elements associated with nano-inclusions in chalcopyrite include ^{208}Pb , ^{66}Zn , ^{111}Cd , ^{107}Ag , ^{59}Co and ^{55}Mn .

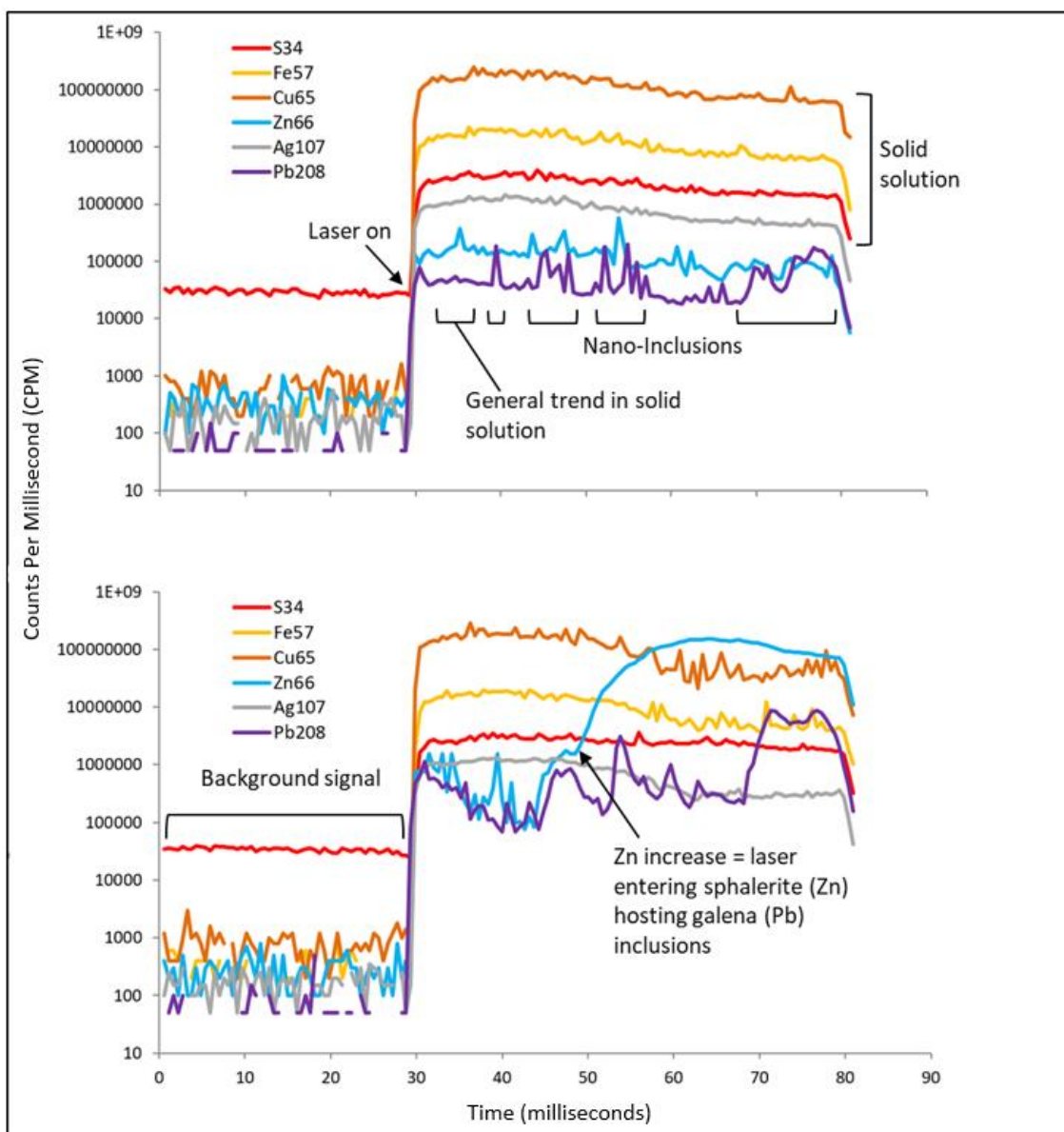


Figure 7: ICP-MS spot data from two chalcopyrite samples. Top displays Cu and associated elements in solid solution with nano-inclusions. Bottom displays the transition of chalcopyrite into sphalerite hosting galena inclusions. The Cu, Fe, S and Ag in solid solution maintains a consistent concentration during acquisition time whereas the presence of sphalerite (Zn) and galena (Pb) nano-inclusions is indicated by the spikes in data. Pb and Zn also peak when laser is on indicating concentrations are also present in solid solution.

Element concentrations against Northing coordinates illustrates the lateral distribution of a selected element (e.g. ^{107}Ag) and mineralisation styles between Hilton and George Fisher. After processing ~350 spots of chalcopyrite geochemical data, silver (^{107}Ag) was observed to be in solid solution with Cu and therefore used to display the lateral distribution of chalcopyrite (Figure 8). No trend in the distribution of ^{107}Ag is observed between Hilton and George Fisher (Figure 8). Overlapping distribution of vein-infill, disseminated and strata-bound mineralisation styles indicates no association between the mineralisation style of chalcopyrite and the concentration of ^{107}Ag (Figure 8).

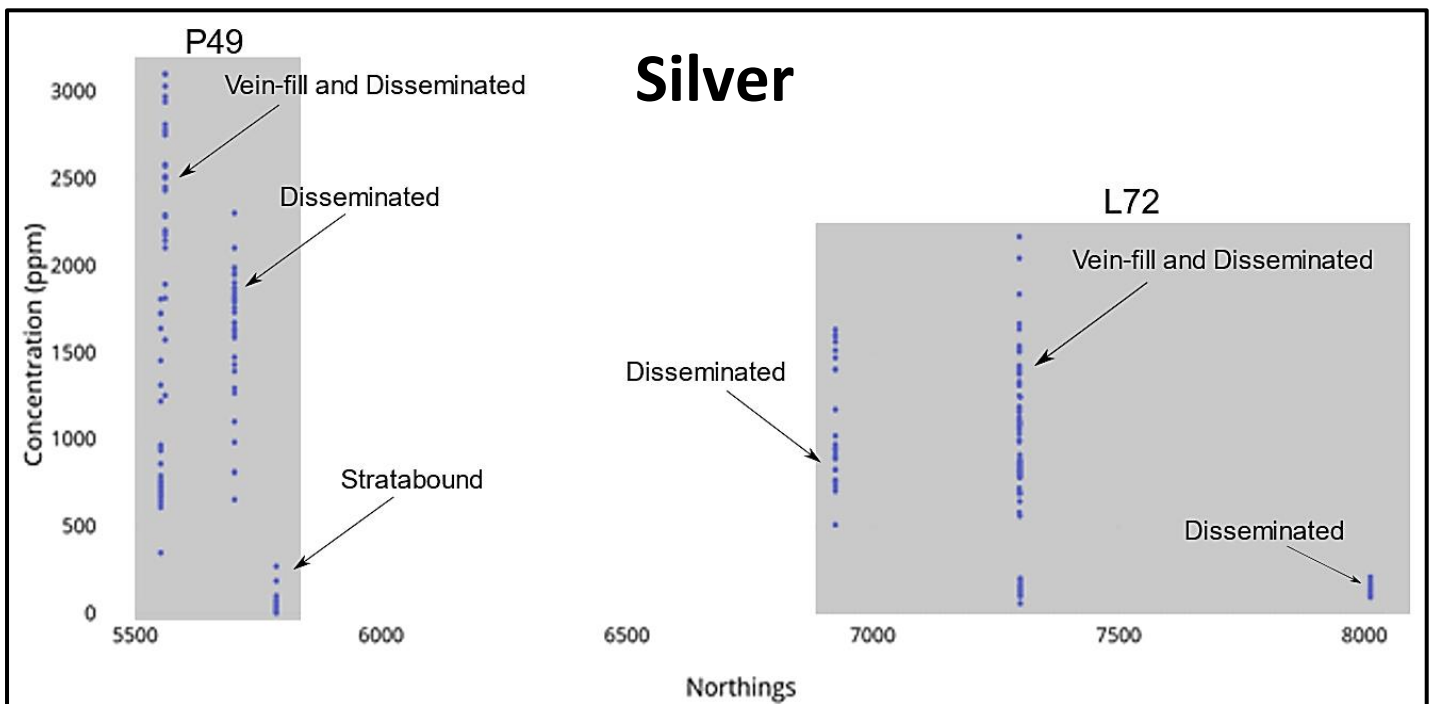


Figure 8: Scatterplot displaying the lateral distribution Silver (^{107}Ag) trace element concentrations of chalcopyrite between Hilton (P49) and George Fisher (L72). Mineralisation styles observed during sampling are indicated to show an absence of relationship between Ag trace element concentration and mineralisation style. Mineralisation styles cannot be discriminated by chalcopyrite trace element geochemistry.

4.32 TRACE ELEMENT CORRELATIONS

Investigating the correlation between chalcopyrite trace elements of Hilton (P49) and George Fisher (L72) can help clarify relationships between ore-forming processes and stages of hydrothermal alteration (Petrov & Popov, 2015). Element correlation coefficients for Hilton and George Fisher can be viewed in Appendix F.

Both Hilton and George Fisher display moderate ($R^2 > 0.5$) trace element correlations between Al-Ga, Zn-Cd and Pb-Bi (Figure 9). Hilton also displays a moderate ($R^2 > 0.5$) trace element correlation between Ag-Ln (Figure 9). George Fisher displays very strong ($R^2 > 0.9$) Zn-Cd correlation.

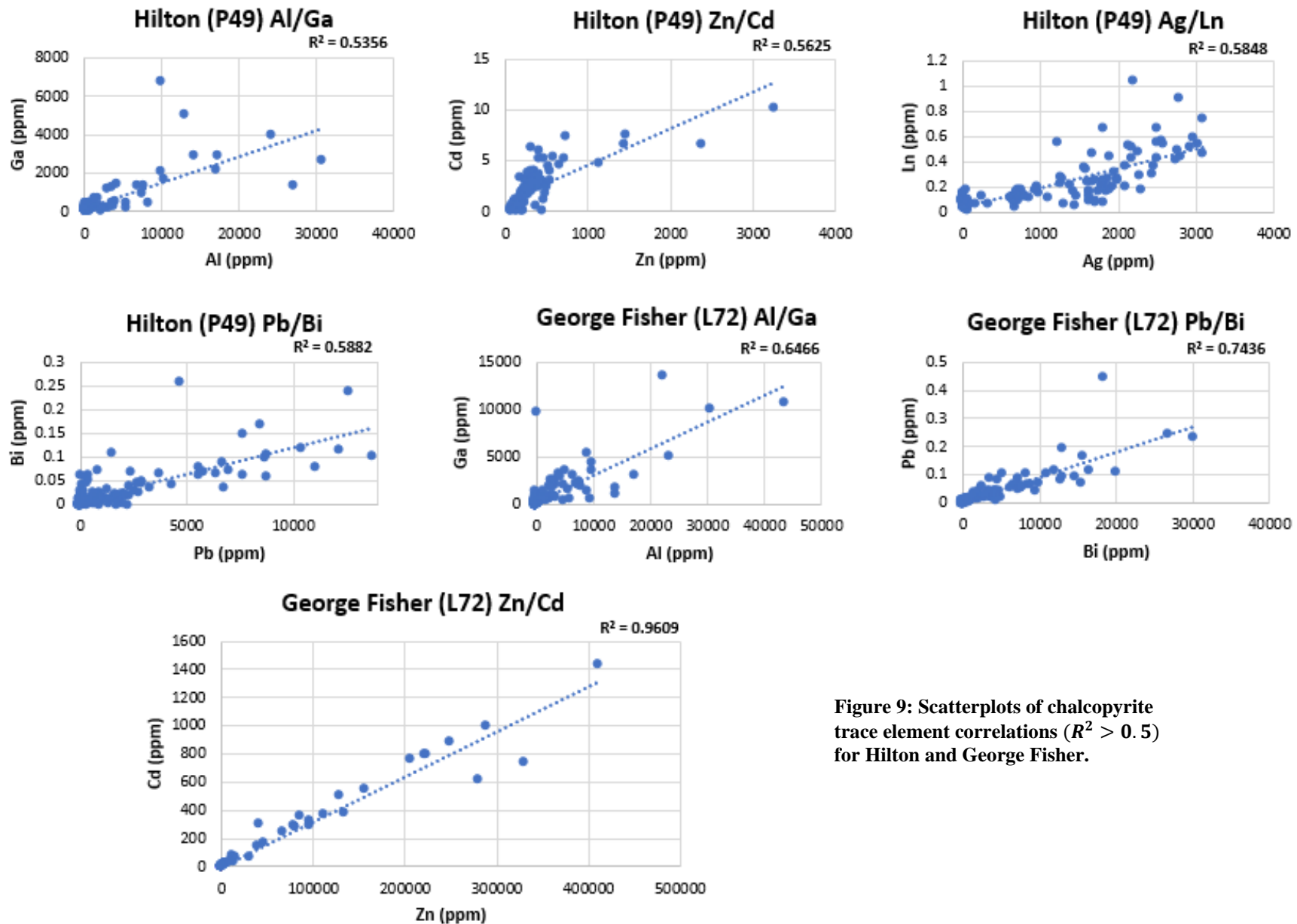


Figure 9: Scatterplots of chalcopyrite trace element correlations ($R^2 > 0.5$) for Hilton and George Fisher.

4.4 Dolerite Dyke Petrology

A suite of 11 dolerite dyke samples from five drill holes and seven different ore domains were collected to reflect the dolerite dyke lithology at Hilton (P49) and George Fisher (L72). Sample descriptions can be found in Appendix D. The range of samples is representative of dolerite dyke intrusion across both deposits with all samples consisting of very fine-grained, strongly altered and sheared rock (Figure 10). The degree of alteration varies between samples with the dominant alteration minerals being chlorite (Figure 10a), biotite (Figure 10b) and carbonate. Varying proportions of pyrite, pyrrhotite, sphalerite and galena were observed as vein-infill textures throughout (Figure 10c, d & f). Minor chalcopyrite was also observed by reflected light optical microscopy (Figure 10e). A single apatite grain was identified indicating potential for future geochronology dating (Figure 10g).

4.5 Structural Setting of Dolerite Dykes

Schematic cross-section of Hilton and George Fisher (Figure 2) displays the position of dolerite dykes within the Pb-Zn ore bodies relative to the major Hangingwall Fault to the west. Intrusion along the Hangingwall Fault indicates the dolerites were emplaced post-deformation of the Urquhart Shale (D₁) allowing for the intrusion up existing fault structures. The heavily deformed and sheared texture of dolerite samples (Figure 10) and the segmentation of dolerite dykes at depth along the Hangingwall Fault (Figure 2) indicates deformation post-dating dolerite intrusion. Mineralised Pb-Zn ore lenses are structurally-controlled and lack major deformation indicating the hydrothermal mineralisation of sulphide ore post-dating the main D₂ deformation episode (Figure 2)

(Murphy, 2004). The input of hydrothermal fluid enriched in Pb-Zn-Cu ore is observed to have infiltrated the system via fault structures created by D₃ deformation (Perkins, 1997; Davis, 2004).

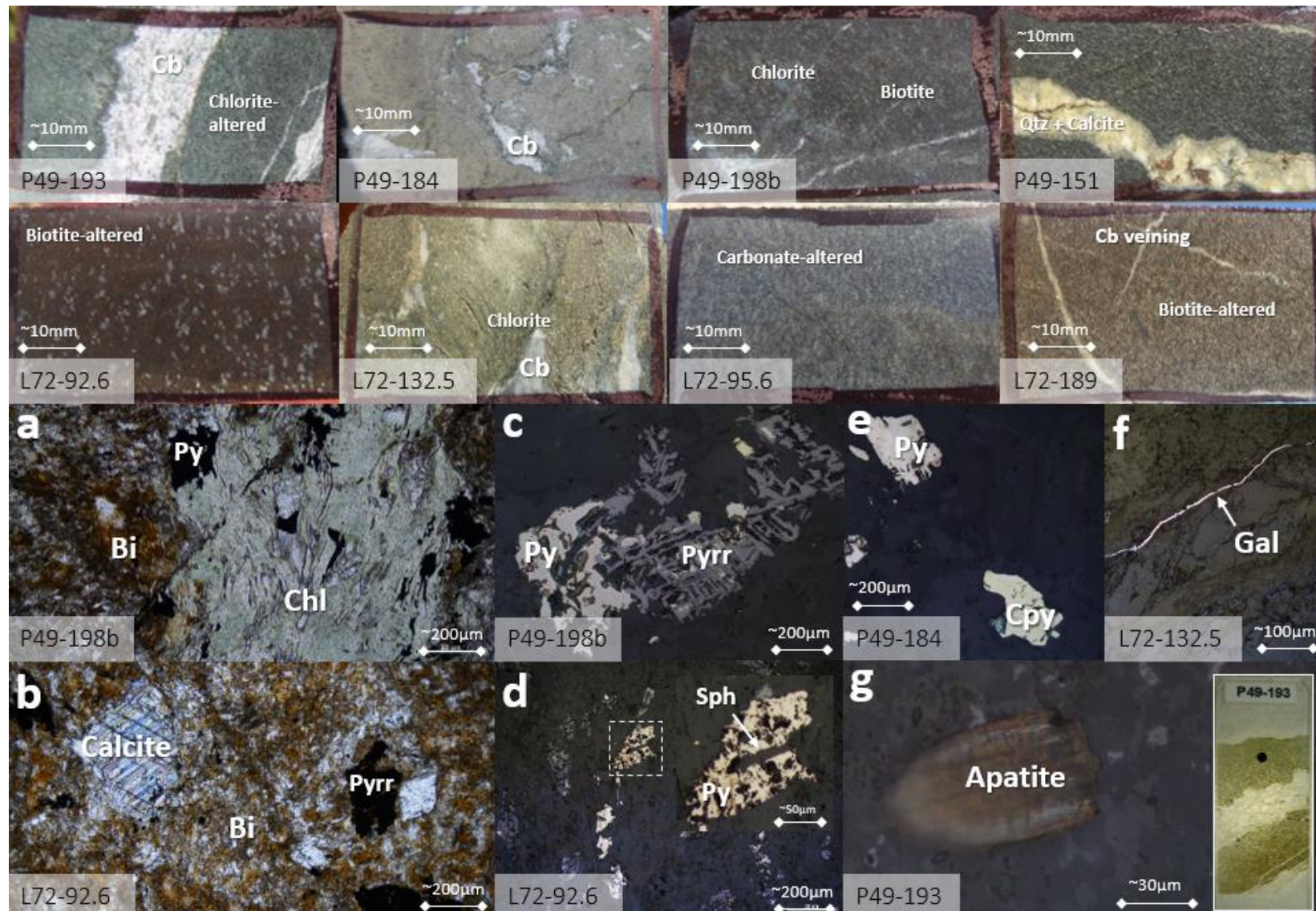


Figure 10: Images of original dolerite dyke samples displaying the heterogeneity of appearance and alteration styles for George Fisher (L72) and Hilton (P49) samples. Note common carbonate veining and deformation textures. a) Optical microscope image of biotite alteration (brown), chlorite alteration (pale green) and pyrite mineralisation (black), b) Optical microscope image of calcite (white with bright birefringence), pyrrhotite (black) and biotite alteration (brown), c) Reflected light image of pyrite (white/cream) and pyrrhotite (light grey), d) Reflected light image of pyrite cross-cut by sphalerite (grey) vein, e) Reflected light image of pyrite and chalcopyrite (pale yellow) infill, f) Reflected light image of galena vein (bright white) cross-cutting chlorite altered host, g) Reflected light image of an apatite grain (slightly out of focus) with the thin-section alongside displaying its location (black dot). Bi = Biotite, Chl = Chlorite, Cpy = Chalcopyrite, Sph = Sphalerite, Pyrr = Pyrrhotite, Py = Pyrite, Gal = Galena.

4.6 Dolerite Dyke Geochemistry

Whole rock and trace element geochemical data for dolerite dyke samples from Hilton (P49) and George Fisher (L72) were collected. Refer to Appendix I for whole rock and trace element values. From initial observations of whole rock geochemical data, two samples (P49-151 & L72-179.5) had relatively low TiO₂ (<0.2 wt%) compared to other samples which had TiO₂ values between 2.31—3.12 wt%. These samples were interpreted to not be dolerite and were excluded from further data analysis. However, it is worth noting that these samples were collected from zones which had been logged as dolerite, demonstrating how difficult it can be to visually distinguish the highly altered dolerites.

Measurable concentrations of ¹³⁷Ba, ¹⁴⁰Ce, ⁵²Cr, ¹³³Cs, ¹⁶³Dy, ¹⁶⁷Er, ¹⁵²Eu, ⁷⁰Ga, ¹⁵⁷Gd, ¹⁷⁸Hf, ¹⁶⁵Ho, ¹³⁹La, ¹⁷⁵Lu, ⁹³Nb, ¹⁴⁴Nd, ¹⁴¹Pr, ⁸⁵Rb, ¹⁵⁰Sm, ¹¹⁹Sn, ⁸⁸Sr, ¹⁸¹Ta, ¹⁵⁹Tb, ²³²Th, ¹⁶⁹Tm, ²³⁸U, ⁵¹V, ¹⁸⁴W, ⁸⁹Y, ¹⁷³Yb, ⁹¹Zr, ¹⁰⁸Ag, ⁷⁵As, ¹¹²Cd, ⁵⁹Co, ⁶⁴Cu, ⁷Li, ⁹⁶Mo, ⁵⁸Ni, ²⁰⁷Pb, ⁴⁵Sc, ²⁰⁴Tl & ⁶⁵Zn were recorded. Elevated concentrations of Cu, Pb and Zn were recorded which continues to support a timing of mineralisation which post-dates dolerite dyke intrusion.

Whole rock geochemistry allows for the classification of dolerite dyke samples to investigate their rock type and composition. According to Na₂O+K₂O and SiO₂ TAS volcanic rock classification (Le Maitre et al., 1989) (Figure 11), the dolerite dyke samples range from Foidite to Trachy-basalt to Tephrite volcanic rocks. However, modification of the primary SiO₂ values is possible during alteration, so these classifications should only be used as a guide.

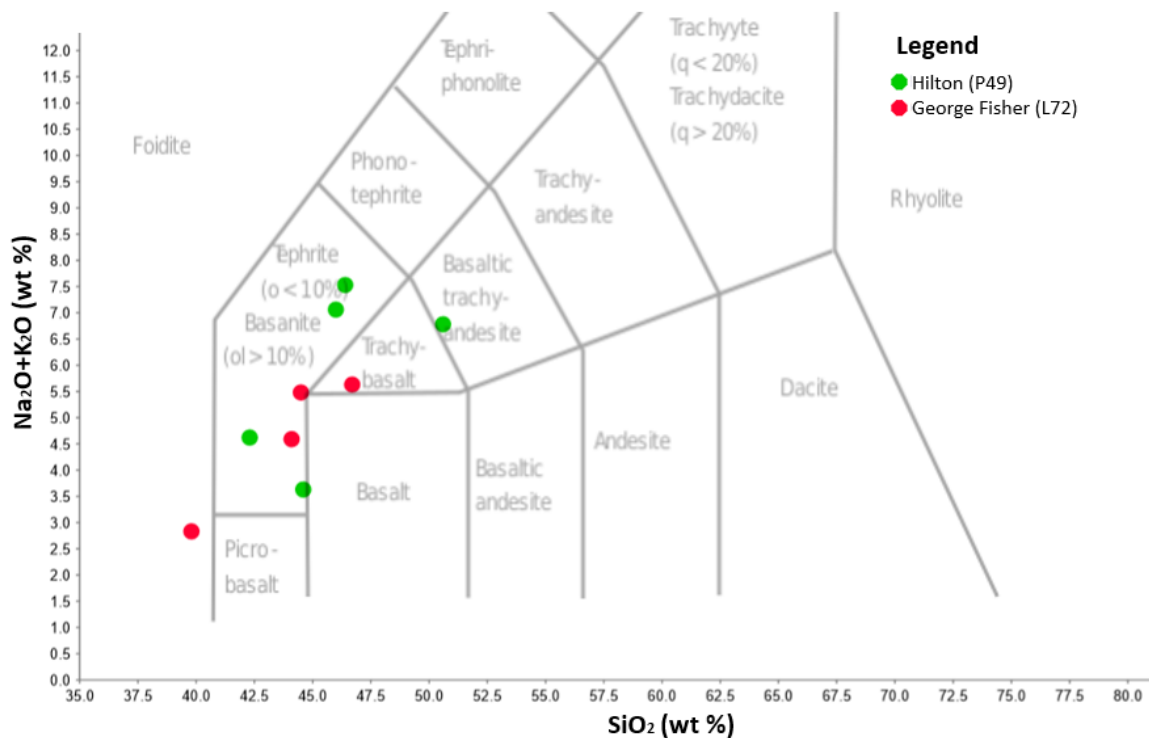


Figure 11: Total alkalis-silica (TAS) classification of dolerite dyke samples from Hilton (P49) and George Fisher (L72). Boundaries of fields implemented from Le Maitre *et al.* (1989). ol = normative olivine, q = normative quartz. TAS diagram does not discriminate between dolerite dyke samples of Hilton and George Fisher.

AFM discrimination (Rollinson, 1993) can be used to illustrate whether dolerite dyke samples from Hilton and George Fisher display a tholeiitic or calc-alkaline composition. According to discrimination diagrams made by Kuno (1968), four dolerite dyke samples are classified as tholeiitic and five are calc-alkaline. According to the diagrams from Irvine & Baragar (1971), seven dolerite dyke samples are classified as tholeiitic and two are calc-alkaline composition (Figure 12). Most dolerite dyke samples sit on the border between the two series with one sample from George Fisher displaying a calc-alkaline series, depleted in FeO. AFM plot poorly illustrates whether dolerite dyke samples represent tholeiitic or calc-alkaline compositions (Figure 12).

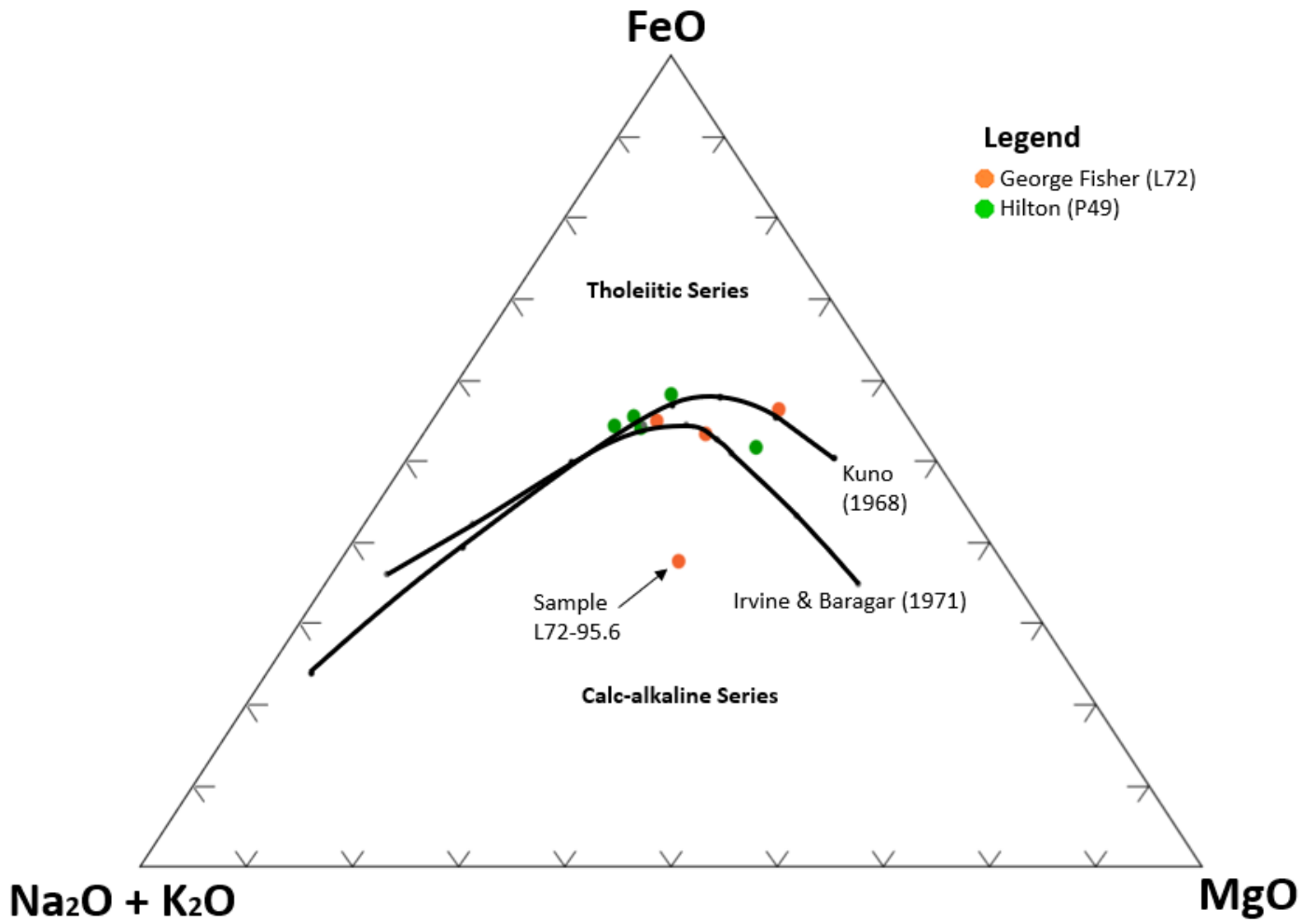


Figure 12: AFM (Na₂O+K₂O-FeO-MgO) ternary classification of dolerite dyke samples from Hilton (P49) and George Fisher (L72). Boundaries between tholeiitic and calc-alkaline series are from Kuno (1968) and Irvine & Baragar (1971). AFM discrimination implemented from Rollinson, (1993).

4.61 ELEMENT MOBILITY

Correlations of zircon (Zr) with trace and whole elements geochemical data can help determine the degree of element mobility and associated tectonic environments of formation. An element that displays a positive correlation is considered immobile (Pearce, 1983) and therefore represents dolerite dyke lithology prior to the biotite, chlorite and carbonate alteration.

Figure 13 displays selected major elements against the immobile element Zr. Plots B, C and E (CaO-K₂O-Na₂O) display a poor linear correlation with Zr compared to Ti₂O displaying a good positive correlation. Plot A (Si₂O) displays a fairly good correlation with Zr. In accordance with Rollinson (1993), the mobility of major elements is related to a low-grade metamorphic history because of Ti being relatively immobile and to an extent, Si, Ca, Na and K being relatively mobile.

Figure 14 displays selected trace elements against the immobile element Zr. Two members of the Rare Earth Elements (REE) are presented in plots B (LREE La) and D (HREE Yb). Samples display an overall poor correlation with Zr apart from Hilton samples on plot D (HREE Yb) displaying a positive correlation. Plot E (HFS Y) displays a poor correlation with Zr which is unexpected since Yttrium (Y) is a high field strength element. Plots A (LILE Ba) and C (LILE Rb) display poor correlations indicating trace element mobilisation. Trace elements that are identified as mobile (Ba & Rb) are unreliable for discrimination and in-turn dismissed from further multi element analysis (Figure 18).

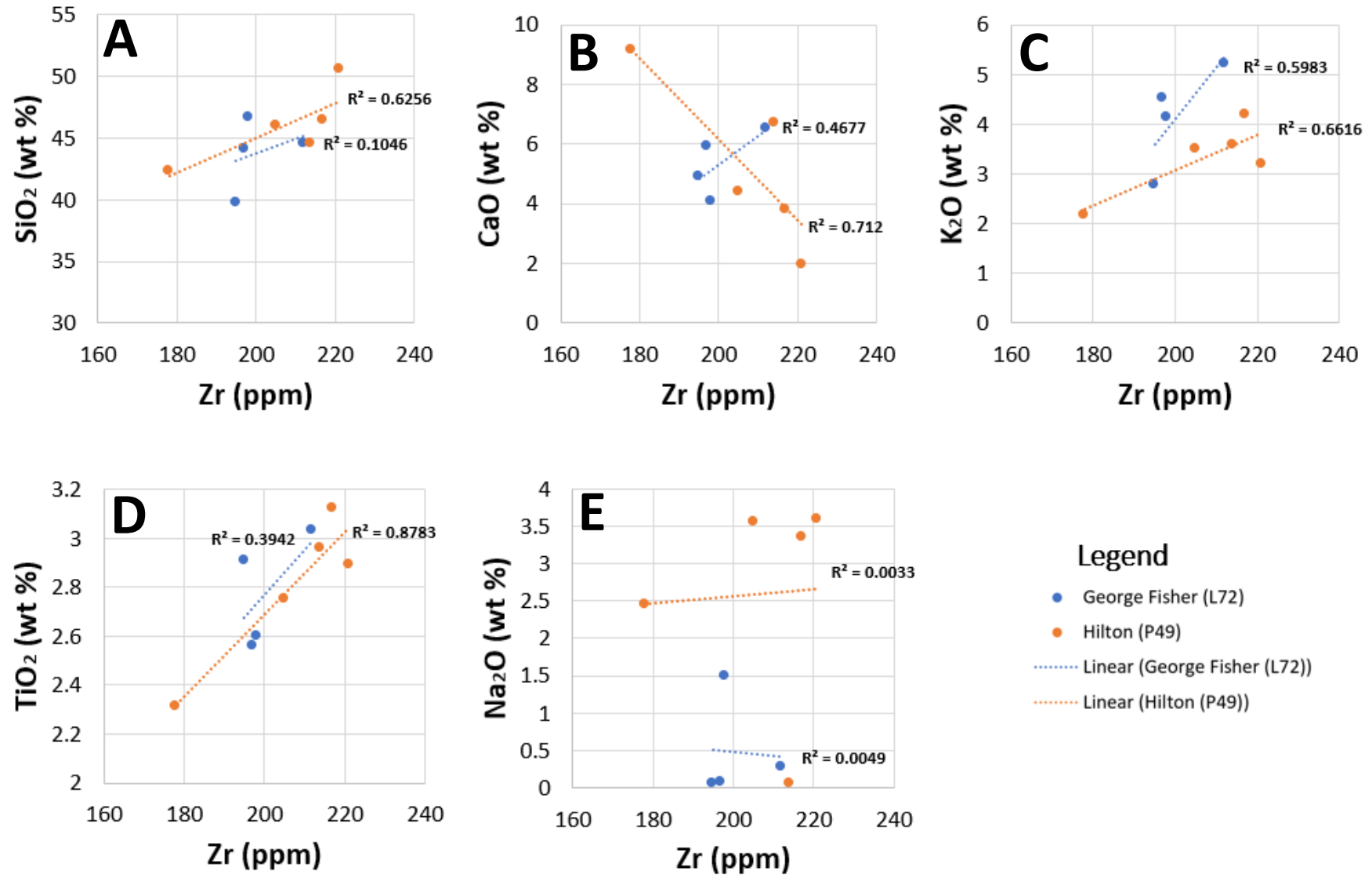


Figure 13: Scatterplots displaying Zircon (Zr) and major element concentrations for dolerite dyke samples of Hilton (orange) and George Fisher (blue). Zircon correlations infer the degree of mobility of elements. A positive correlation infers the major element is immobile.

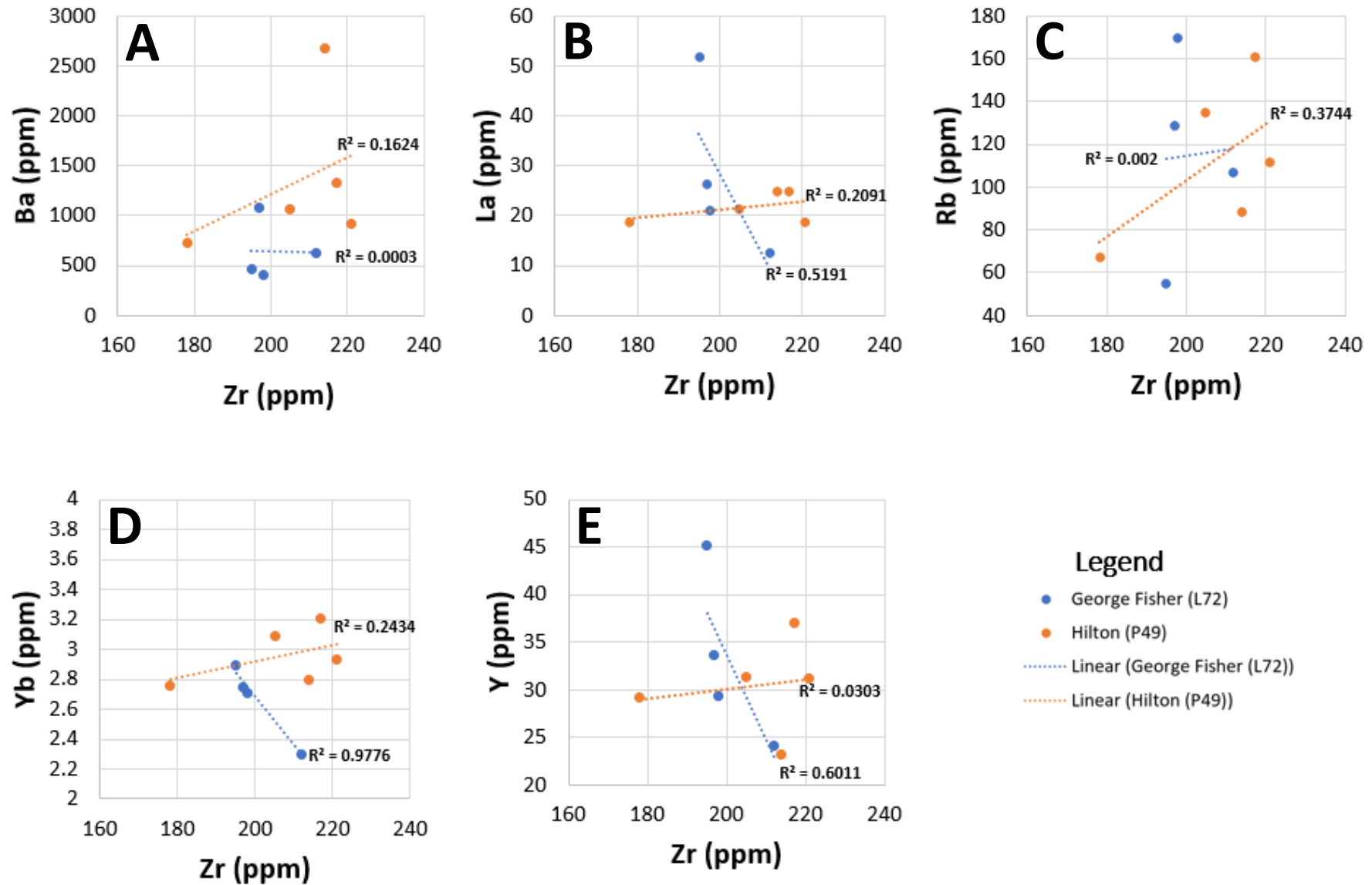


Figure 14: Scatterplots displaying Zircon (Zr) and trace element concentrations for dolerite dyke samples of Hilton (orange) and George Fisher (blue). Zircon correlations infers the degree of mobility of elements. A positive correlation infers the trace element is immobile.

5. DISCUSSION

From observations of chalcopyrite mineralisation styles, associations with Pb-Zn ore-bearing minerals and trends in trace element distribution for Hilton (P49) and George Fisher (L72) deposits, interpretations can be made regarding the continuity and paragenesis of mineralisation.

5.1 Chalcopyrite Petrology

Sulphide mineral relationships were observed from Cu samples of Hilton and George Fisher illustrating the paragenetic timing of chalcopyrite in association with the main Pb-Zn mineralisation event, consistent with observations of chalcopyrite at the Mount Isa deposit (Cave, Bavorich, Lilly, 2019; Perkins, 1997). At Hilton and George Fisher, relatively early sphalerite appears to be overprinted by galena and then both are overprinted by chalcopyrite indicating an extended hydrothermal system of concurrent Zn-Pb-Cu mineralisation, and consistent with temperature-related solubility (Figure 4). This concept was initially depicted for the Mount Isa system by Perkins (1997) and is supported by data collected in this study at Hilton and George Fisher.

Paragenesis of Hilton by Taylor (2019) supports observations and key sulphide mineral relationships previously stated. According to Taylor (2019), the Hilton samples display an extended paragenesis of hydrothermal stages with a pre-ore assemblage of magnetite, chlorite, biotite, feldspar followed by three subsequent stages of sulphide input: (1) sphalerite dominant; (2) pyrrhotite dominant; and (3) galena dominant \pm sphalerite with chalcopyrite and pyrrhotite. However, three characteristics observed within the Cu

orebodies of Mount Isa can determine the continuity between Mount Isa, Hilton and George Fisher. Cu orebodies at Mount Isa host (1) major and distinct carbonate alteration, (2) major silicification ('silica dolomite') and (3) chalcopyrite mineralisation associated with pyrrhotite \pm pyrite \pm cobaltite. Most of these characteristics are also present within Hilton and George Fisher deposits however, the lack of identified cobaltite and major silicification in samples infers the deposits, while sharing a very similar paragenesis, have a slightly different genesis to the Mount Isa system.

Relatively high temperature minerals including biotite, magnetite and celsian (Ba) feldspar were observed within high-grade Cu zones at Hilton. Magnetite, a relatively high temperature mineral, indicates a relatively high temperature during an early stage of alteration. These minerals could also reflect D₂ (~1575 Ma) or peak metamorphism (Bell & Hickey, 1998; Waring, Heinrich, & Wall, 1998). Perkins (1987) and Gregory et al. (2005) also report magnetite, biotite and K-feldspar within the Mount Isa system and interpreted this to be the product of high temperature (potassic) alteration. The continued presence of these minerals with the same paragenetic relationship to the ore minerals over 22km strike provides evidence that mineralisation at Mount Isa, Hilton and George Fisher formed during related hydrothermal events.

Reflected light images and MLA mapping of Cu samples from Hilton and George Fisher displayed an association between Cu mineralisation, pyrrhotite (Figure 4f) and pyrite (Figure 5c). These associations are also evident at Mount Isa (Connell, 2016; Hitzman, Kirkham, Broughton, Thorson, & Selley, 2005). The presence of pyrite (coarse and fine-grained) is proposed to be an important chemical control for Cu mineralisation influencing the distribution of Cu ore (Robertson, 1975, 1982; Waring,

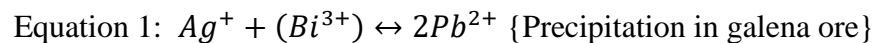
Heinrich, & Wall, 1998; Wilson, 1992). MLA maps of chalcopyrite-bearing samples from Hilton and George Fisher indicate that chalcopyrite is typically associated with pyrite-rich zones providing evidence that pre-ore pyrite (FeS_2) may provide a source of sulphur for the subsequent precipitation of chalcopyrite (CuFeS_2).

5.2 Chalcopyrite Geochemistry

Trace element and whole rock geochemistry has allowed for detailed discrimination of chalcopyrite between Mount Isa, Hilton and George Fisher (Figure 6).

Chalcopyrite with inclusions of sphalerite and galena is commonly observed throughout the samples at Hilton and George Fisher (Figure 7). The coexistence of co-crystallising sphalerite, galena and chalcopyrite allows for the substitution of selected trace elements (e.g. Ag^+ , Bi^{3+} , Ni^{2+} and Pb^{2+}) of similar physical properties (i.e. oxidation state, ionic radius) (George, Cook, & Ciobanu, 2016).

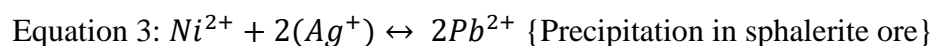
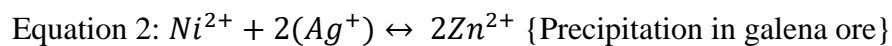
According to Goldschmidt's (1954) rules of substitution, Ag and Bi are able to substitute with Pb from galena shown by the equation below;



The substitution of Ag and Bi of chalcopyrite with Pb of galena could be responsible for enriched Ag and depleted Bi concentrations throughout Hilton and George Fisher relative to Mount Isa.

According to Cave et al. (2018), the concentration of Bi and Pb transitioning from Cu to Pb-Zn mineralisation systematically decrease. Bi concentrations progressively decrease and Pb concentrations progressively increase from Mount Isa to Hilton to George Fisher. Chalcopyrite from high-grade Cu zones contains relatively high concentrations of Bi and relatively low concentrations of Pb representative of Mount Isa (Cave, Bavorich, Lilly, 2019). Comparatively, chalcopyrite sourced from a galena mineralized zone beneath the Paroo Fault of the Mount Isa system contains relatively lower Bi concentrations and relatively higher Pb concentrations. The co-crystallisation of chalcopyrite and galena relates to the sample observations from Hilton and George Fisher (Figure 4) and reflects the depleted Bi and elevated Pb concentration results for Hilton and George Fisher relative to Mount Isa.

Clustering of data observed for Ni and Ag (Figure 6) was initially interpreted to be controlled by the influx of different Cu-rich fluids. Chalcopyrite at Hilton and George Fisher contains abundant inclusions of sphalerite and galena, allowing for the substitution of Ni and Ag with Zn (Equation 1) and Pb (Equation 2). This interpretation infers that the intergrown nature of chalcopyrite with galena and sphalerite is responsible for the clustering of data.



5.21 DEPOSIT GEOTHERMOMETRY

Mount Isa Group rocks at the Mount Isa deposit are considered to have higher peak metamorphic temperatures of ~300-350°C relative to George Fisher (Rubenach, 1992; Chapman, 1999; Davis, 2004). Bitumen reflectance analysis indicated peak metamorphic temperatures at George Fisher of ~200°C during D₂ and ~280°C during D₄, significantly cooler than the Mount Isa system (Chapman, 1999, 2004). Since Mount Isa is considered as a 'hotter' system relative to Hilton and George Fisher, ⁷¹Ga displays elevated concentrations at Hilton and George Fisher because of its incompatibility, preference for the 'melt' phase and concentration in 'cooler' systems (Bauer et al., 2019).

Hilton and George Fisher both display significant Cd/Zn correlations in chalcopyrite with George Fisher being very strong at $R^2 = 0.9609$. Since sphalerite is a main carrier of Cd (Cave, Bavorich, & Lilly, 2019), the strong Cd/Zn correlation is most likely because of sphalerite inclusions within the chalcopyrite.

According to George, Cook, Crowe, & Ciobanu (2018), ratios of Cd:Zn in chalcopyrite increases with temperature which allows for the interpretation of crystallisation temperatures (Figure 15) to be made. Chalcopyrite co-existing with other sulphide metals displays the same trends as chalcopyrite from Cu-dominated zones. Controlling factors of Cd:Zn ratios are influenced by crystallisation temperature however other factors include the concentrations and stability of each element in the ore-forming fluid, for example, pH and sulphur activity (George et al., 2018). Hilton has a considerably lower correlation ($R^2 = 0.5625$) between Cd and Zn which proposes the crystallisation

of chalcopyrite has less geochemical influence from sphalerite and galena mineralisation.

Plotting Cd/Zn concentrations of chalcopyrite from Hilton and George Fisher with deposits of known crystallisation temperature illustrates that Hilton samples have a slightly 'hotter' crystallisation temperature compared to George Fisher. With Hilton located closer to the 'hot' Mount Isa system, this interpretation is expected. The mean concentration of Cd/Zn for each deposit is used to infer the crystallisation temperature of chalcopyrite at Hilton and George Fisher ranging from ~280-350°C following the trend of known crystallisation temperatures (between Vorta (~280°C) & Toroiaga (~350°C) deposits) (Figure 15). Inferred crystallisation temperatures of chalcopyrite from Hilton and George Fisher overlap with chalcopyrite from Mount Isa (Cave, Bavorich, & Lilly, 2019) possibly indicating a semi-continuous and/or linked hydrothermal system between Mount Isa, Hilton and George Fisher.

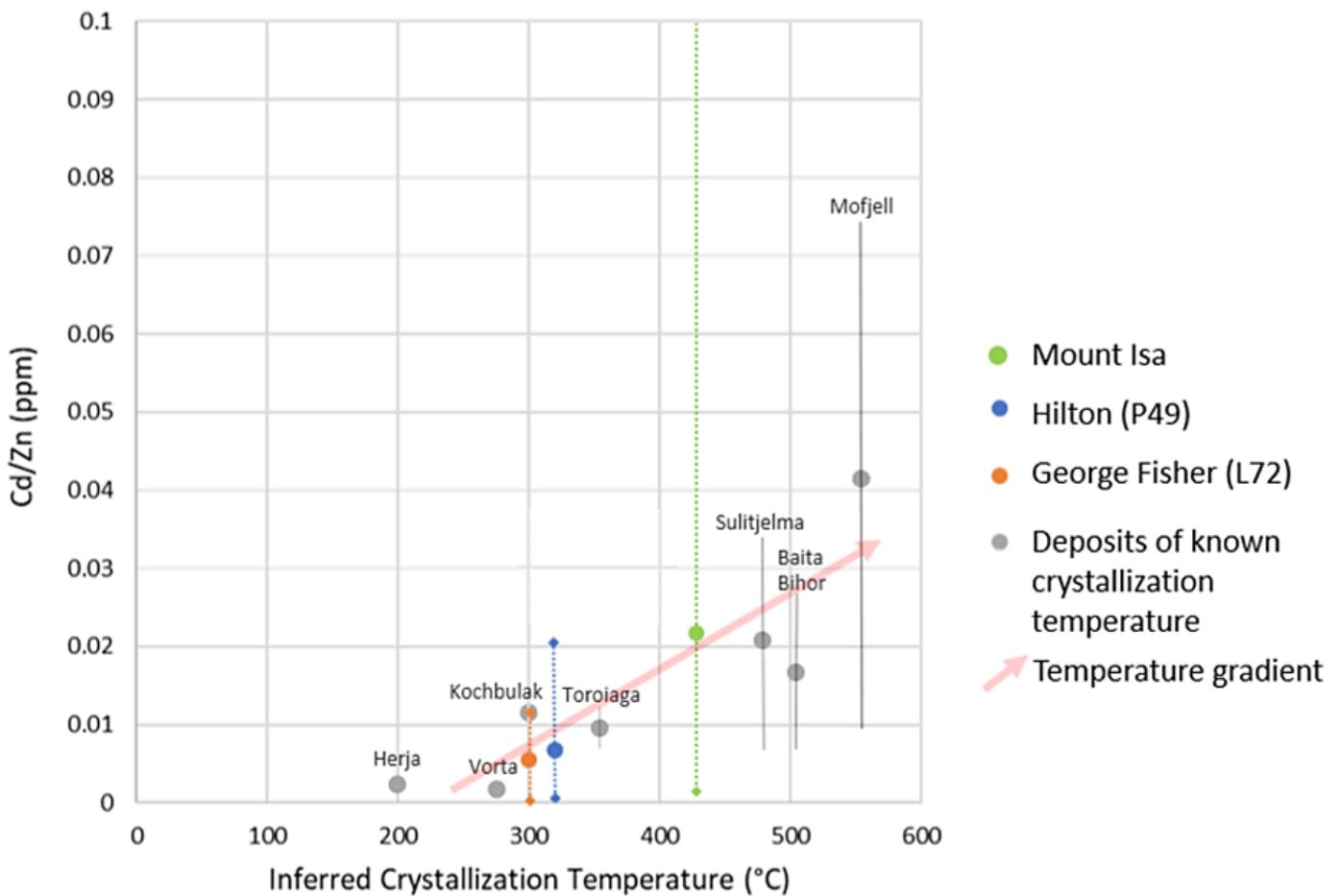


Figure 15: Plot showing the correlation between Cd/Zn ratios in chalcopyrite at Hilton (P49) and George Fisher (L72) and inferred chalcopyrite crystallisation temperatures. Grey data points are deposits with known crystallisation temperature. Coloured dots represent the mean value of Cd/Zn for each deposit. Black arrow illustrates decreasing inferred crystallisation temperature in the northward direction. Inferred crystallisation temperatures are only estimates for chalcopyrite. Error bars for deposits of known crystallisation temperature indicate one standard deviation. The dotted lines for Hilton and George Fisher displays the range of Cd/Zn values for each deposit. The Cd/Zn vs Inferred Crystallisation Temperature plot has been implemented from George et al. 2018. Deposits of known crystallisation temperature include epithermal (Herja, Toroiaga, Kochbulak), skarn (Baita Bihor), VMS (Vorta), Recrystallized SEDEX (Mofjell) and Recrystallized VMS (Sulitjelma).

5.3 Dolerite Dyke Petrology

Groundmass of dolerite dyke samples are dominated by fine-grained chlorite, biotite, quartz, calcite and minor rutile (TiO_2) supported by Hannan et al. (1993) and Valenta (1994) inferring emplacement prior to peak metamorphism (D_2). Taylor (2019) also identified the dolerites have experienced high temperature biotite, chlorite and rutile (TiO_2) alteration indicating the dykes were emplaced during a relatively 'hot' mineralisation episode.

The dolerite dykes host pyrite, pyrrhotite and Pb-Zn ore minerals, sphalerite and galena, while lacking major chalcopyrite mineralisation (Figure 10). Valenta (1994) also identified the presence of chalcopyrite, minor sphalerite and minor galena in the dolerites at Hilton and interpreted this as evidence of remobilisation of the pre-existing 'SEDEX' mineralisation during deformation. Valenta (1994) also used the location of the dolerite dykes proximal to the controlling Hangingwall Fault Cu zone as evidence that the dykes were associated with Cu mineralisation. However, this study and other studies that identify co-genetic Cu-Pb-Zn mineralisation for the George Fisher and Hilton deposits (e.g. Murphy, 2004 and Taylor, 2019) interpret the sulphide mineralisation post-dating dolerite intrusion (and biotite-chlorite alteration) (Figure 10). Chalcopyrite mineralisation found throughout dolerite lithologies is interpreted to be controlled by post-deformation of dykes and crystallisation temperature.

5.4 Dolerite Dyke Geochemistry

Dolerites sampled from Hilton and George Fisher display a range of compositions using the TAS and AFM classification schemes. Samples are identified as Foidite to

Trachy-basalt to Tephrite volcanic rocks in the TAS discrimination diagram (Figure 11) with compositions positioned along the boundary between a tholeiitic and calc-alkaline series in the AFM discrimination diagram (Figure 12), requiring further discrimination.

Correlations of trace and whole rock elements with Zircon (Zr) identified the mobility of elements allowing a more refined analysis of dolerite dyke samples and their association with two ECV members; Cromwell and Pickwick. TiO_2 displayed a strong positive correlation with Zr indicating its immobile nature making it a very reliable element for further discrimination of dolerite dyke samples. TiO_2 values from mine assay data are a good way to identify dolerites.

Ti/1000:V discrimination is used to correlate Hilton and George Fisher samples with the Cromwell and Pickwick ECV members and is typically used to distinguish between modern volcanic-arc tholeiites, MORBs and alkali basalts (Shervais, 1982). Hilton and George Fisher samples display lower Ti concentrations relative to both ECV members and a Ti/V ratio less than ten (Figure 16). According to Shervais (1982), low Ti values (2-10 ppm/1000) and moderate V concentrations (100-500 ppm) infer the dolerite dyke samples were derived from a mantle source with island-arc tholeiitic geochemical associations. Dolerite dyke samples from Hilton and George Fisher also partially lie within the W3 dolerite zone recorded in the Western Succession by Ellis & Wyborn (1984) inferring a similar mantle source region (Figure 16).

Y/Nb-Zr/Nb scatterplots are essential for illustrating a sample's evolution from bulk continental crust (Figure 17). Overall, the dolerite dyke samples from both Hilton and George Fisher are depleted in Y relative to the Isa Cromwell and Pickwick members

however are enriched relative to bulk continental crust inferring some samples have experienced a degree of contamination (possibly during emplacement). The field of samples overlaps with data from both ECV members inferring that dolerite dyke samples were generated from a similar mantle source. Interpretation of a similar mantle source is also supported by the emplacement of dolerite dykes splaying from NE—SW trending faults that bound the ECV complex (Figure 2). Intrusion of these dolerites most likely occurred during E-W shortening of D₂ and developed prior to the mineralisation of co-genetic Cu-Zn-Pb (Valenta, 1994).

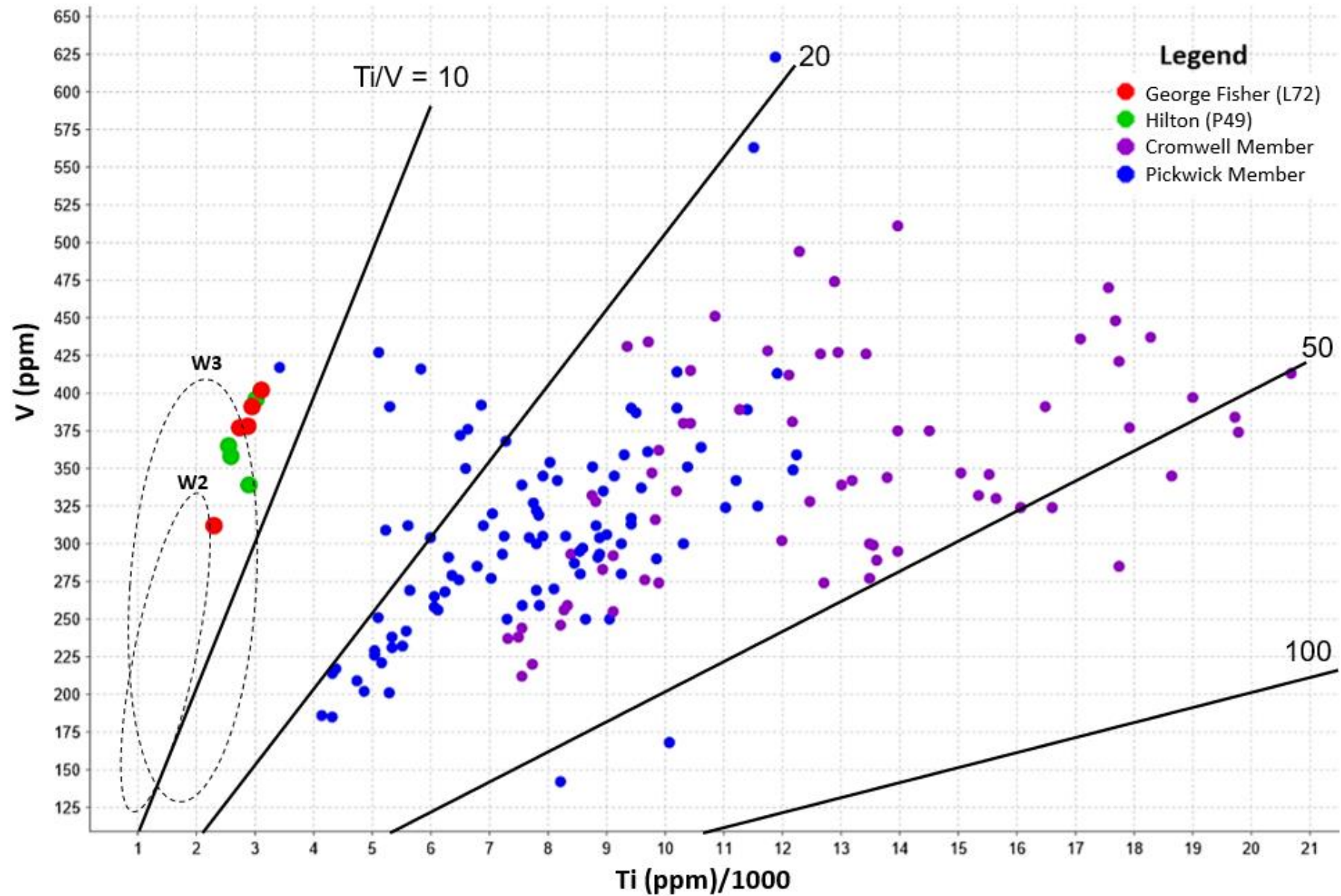


Figure 16: Ti-V discrimination diagram displaying dolerite dyke samples from Hilton (P49) and George Fisher (L72) relative to the Cromwell and Pickwick ECV members. W2 and W3 zones refer to dolerite samples within the Western Succession recorded by Ellis & Wyborn (1984) (Table 1). Black lines display the Ti/V ratios. Data of ECVs is from unpublished data provided by Mount Isa Mines.

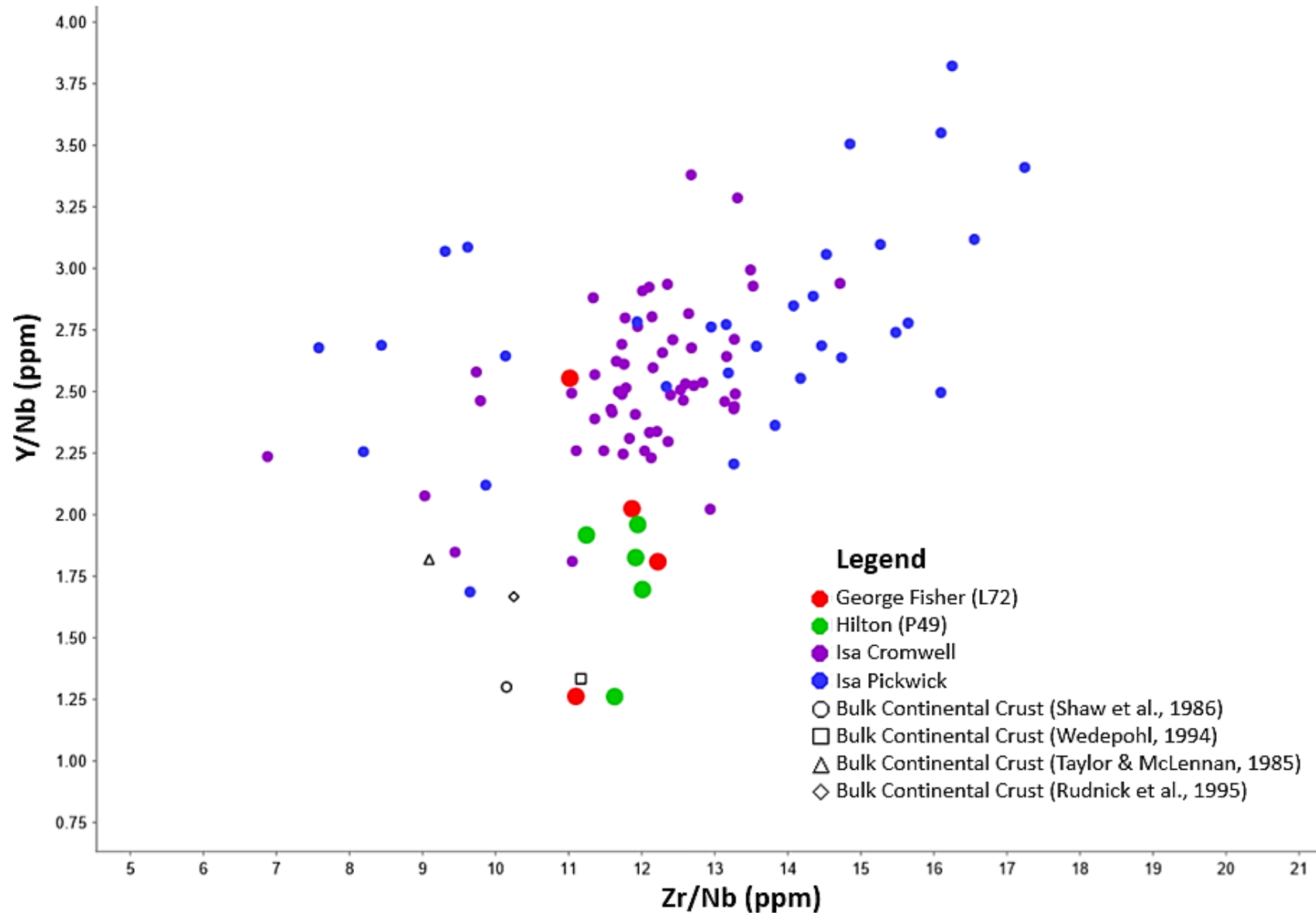


Figure 17: Y/Nb-Zr/Nb scatterplot displaying the degree of contamination of dolerite dyke samples from Hilton (P49) and George Fisher (L72) relative to the Isa Cromwell and Pickwick Members. Bulk continental crust estimates are displayed to show the degree of contamination. Supplementary data of Isa Cromwell and Pickwick Metabasalt Members from Wilson, Derrick, & Perkin, (1985) and bulk continental crust estimates from Rudnick & Fountain, (1995), Taylor & McLennan, (1995), Wedepohl, (1995), Shaw et al. (1986) and Weaver & Tarney (1984).

N-MORB normalised multi-element plots provide the ability to compare REE being the least soluble trace elements and relatively immobile under hydrothermal conditions (Rollinson, 1993). When comparing the REE from dolerite dyke samples of Hilton and George Fisher to ECV data, similarities and differences with the Pickwick Member can be illustrated (Figure 18). Dolerite dyke samples closely resemble REE concentrations of the Pickwick (Trachy-Basalt) Member. According to Gregory, Keays, & Wilde, (2005), the Pickwick Metabasalt Member formed by the injection of S-undersaturated magma enriched in platinum-group elements (PGEs) but depleted in Cu, consistent with Hilton and George Fisher samples. Similarities of dolerite dyke samples at Hilton and George Fisher with ECV data of the Pickwick Member infers the dolerites were a product of re-melting of the same mantle material which sourced the ECVs.

Samples from Hilton and George Fisher display a negative Nb anomaly representing contamination from continental crust during magma processes (Rollinson, 1993) most likely because of the exhumation and intrusion of the dolerite dykes. Positive Dy anomaly, also observed in dolerite dyke samples, helps measure the ‘concavity’ of a REE pattern. When the slope between Dy and Yb is decreasing, it is inferred the dolerite dyke samples are from a single co-genetic volcanic source controlled by amphibole and increasing SiO₂ (Davidson, Turner, & Plank, 2012).

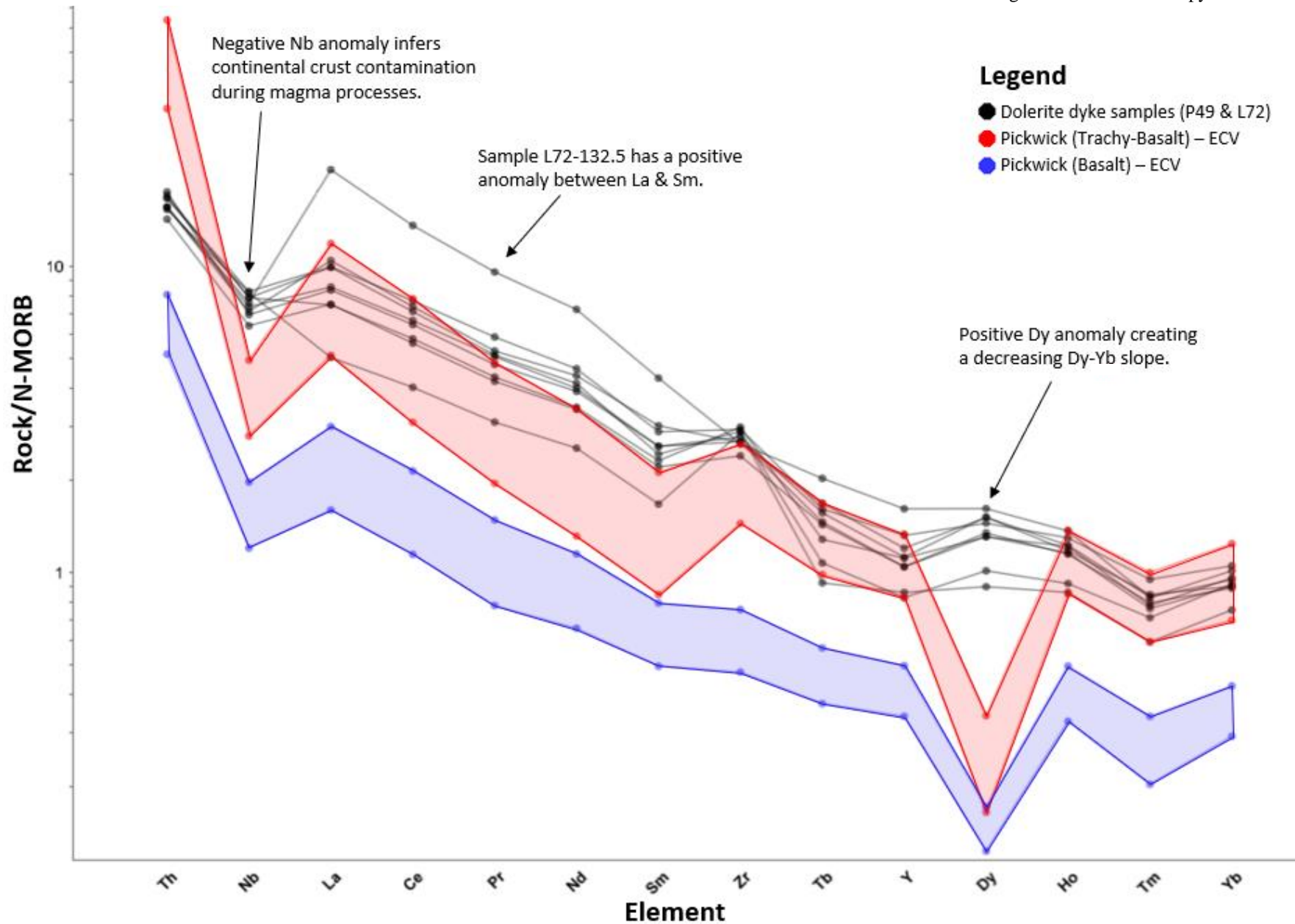


Figure 18: N-MORB normalised multi-element plot displaying REE of dolerite dyke samples from Hilton (P49) and George Fisher (L72) relative to the Parsons Knob Pickwick Trachy-Basalt Member. Pickwick Member ECV geochemical data is unpublished and provided by Mount Isa Mines. 57

5.5 Relationship between Cu and Dolerite Dyke distribution

Valenta (1988) inferred a strong spatial association between Cu and the major subvertical sheared dyke system within the Hilton deposit. However, after observing dolerite dyke samples collected from Hilton and George Fisher, modest mineralisation of Cu, Pb and Zn is present in most samples. The lack of Cu-only mineralisation within dolerite dyke samples at Hilton and George Fisher infers that Cu mineralisation is not uniquely associated with the dolerite dyke system. Since an epigenetic Cu-Pb-Zn mineralised system is inferred from the data generated by this study, the distribution of Cu near dolerite dykes is interpreted as a result of the dykes being structurally located in the Hangingwall of a zoned, temperature-controlled Cu-Pb-Zn system.

5.6 Interpreted Timeline of Events

- 1) Formation of Urquhart Shale, fine-grained pyrite and carbonate bedding.
- 2) N—S directed shortening creating east-west oriented folds (D_1).
- 3) E—W horizontal shortening characteristic of the Isan Orogeny (D_2).
- 4) Intrusion of dolerite dyke lithologies hosting quartz, calcite and minor apatite with major chlorite, biotite and carbonate alteration (Early D_2).
- 5) D_2 peak metamorphism and related hydrothermal event associated with quartz, carbonate, magnetite, celsian (Ba) feldspar, biotite and rutile (TiO_2) formation.
- 6) Hydrothermal event resulting in co-genetic Cu-Pb-Zn within an epigenetic system, synchronous with trans-tensional D_3 , hosting sphalerite, galena, pyrrhotite, pyrite and chalcopyrite.

6. CONCLUSIONS

- Chalcopyrite mineralisation is closely associated with galena and sphalerite and is interpreted to be part of the same extended epigenetic hydrothermal event.
- The presence of co-genetic Pb-Zn-Cu mineralisation within the altered and sheared dolerites provides strong field evidence for an epigenetic mode of origin for the Hilton and George Fisher deposits with a closely related ore genesis to the Mount Isa deposit.
- Economic sulphide mineralisation post-dates the deformation of the host shales and major deformation of the Isan Orogeny (D_1 — D_2).
- Cd:Zn ratios of chalcopyrite indicate that the greater mineralising system is most likely focused at Mount Isa and cools to the north, subsequently Hilton represents a ‘hotter’ mineralised system relative to George Fisher.
- Chalcopyrite mineralisation is associated with hotter systems, so it is interpreted that Hilton has more prospectivity for additional (deep) Cu mineralisation than George Fisher.
- There is potential for additional Pb-Zn-Cu mineralisation in the Urquhart Shales between Mount Isa and Hilton, and Pb-Zn mineralisation the north of George Fisher.
- The dolerite dykes have experienced significant biotite, chlorite and/or carbonate alteration and host sphalerite, galena and chalcopyrite indicating intrusion prior to Pb-Zn-Cu mineralisation.
- The structural controls to the dolerites and their subsequent deformation and alteration indicates that the dolerites were most likely introduced during D_2 (~1575 Ma).

- Ti/1000:V diagram illustrates a geochemical similarity between W3 dolerites of the Western Succession and dolerites at Hilton and George Fisher.
- Dolerite dykes at Hilton and George Fisher can be broadly categorised as tholeiites and have similar geochemistry to the Pickwick Member of the ECVs providing evidence that the dolerites are a product of re-melting from the same mantle source as the ECVs most likely during D₂ orogenesis and prior to peak metamorphism.

ACKNOWLEDGMENTS

Thank you to Vincent Wai and the rest of the team at George Fisher for assisting with field work and financially supporting this project. Thanks to Sarah Gilbert and Benjamin Wade from Adelaide Microscopy for their expert knowledge and welcoming nature. Big thanks to Brad Cave for helping with sampling, preparation, data analysis, supplementary Mount Isa data and overall structure of the honours project. Last but most definitely not least I would like to thank Richard Lilly, my supervisor, for his drive and passion of the industry and the outstanding hard work and commitment made towards his honours students. Richard has provided me with the confidence, knowledge and expertise required to succeed in the exploration and mining industry. Thanks immensely!

REFERENCES



- Bell, T. H., & Hickey, K. A. (1998). Multiple deformations with successive subvertical and subhorizontal axial planes: their impact on geometric development and significance for mineralization and exploration in the Mount Isa region. *Economic Geology*, 93, 1369-1389.
- Blake, D. H. (1987). Geology of the Mount Isa Inlier and environs: Queensland and Northern Territory. 1.
- Blake, D. H., & Stewart, A. J. (1992). Stratigraphic and tectonic framework, Mount Isa inlier. *Australian Geological Survey Organisation Bulletin*, 243, 1-11.
- Broadbent, G. C., Myers, R. E., & Wright, J. V. (1998). Geology and origin of shale-hosted Zn-Pb-Ag mineralization at the Century Deposit, Northwest Queensland, Australia. *Economic Geology*, 93, 1264-1294.
- Cave, B., Lilly, R., & Bavorich, K. (2018). Geology and geochemistry of chalcopyrite, galena and sphalerite across the Mount Isa Cu to Pb-Zn transition: Implications for a zoned Cu-Pb-Zn system. *Mawson Centre for Geoscience, Department of Earth Sciences, The University of Adelaide*.
- Chapman, L. H. (1999). Geology and genesis of the George Fisher Zn-Pb-Ag deposit Mount Isa, Australia. *School of Earth Sciences, James Cook University*, 2.
- Chapman, L. H. (2004). Geology and Mineralization Styles of the George Fisher Zn-Pb-Ag Deposit, Mount Isa, Australia. *Economic Geology*, 99(2), 233-255. doi:10.2113/gsecongeo.99.2.233
- Conaghan, E. L., Hannan, K. W., & Tolman, J. (2003). Mount Isa Cu and Pb-Zn-Ag deposits, NW Queensland Australia. *Mount Isa Mines Exploration Pty Ltd*.
- Connell, S. (2016). Fine-grained pyrite within the Mount Isa copper system, NW Queensland; geological relationships, modelled distribution and links to reactive ground. *Honours Thesis, The University of Adelaide*.
- Cox, R., & Curtis, R. (1977). The discovery of the Lady Loretta zinc-lead-silver deposit, northwest Queensland, Australia - A geochemical exploration case history. *Journal of Geochemical Exploration*, 8(1-2), 189-202. doi:10.1016/0375-6742(77)90051-6
- Davidson, J., Turner, S., & Plank, T. (2012). Dy/Dy*: Variations arising from mantle sources and petrogenetic processes. *Journal of Petrology*, 54(3), 525-537. doi:<https://doi.org/10.1093/petrology/egs076>
- Davis, T. P. (2004). Mine-scale structural controls on the Mount Isa Zn-Pb-Ag and Cu Orebodies. *School of Earth Sciences, James Cook University*, 99, 543-559.
- Ellis, D. J., & Wyborn, L. A. I. (1984). Petrology and geochemistry of Proterozoic dolerites from Mount Isa Inlier. *Journal of Australian Geology & Geophysics*, 9, 19-32.
- Etheridge, M., & Wall, V. (1994). Tectonic and structural evolution of the Australian Proterozoic. *Geological Society of Australia*, 102-103.
- Finlow-Bates, T., & Stumpfl, E. F. (1980). The copper and lead-zinc-silver orebodies of Mt Isa mine, Queensland: products of one hydrothermal system. *Conference Proceedings*.
- Forrestal, P. J. (1990). Mount Isa and Hilton silver-lead-zinc deposits. *Geology of the Mineral Deposits of Australia & Papua New Guinea*, 14, 927-934.

- George, L., Cook, N. J., & Ciobanu, C. L. (2016). Partitioning of trace elements in co-crystallized sphalerite-galena-chalcopyrite hydrothermal ores. *Ore Geology Reviews*, 77, 97-116.
- George, L., Cook, N. J., Crowe, B. B. P., & Ciobanu, C. L. (2018). Trace elements in hydrothermal chalcopyrite. *Mineralogical Society of Great Britain and Ireland*, 82(1), 59-88. doi:10.1180/minmag.2017.081.021
- Glencore. (2014). Resources & Reserves.
- Gregory, M. J., Keays, R. R., & Wilde, A. R. (2005). Platinum-group element geochemistry of the Eastern Creek Volcanics, Mount Isa, Australia. *School of Geoscience*, 961-964.
- Grondijs, H. F., & Schouten, C. (1937). A study of the Mount Isa ores. *Economic Geology*, 32(4), 407-450.
- Gulson, B. L., Perkins, W. G., & Mizon, K. I. (1983). Lead isotope studies bearing on the genesis of copper orebodies at Mount Isa, Queensland. *Economic Geology*, 78, 1466-1504.
- Hannan, K. W., Golding, S. D., Herbert, H. K., & Krouse, H. R. (1993). Contrasting Alteration Assemblages in Metabasites from Mount Isa, Queensland: Implications for Copper Ore Genesis. *Economic Geology*, 88, 1135-1175.
- Hitzman, M., Kirkham, R., Broughton, D., Thorson, J., & Selley, D. (2005). The sediment-hosted stratiform copper ore system. *Economic Geology*, 100, 609-642.
- Large, R., McGoldrick, P., Bull, S., & Cooke, D. (2004). Proterozoic strataform sediment-hosted zinc-lead-silver deposits of northern Australia. *Centre of Ore Deposit Research*, 1-17.
- McGoldrick, P. J., & Keays, R. R. (1990). Mount Isa copper and lead-zinc-silver ores; coincidence or cogenesis? *Economic Geology*, 85(2), 641-650.
- Murphy, T. E. (2004). *Structural and stratigraphic controls on mineralization at the George Fisher Zn-Pb-Ag Deposit, Northwest Queensland, Australia*. (Doctor of Philosophy PhD). James Cook University, Retrieved from <http://researchonline.jcu.edu.au/1282/>
- Neudert, M. K. (1983). A depositional model for the upper Mount Isa Group and implications for ore formation. *PhD Thesis, Australian National University*, 324.
- O'Dea, M. G. (1997). Geodynamic evolution of the Proterozoic Mount Isa terrain. *Geological Society of London Special Publication*, 121, 99-122.
- Page, R. W., & Bell, T. H. (1986). Isotopic and structural responses of granite to successive deformation and metamorphism. *Journal of Geology*, 94, 365-379.
- Pearce, J. A. (1983). Role of the sub-continental lithosphere in magma genesis at active continental margins. *Continental basalts and mantle xenoliths*, 230-249.
- Perkins, W. G. (1997). Mount Isa lead-zinc orebodies: replacement lodes in a zoned syndeformational copper-lead-zinc system? *Ore Geology Reviews*, 12, 61-110.
- Perkins, W. G., & Bell, T. H. (1998). Stratiform replacement Lead-Zinc deposits: a comparison between Mount Isa, Hilton, and McArthur River. *Economic Geology*, 93, 1190-1212.

- Petrov, D., & Popov, K. (2015). Correlations between elements in ores from the Gold-Copper deposit Chelopech, Bulgaria. *University of Mining and Geology*, 58, 1-6.
- Robertson, C. W. (1975). The stratigraphy and geochemistry of the southern portion of the 110 copper orebody at Mount Isa, north west Queensland, and its implication on the genesis of the copper mineralization. *Unpublished MSc thesis, James Cook University*.
- Robertson, C. W. (1982). The role of pre-existing sulphides in copper-ore formation at Mount Isa, Queensland. *Journal of Australian Geology & Geophysics*, 7, 119-124.
- Rollinson, H. (1993). Using geochemical data: evaluation, presentation, interpretation. *Longman Scientific & Technical*, 352.
- Rubenach, M. J. (1992). Proterozoic low-pressure/high-temperature metamorphism and an anticlockwise P-T-t path for the Hazeldene area, Mount Isa inlier, Queensland, Australia. *Journal of Metamorphic Geology*, 10, 333-346.
- Scott, D. L., Rawlings, D. J., Page, R. W., Tarlowski, C. Z., Idnurm, M., Jackson, M. J., & Southgate, P. N. (2000). Basement framework and geodynamic evolution of the Palaeoproterozoic superbasins of north-central Australia: an integrated review of geochemical, geochronological and geophysical data. *Australian Journal of Earth Sciences*, 47, 341-380.
- Shervais, J. W. (1982). Ti-V plots and the petrogenesis of modern and ophiolitic lavas. *Earth and Planetary Science Letters*, 59(1), 101-118.
- Sinyakova, E., Kosyakov, V., Distler, V., & Karmanov, N. (2016). Behaviour of Pt, Pd, and Au during crystallisation of Cu-rich magmatic sulfide minerals. *The Canadian Mineralogist*, 54(2), 491-509.
- Smith, J. W., Burns, M. S., & Croxford, N. J. W. (1978). Stable isotope studies of the origins of mineralization at Mount Isa. *Mineralium Deposita*, 13(3), 369-381.
- Stanton, R. L. (1963). Constitutional features of the Mount Isa sulfide ores and their interpretation. *Australas. Inst. Min. Metall. Proc.*, 205, 31-153.
- Taylor, R. G. (2019). Paragenetic interpretation -derived via petrological investigation of 19 samples from drill hole P49, Hilton Mine Mt Isa, Queensland Australia.
- Valenta, R. (1994). Syntectonic discordant copper mineralization in the Hilton Mine, Mount Isa. 89, 1031-1052.
- Valenta, R. K. (1988). Deformation, fluid flow and mineralization in the Hilton area, Mt Isa, Australia. *PhD Thesis, Monash University*, 269.
- Waring, C. L., Heinrich, C. A., & Wall, V. J. (1998). Proterozoic metamorphic copper deposits. *Australian Geological Survey Organisation - Journal of Australian Geology and Geophysics*, 17, 239-246.
- Williams, P. J. (1998). An Introduction to the Metallogeny of the McArthur River-Mount Isa-Cloncurry Minerals Province. *Economic Geology Research Unit, School of Earth Sciences*, 93, 1120-1131.
- Wilson, A. (1992). Metal distribution in the Hilton Mine, Mount Isa, and its genetic implications. *Unpublished B.Sc. honours thesis, Monash University*, 159.

Wilson, I. H., Derrick, G. M., & Perkin, D. J. (1985). Eastern Creek Volcanics; their geochemistry and possible role in copper mineralisation at Mount Isa, Queensland. *BMR Journal Australian Geology & Geophysics*, 9, 317-328.

APPENDIX A: HOST LITHOLOGY DESCRIPTIONS

<p>Medium-bedded stylolitic mudstone (MM)</p>	<p>Consistent 5-15m unit thickness with continuity throughout the deposit. Mineralogy ranges from quartz, calcite, K-feldspar and/or ferroan dolomite with remnant white mica. Bedding within this unit is planar, 5-10cm thickness beds and lacks banding of carbonate. Prominent carbonaceous stylolites evident throughout.</p>  <p>Photo from Chapman (1999)</p>
<p>Banded mudstone (BM)</p>	<p>10-100m long, discontinuous lenses throughout the deposit approximately 2-5cm thickness. Mineralogy same as MM host rock however parallel carbonate bands are common in BM host rock. Minor cross-bedding observed in massively bedded, 2-5cm shale-rich intervals with gradational contact between siltstone units.</p> 

**Pyritic
siltstone (PS)**

1-5m unit thickness hosts the majority of ore mineralisation. Millimetre-scale laminations same as CS host rock however mineralogy of the dark laminations composes fine-grained spheroidal pyrite and minimalistic carbonaceous material. Contact between banded mudstones is gradational at metre-scale whereas a sharp contact with medium-bedded mudstones. Nodular and banded carbonate common throughout.

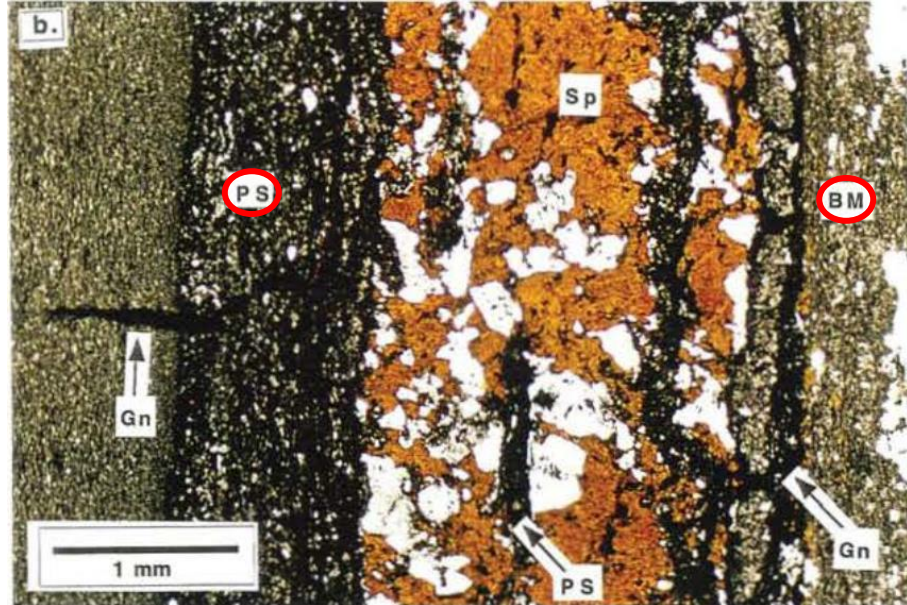
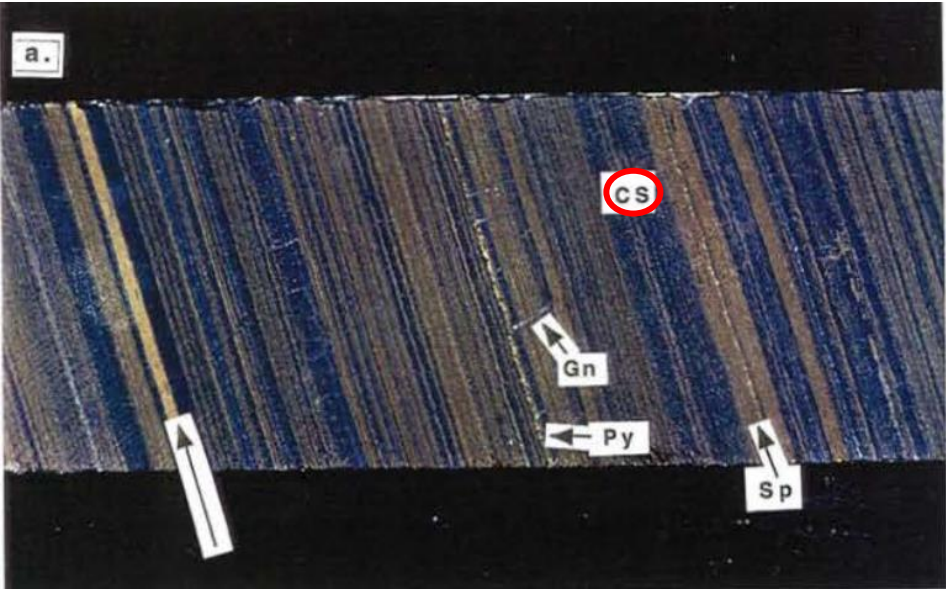



Photo from Chapman (1999)

<p>Carbonaceous siltstone (CS)</p>	<p>2-50cm unit thickness with alternating light and dark laminations, gradational between banded mudstones. Mineralogy ranges from ferroan dolomite and quartz composing the light grey laminations and concentrated carbonaceous material making up the darker laminations. Stratigraphically horizontal, discontinuous bedding of millimetre-scale with minor nodular and banded carbonate.</p>  <p>Core photo from Chapman (1999)</p>
<p>Tuffaceous marker bed (TMB)</p>	<p>Continuous, stratigraphically oriented beds lengthening the entire deposit. At approximately 0.5-10cm thickness, the TMB typically has cross fracturing of bedforms and sharp boundaries between units. Mineralogy predominantly consists of quartz and K-feldspar with additional chlorite and white mica mineralisation.</p>  <p>Core photo from George Fisher</p>

APPENDIX B: PB-ZN MINERALISATION STYLE DESCRIPTIONS

<p>Layer-parallel disseminated sphalerite</p>	<p>Strata-bound and conformable with bedding comprised of very fine grained, sub- to anhedral light brown and reddish-brown sphalerite. The sphalerite is parallel with the host rock at millimetre- to centimeter-scale and is considered sub-economic. Disseminated sphalerite is dispersed throughout dolomite laminations and tuffaceous marker beds however sporadic within pyritic and carbonaceous laminations (Chapman, 2004).</p>
<p>Layer-parallel vein-hosted sphalerite</p>	<p>Typically fine-medium grained, reddish-brown, crystalline sphalerite formed as parallel bands, interpreted as veins. Deposition of vein-hosted sphalerite is associated with material in open fractures and range from 1mm to 3cm thickness. Textural features within veining suggests earlier small scale brecciation of silicate and carbonate vein infill was dissolved or replaced by a later stage precipitation of sphalerite (Chapman, 2004).</p>
<p>Breccia-hosted sphalerite</p>	<p>More structural complexity and finer grain size relative to vein-hosted sphalerite. The strata-bound breccia-hosted sphalerite contains very fine-grained sphalerite with traces of pyrrhotite and galena. Folded and deformed fragments of mudstone, pyritic siltstone and clasts of dolomitic veins are dispersed throughout the breccia indicating breccia formation was synchronous with fold development (Chapman, 2004).</p>
<p>Vein- and breccia-hosted galena</p>	<p>Structurally continuous however irregularly distributed. Vein-hosted galena ranges from fine to coarse-grained, subhedral mineralisation typically interlocking with sphalerite and pyrrhotite. Veins are millimetre-scale and display orthogonal networks with</p>

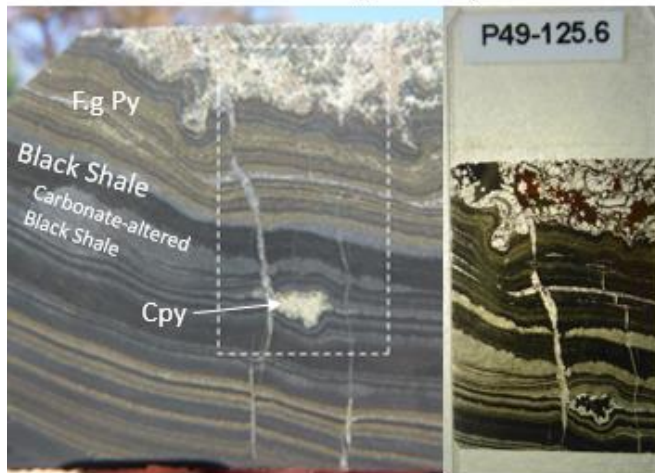
	<p>bedding. Breccia-hosted galena is also fine- to coarse-grained composed of millimetre- to centimetre-scale sub-rounded clasts of mudstone, pyritic siltstone and disseminated sphalerite. Thickness ranges from 2-10cm and remains parallel and concordant with host rock (Chapman, 2004).</p>
--	---

APPENDIX C: LIST OF DRILL HOLES

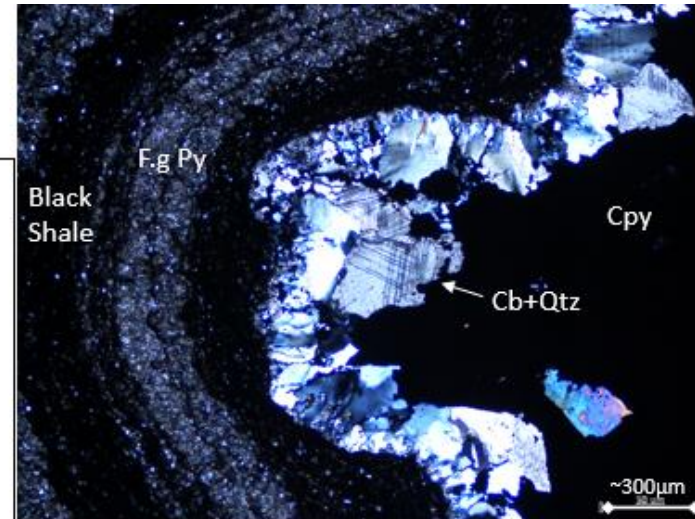
Drillhole List	
Hilton (P49)	George Fisher (L72)
12L_H558_08	201504162
12L_H558_09	16C_I696_04
5L_K579_03	201406212
14L_J558_01	12L_K796_01
14L_J573_03	5L_2685_02
	16C_I692_04

APPENDIX D: SAMPLE DESCRIPTIONS

P49-125.6



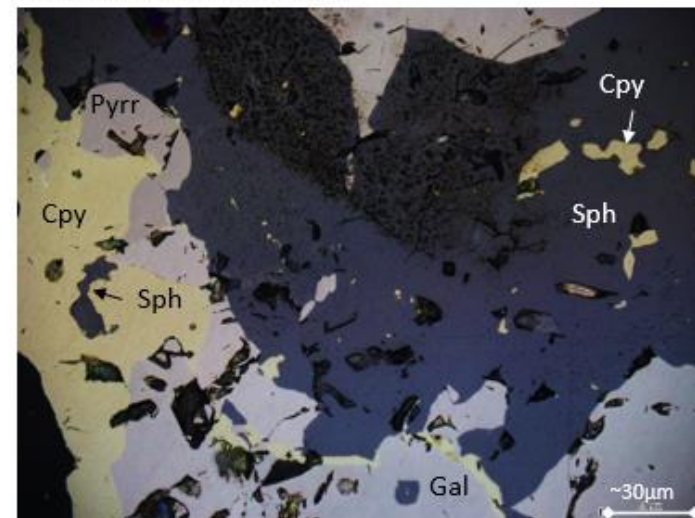
Core Sample:
Heavily interbedded black shale and fine-grained pyrite with carbonate, quartz, chalcopyrite, sphalerite, galena and pyrrhotite. Vein-infill cross-cutting beds undergone folding deformation.



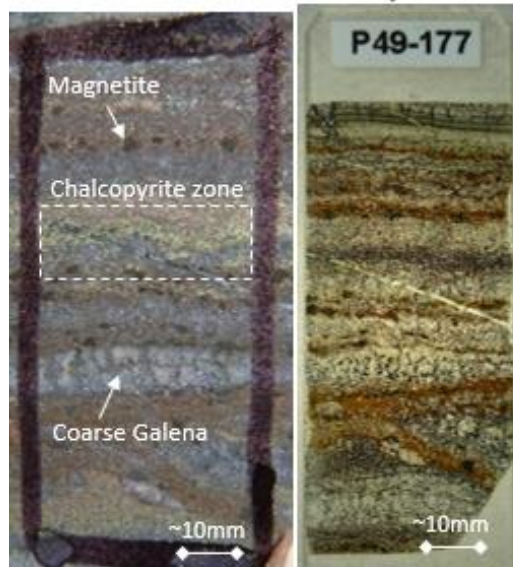
Above: Plain-polarized light image of zonation of chalcopyrite and bedding layers separated by quartz and calcite.

Below: Reflected light image displaying inclusions of chalcopyrite within sphalerite and galena inferring Cu entered the system at the same time as the Pb-Zn ore-forming minerals.

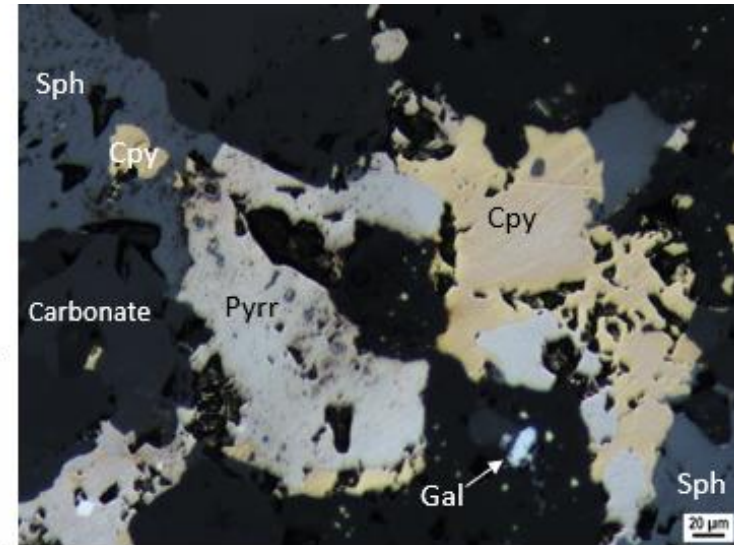
<p>Host Rock: Carbonaceous and slightly folded/deformed rock with cross-cutting vein-infill, carbonate-rich mineralization. Beds deformed around infill chalcopyrite. Entire rock undergone strong carbonate alteration</p>
<p>Veins/infill: Carbonate-rich veins post-date fine-grained pyrite and black shale beds. Composition predominantly chalcopyrite, sphalerite, galena and minor pyrrhotite with quartz and calcite throughout. Carbonate alteration entered the rock with sulphide mineralization.</p>
<p>Modal Proportions: 60% shale, 25% pyrite, 12% carbonate (quartz & calcite), 1.7% chalcopyrite, 0.5% sphalerite, 0.5% galena, 0.3% pyrrhotite</p>
<p>Summary: Interbedded black shale and fine-grained pyrite with abundant carbonate alteration, cross-cutting carbonate-rich veins, chalcopyrite sphalerite, galena and minor pyrrhotite infill.</p>



P49-177



Core Sample: High-grade Pb-Zn ore with significant strata-bound chalcopyrite, pyrrhotite, remnant shale beds and patchy magnetite grains.



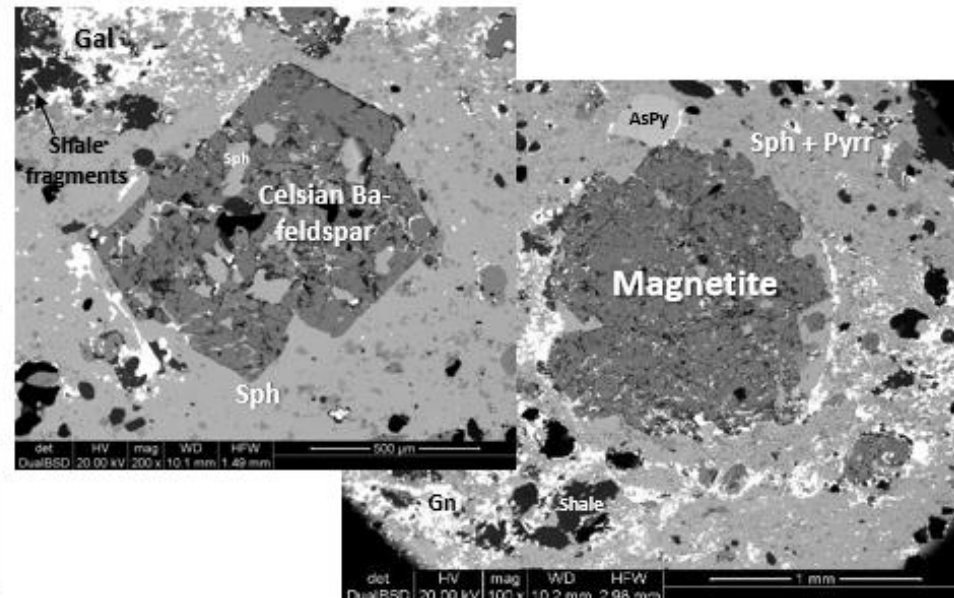
Above: Reflected light image displaying the intergrown nature of chalcopyrite with pyrrhotite and sphalerite implying the same mineralization event.
Below: SEM image of a celsian feldspar (left) and magnetite grain (right) imbedded within a high-grade Cu zone surrounded by sphalerite and pyrrhotite (R. Lilly 2019).

Host Rock: Chalcopyrite hosted within high-grade Pb-Zn ore with remnant shale bed overprinted by coarse galena. Carbonate alteration throughout ore. Chalcopyrite disseminated throughout pyrrhotite, galena and sphalerite. Magnetite and celsian feldspar common in Cu-rich zone.

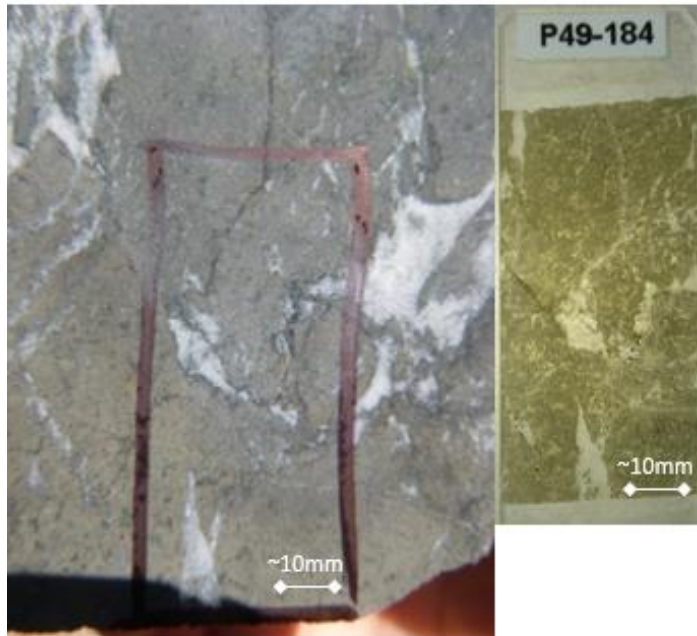
Veins/infill: Late carbonate vein hosting galena cross-cutting strata-bound ore lenses post-dating main ore forming stage, cutting through chalcopyrite zone.

Modal Proportions: 35% sphalerite, 20% galena, 20% remnant shale, 5% pyrrhotite, 4% magnetite, 6% chalcopyrite, 10% carbonate (quartz & calcite)

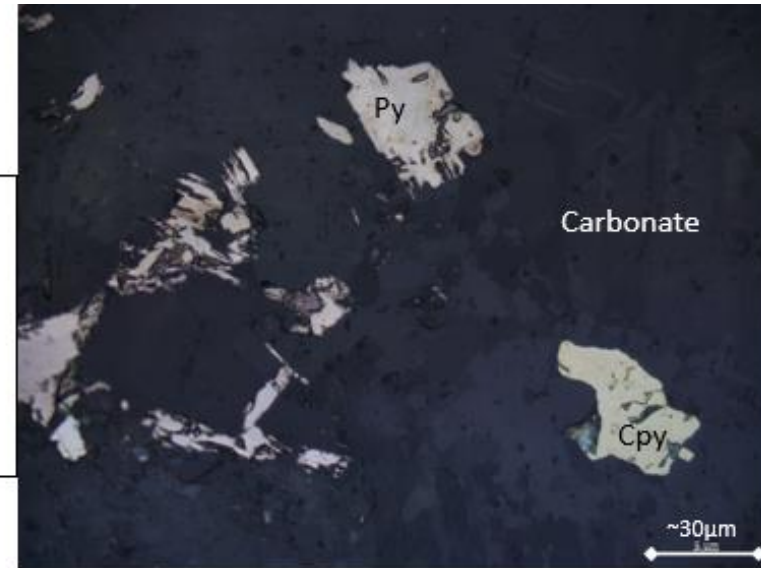
Summary: Massive sphalerite (Zn) and galena (Pb) ore with high-grade chalcopyrite (Cu) throughout. Carbonate vein hosting galena post-dates main ore stage. Chalcopyrite entered system with main ore-forming stage.



P49-184



Core Sample: Very fine-grained rock undergone biotite alteration. Minor patchy mineralization throughout. Riddled with carbonate.



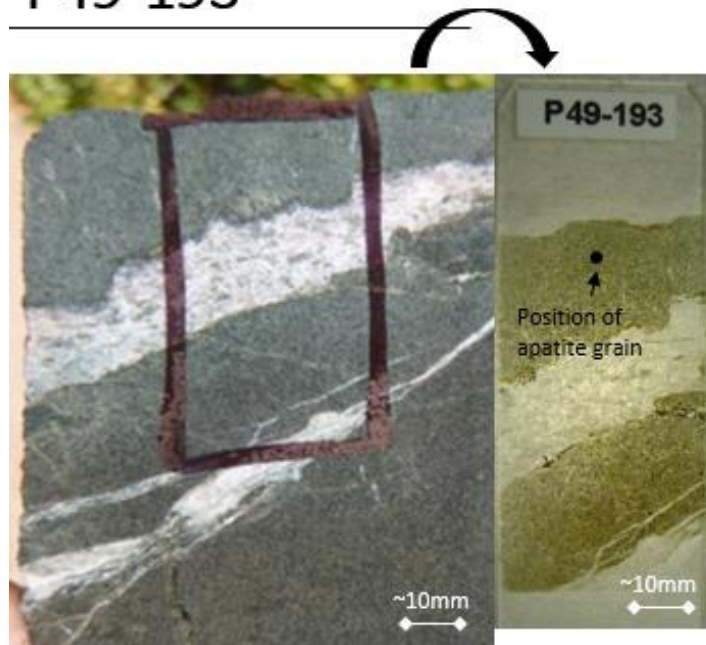
Above: Reflected light image displaying the presence of pyrite and chalcopyrite mineralization within 'dolerite dyke' sample. This infers mineralization stage post-dating 'dolerite dyke' intrusion.

Below: Plain polarized light image displaying massive biotite and carbonate alteration which correlates with Taylor's (2019) paragenetic interpretation.

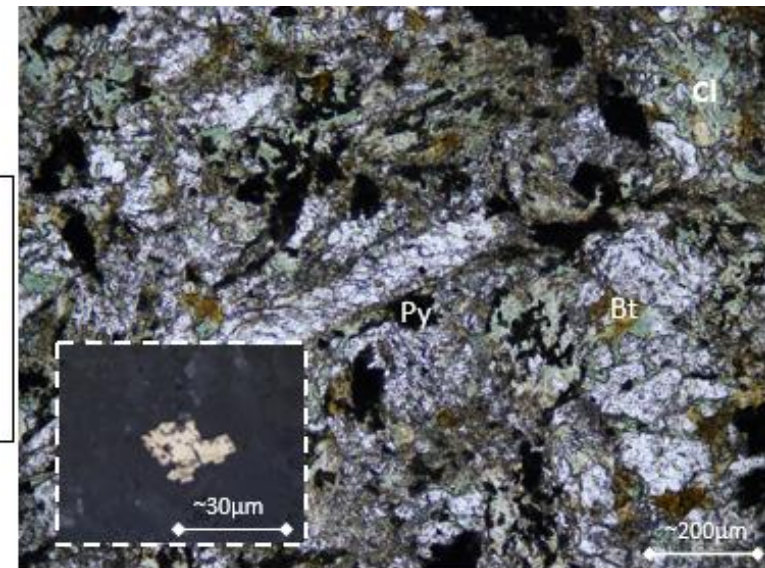


<p>Host Rock: Intensely biotite altered, very fine-grained rock with patchy pyrite and minor chalcopyrite mineralization. Grain structure are NOT preserved inferring heavily deformed nature.</p>
<p>Veins/infill: Carbonate infill of veins due to heavily fractured host rock. Mineralization in veins. Calcite and quartz-rich.</p>
<p>Modal Proportions: 40% carbonate (quartz + calcite), 35% biotite, 15% pyrite, 9% pyrite, 1% chalcopyrite</p>
<p>Summary: So-called 'dolerite dyke' sample experienced intense biotite alteration and hosts pyrite and chalcopyrite mineralization. This infers a mineralization stage post-dating intrusion.</p>

P49-193

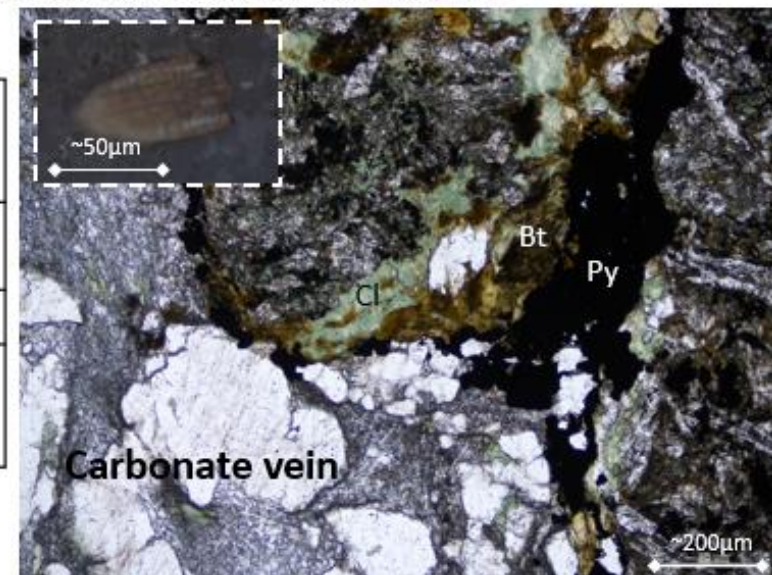


Core Sample: Very fine-grained rock undergone chlorite, biotite and carbonate alteration with a >10mm carbonate vein.

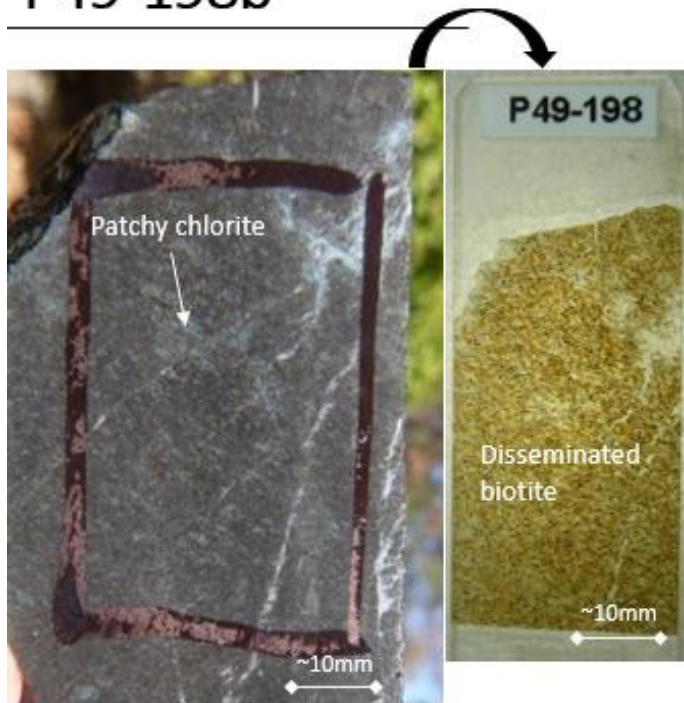


Above: Plain polarized light image displaying rock undergone significant chlorite and biotite alteration with inset reflected light image of patchy pyrite.
Below: Plain polarized light image of the contact between large >10mm carbonate vein and host rock. Chlorite, biotite and pyrite at contact. Inset indicates a possible apatite grain found in host rock.

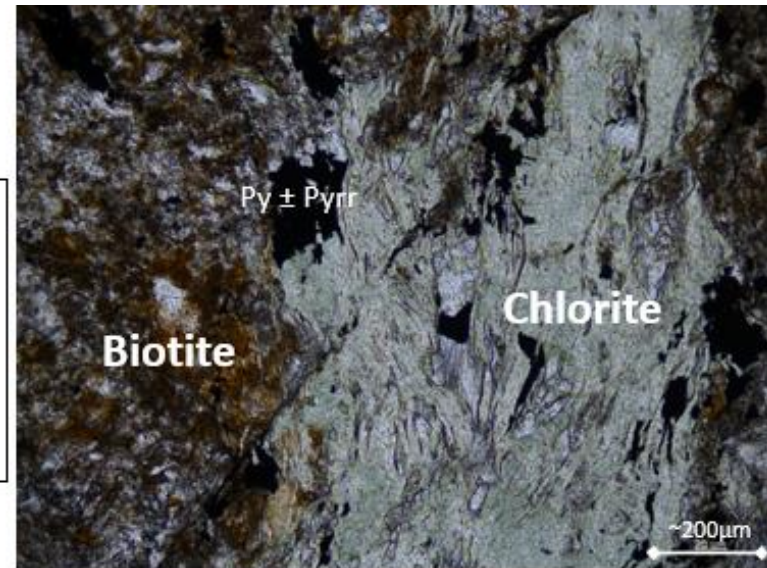
<p>Host Rock: Very fine-grained chlorite, biotite and carbonate altered rock with major carbonate veining (>10mm). Pyrite mineralization disseminated throughout. Fragments of host rock within carbonate vein.</p>
<p>Veins/infill: Carbonate vein (>10mm) with minor mineralization inferring veining post-dates mineralization and alteration of biotite and chlorite.</p>
<p>Modal Proportions: 50% carbonate, 25% chlorite, 15% biotite, 10% pyrite</p>
<p>Summary: Rock undergone massive chlorite, biotite and carbonate alteration and hosts intergrown pyrite mineralization inferring a stage of mineralization post-dating intrusion.</p>



P49-198b



Core Sample: Very fine-grained massively chloritized and undergone significant biotite alteration with patchy mineralization.



Above: Plain polarized light image of both biotite and chlorite alteration within the host rock. Mineralization is not constrained to one alteration event.

Below: Reflected light image of pyrite and pyrrhotite within host rock signifying a mineralization event post-dating intrusion.



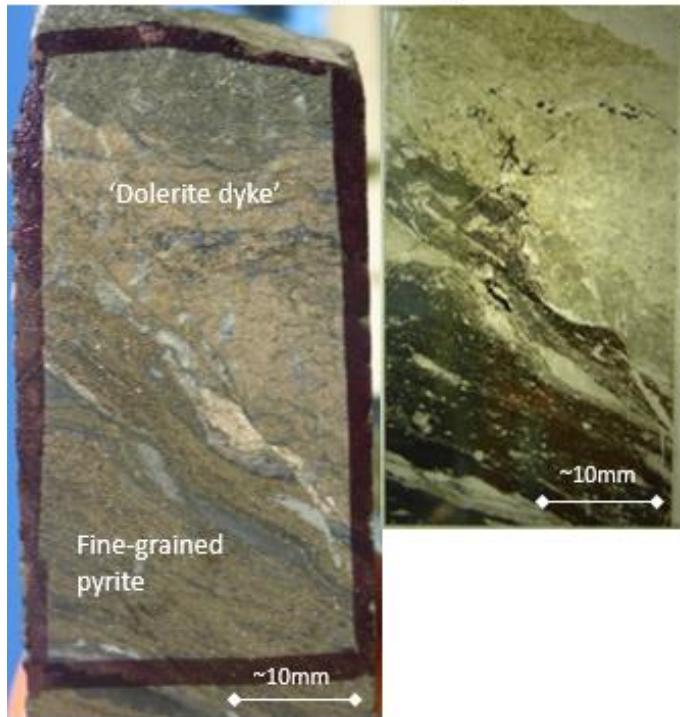
Host Rock: Very fine-grained with minor carbonate veining with significant patchy chlorite and disseminated biotite alteration.

Veins/infill: Carbonate infill throughout biotite and chlorite with patchy pyrite and pyrrhotite mineralization interpreted to post-date intrusion.

Modal Proportions: 40% biotite, 25% chlorite, 30% carbonate (quartz & calcite), 3% pyrite, 2% pyrrhotite

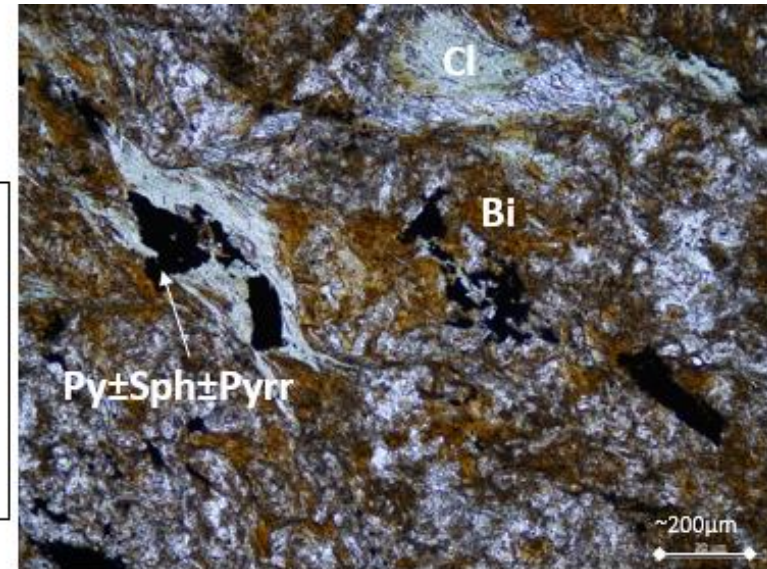
Summary: Very fine-grained rock heavily altered by chlorite and biotite with patchy disseminated pyrite and pyrrhotite mineralization.

P49-198a



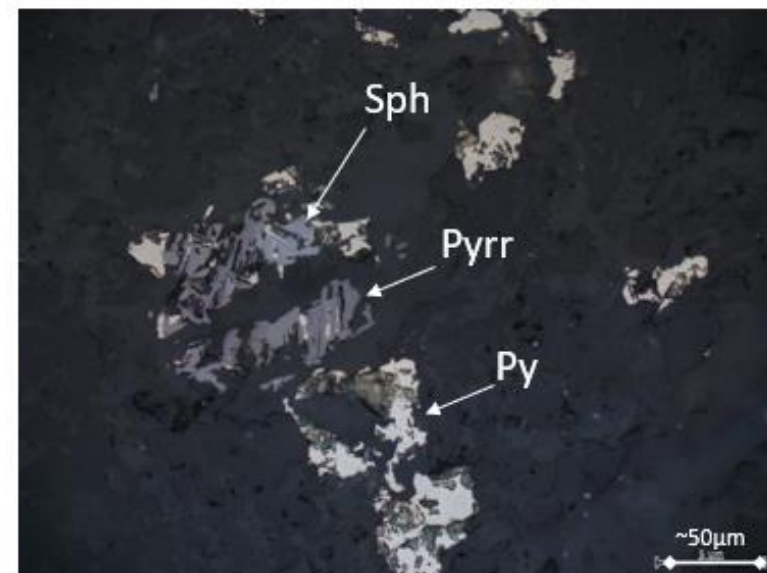
Core Sample: Contact between 'dolerite dyke' and fine-grained pyrite bedding. 'Dolerite dyke' composed of carbonate, biotite, minor chlorite and minor mineralization.

<p>Host Rock: The contact of a 'dolerite dyke' rock with fine-grained pyrite beds. Dominated by biotite and carbonate alteration with minor ore-bearing minerals throughout.</p>
<p>Veins/infill: Sphalerite, pyrrhotite and pyrite infill observed. Carbonate-rich vein infill in 'dolerite dyke' with ~4mm carbonate veining throughout fine-grained pyrite.</p>
<p>Modal Proportions: 40% carbonate (quartz & calcite), 30% biotite, 20% chlorite, 7% pyrite, 2.5% pyrrhotite, 0.5% sphalerite</p>
<p>Summary: Massive biotite and carbonate alteration with patchy chlorite and disseminated sulphide mineralization.</p>

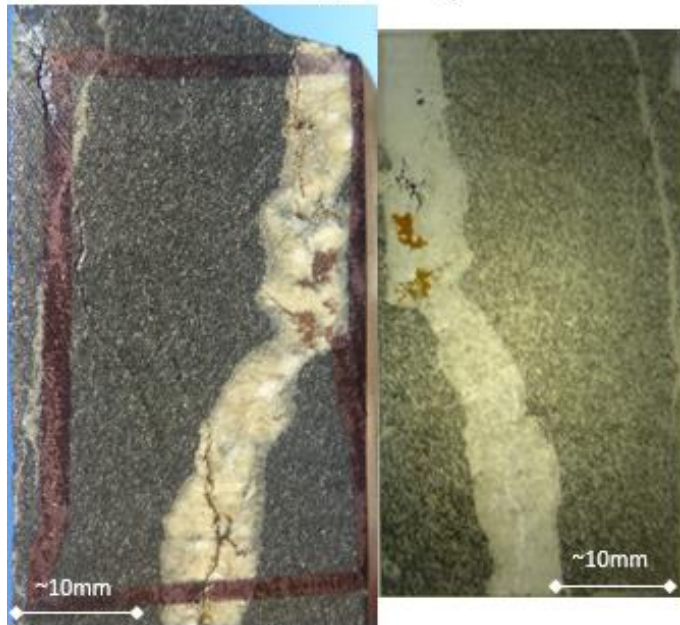


Above: Plain polarized light image displaying massive biotite and carbonate alteration with patchy chlorite and minor sulphide mineralization.

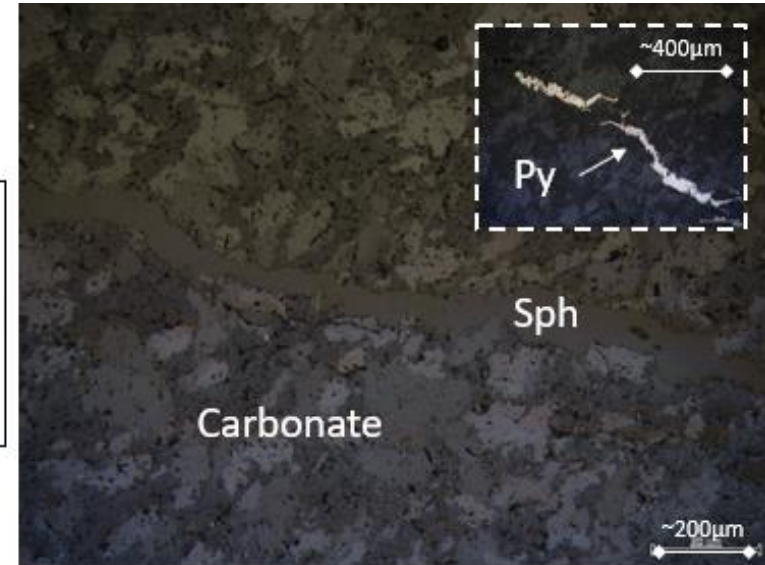
Below: Reflected light image displaying sulphide mineralization post-dating 'dolerite dyke' intrusion. Ore-bearing minerals identified.



P49-151



Core Sample: Fine-grained quartz and calcite-rich rock with a large 8mm carbonate vein throughout, hosting sphalerite and galena.



Above: Reflected light image of sphalerite vein infill post-dating the intrusion of the host rock. Inset displays pyrite vein-infill throughout.

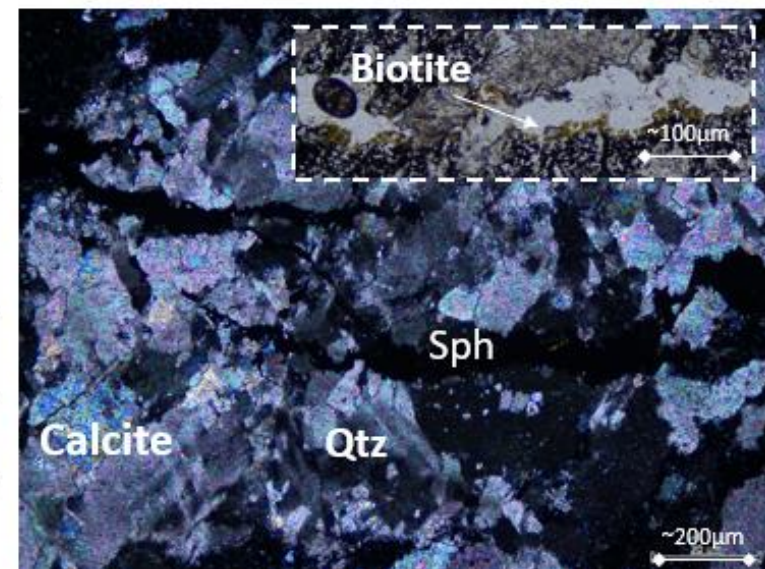
Below: Cross-polarized light image displaying massive calcite and quartz composition with late sulphide veining. The plain polarized inset shows biotite at the edges of carbonate veining inferring initial stages of alteration. Late carbonate veining may be the cause of biotite alteration.

Host Rock: Fine-grained quartz and calcite-rich rock disseminated with a black mineral and minor vein-infill mineralization.

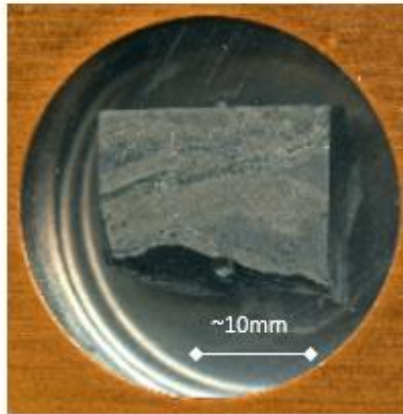
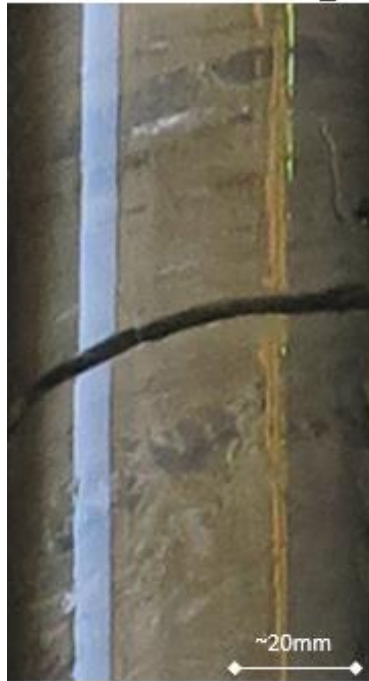
Veins/infill: Large ~8mm carbonate vein infilled with sphalerite and minor galena post-dating intrusion of host rock. Minor vein-infill of sphalerite and pyrite observed within host rock.

Modal Proportions: 45% quartz, 40% calcite, 13% black mineral, 1% sphalerite, 0.5% pyrite, 0.5% biotite

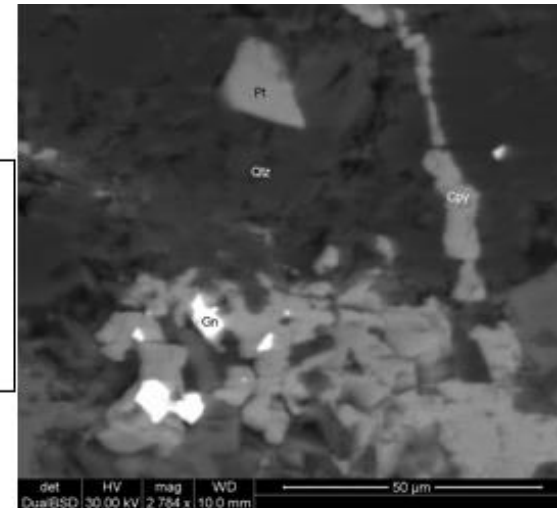
Summary: Fine-grained quartz and calcite-rich rock hosting carbonate and sulphide veining with trace biotite.



P49-17.4



Core Sample: Massive fine-grained pyrite beds with minor black shale fragments and associated chalcopyrite mineralization.



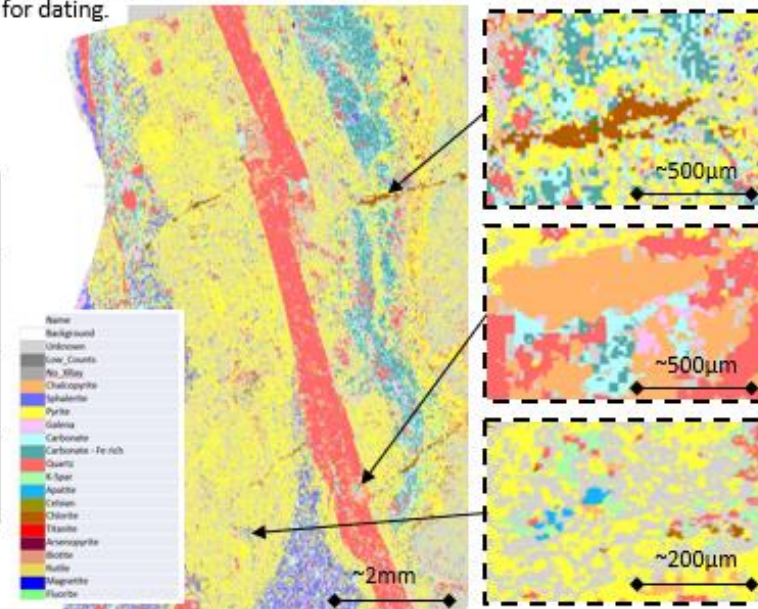
Above: An SEM image displaying the presence of a Pt-Pd-rich mineral nearby vein-infill chalcopyrite and galena mineralization.
Below: MLA map of sample displaying chalcopyrite mineralization within a remnant strata-bound black shale bed. Top inset displays late chlorite vein-infill crosscutting carbonate and fine-grained pyrite. Middle inset displays intergrown galena and chalcopyrite inferring the same mineralization stage. Bottom inset displays apatite possible for dating.

Host Rock: Fine-grained pyrite beds with remnant black shale beds with lenses of carbonate and minor disseminated carbonate alteration.

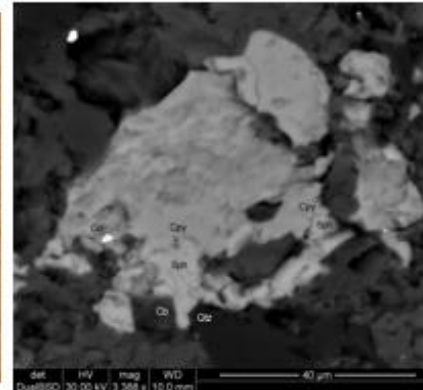
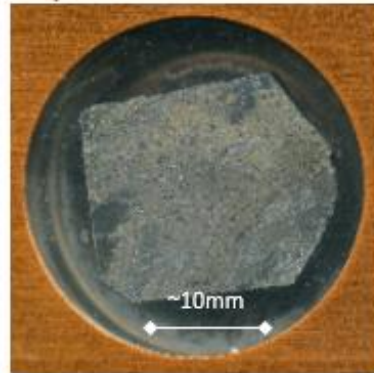
Veins/infill: Remnant black shale bed contains chalcopyrite and galena infill. Late chlorite vein-infill cross-cutting carbonate and fine-grained pyrite.

Modal Proportions: 70% pyrite, 15% black shale, 12.5% carbonate, 1% chlorite, 1% chalcopyrite, 0.5% galena

Summary: Massive fine-grained pyrite with remnant black shale hosting chalcopyrite and galena mineralization



P49-154.3



Above: An SEM image displaying intergrown sphalerite, galena and chalcopyrite inferring the same mineralization event.

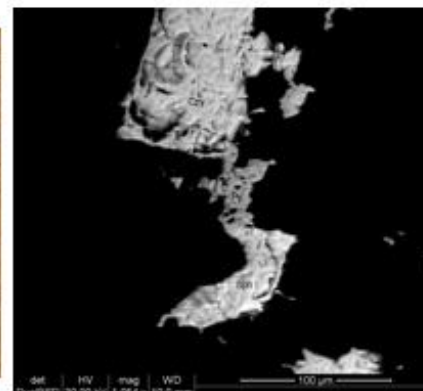
Host Rock: Massive sphalerite and galena ore disseminated by black shale fragments.

Veins/infill: Disseminated chalcopyrite throughout sphalerite and galena ore.

Modal Proportions: 65% sphalerite, 15% black shale, 15% galena, 5% chalcopyrite

Summary: Massive sphalerite and galena ore with high-grade zone of chalcopyrite.

P49-213.7



Above: An SEM image displaying chalcopyrite, pyrite and sphalerite as the same mineralization event.

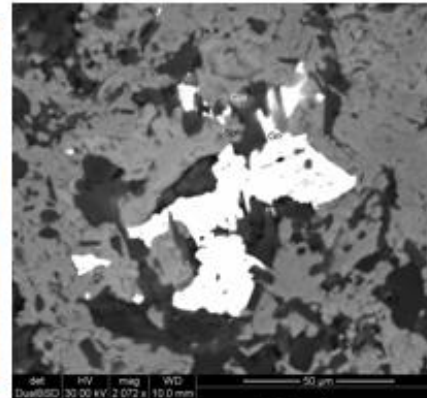
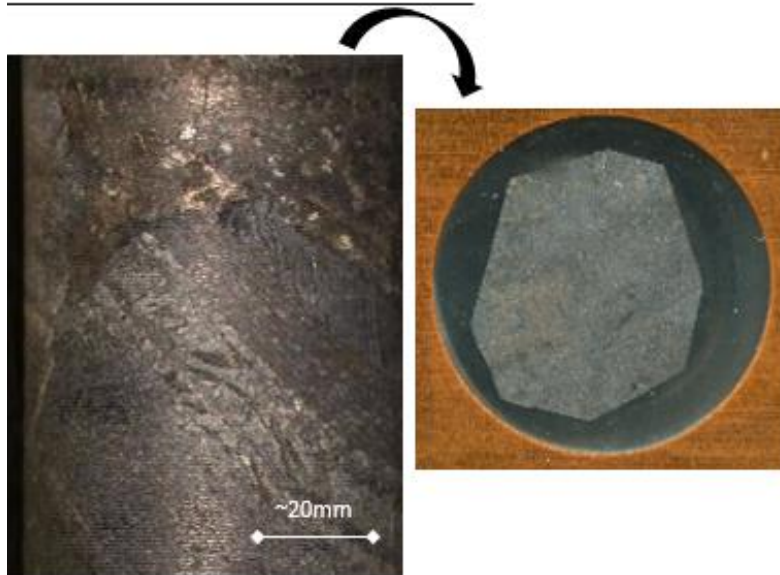
Host Rock: Black shale fragments with carbonate veining.

Veins/infill: Carbonate veining hosts vein-infill chalcopyrite and surrounding black shale fragments carbonate altered sphalerite, pyrite and chalcopyrite

Modal Proportions: 65% black shale, 25% carbonate, 5% chalcopyrite, 4% sphalerite, 0.5% pyrite, 0.5% galena.

Summary: Carbonate veining throughout black shale infilled with chalcopyrite, sphalerite and minor pyrite.

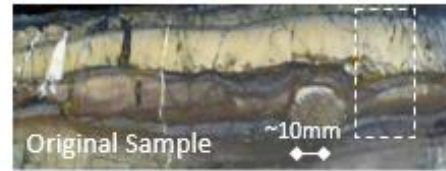
P49-194.2



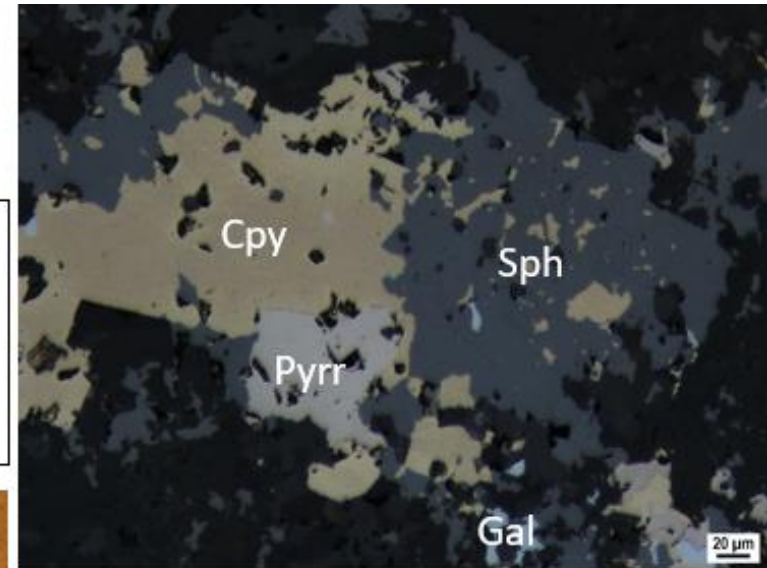
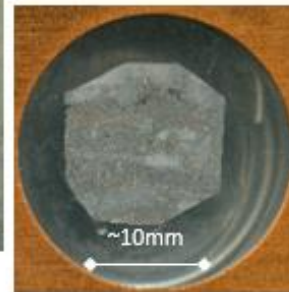
Above: An SEM image displaying intergrown galena, sphalerite and chalcopyrite inferring a single stage of mineralization.

Host Rock: Massive sphalerite and patchy galena with minor fragments of black shale and carbonate.
Veins/infill: Disseminated chalcopyrite throughout sphalerite and galena ore.
Modal Proportions: 45% sphalerite, 5% black shale, 35% carbonate 10% galena, 5% chalcopyrite
Summary: Massive sphalerite and galena ore with disseminated chalcopyrite.

L72-149

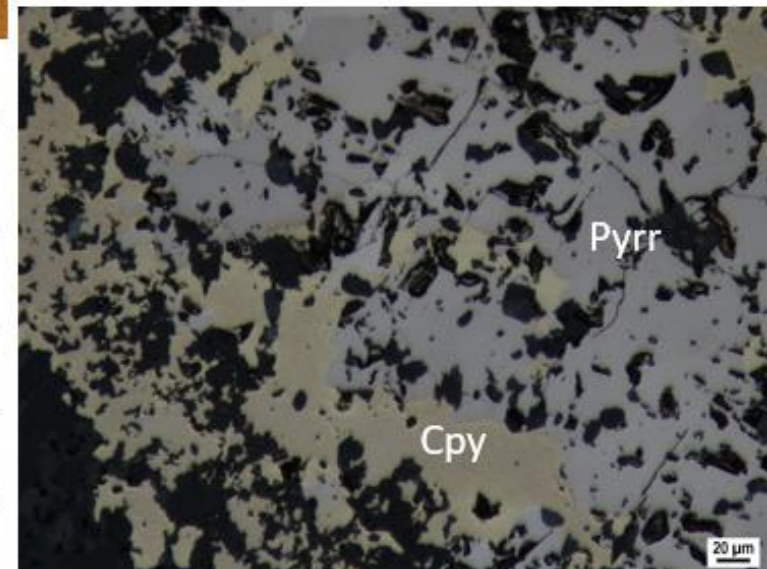


Core Sample: High-grade Zn ore with remnant beds of shale and a heavily 'buff' altered shale bed with chalcopyrite vein-infill.



Above: Reflected light image of the intergrown nature of chalcopyrite with Zn ore-bearing mineral (sphalerite) inferring a congruent stage of mineralization.

Below: Reflected light image displaying the association of chalcopyrite and pyrrhotite inferring mineralization during the same event.



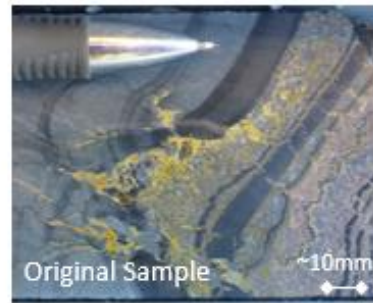
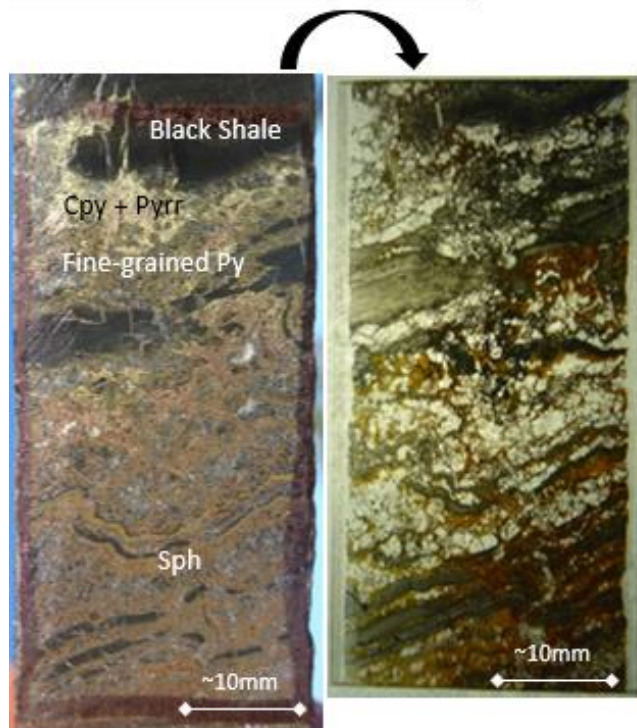
Host Rock: Heavily 'buff' altered shale bed overlying high-grade sphalerite with remnant shale beds. Carbonate alteration throughout sphalerite and pyrrhotite.

Veins/infill: Chalcopyrite disseminated in high-grade Zn ore and infill within altered shale bed. Minor carbonate veining.

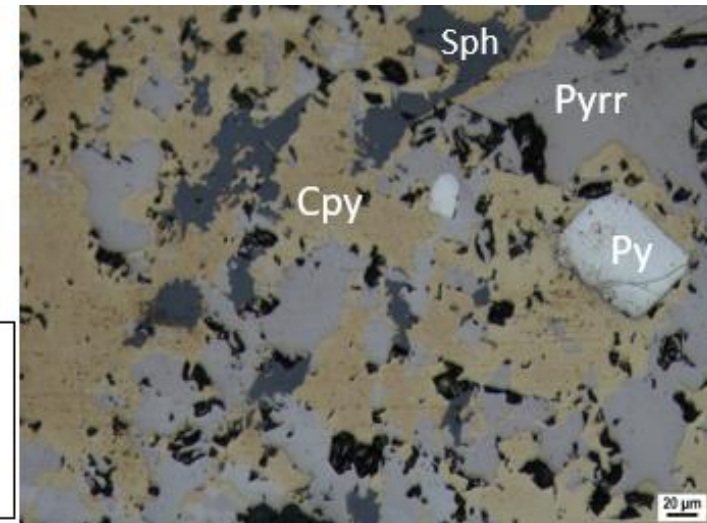
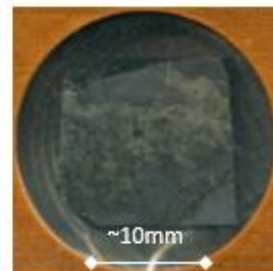
Modal Proportions: 70% shale remnants, 20% carbonate, 6% sphalerite, 2% pyrrhotite, 1.5% chalcopyrite, 0.5% galena

Summary: Heavily 'buff' altered shale bed within a high-grade Zn ore zone with remnant shale fragments, chalcopyrite, pyrrhotite and minor galena.

L72-201.4

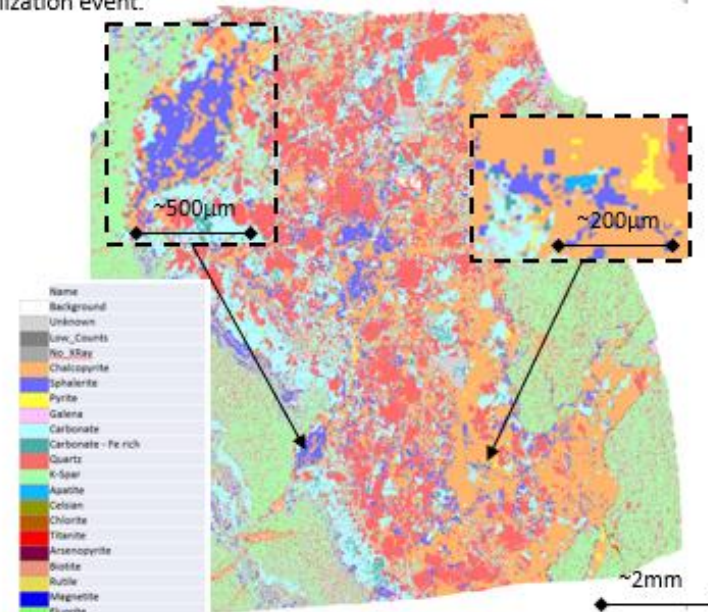


Core Sample: Heavily deformed and brecciated black shale beds overprinted by Zn ore and fine-grained pyrite with trace chalcopyrite.



Above: Reflected light image displaying pyrite pre-dating the single stage of chalcopyrite, pyrrhotite and sphalerite mineralization.

Below: MLA map displaying chalcopyrite distribution associated with sphalerite, pyrite and carbonate. Right inset identifies dateable apatite. Left inset display intergrown sphalerite and chalcopyrite indicating the same mineralization event.



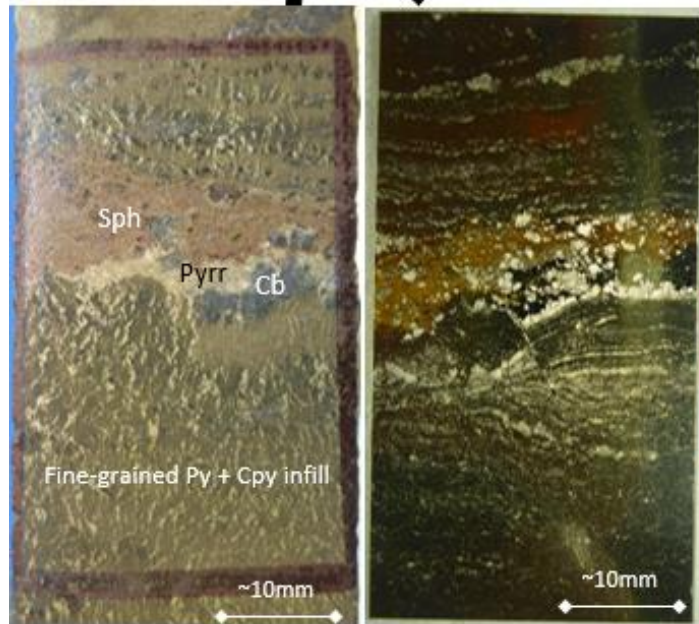
Host Rock: Black shale beds undergone little alteration but fragmented and brecciated by sphalerite, fine grained pyrite and carbonate. Host rock undergone significant deformation.

Veins/infill: Chalcopyrite, pyrrhotite and sphalerite vein infill within black shale fragments with significant carbonate alteration.

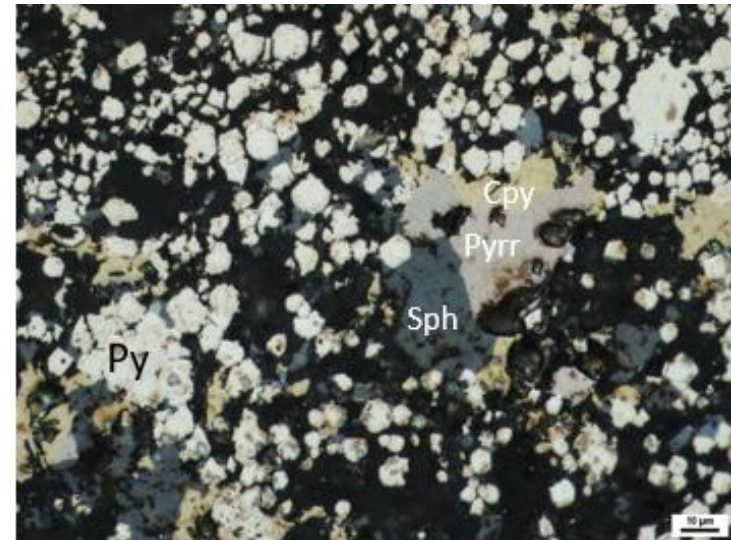
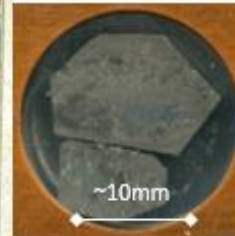
Modal Proportions: 30% black shale fragments, 35% carbonate, 15% pyrite (fine-grained & crystalline), 15% sphalerite, 2.5% pyrrhotite, 1% chalcopyrite, 0.5% galena.

Summary: Brecciated and fragmented black shale rock interbedded with fine-grained pyrite and sphalerite ore that has undergone deformation by the introduction of carbonate, pyrrhotite and another sphalerite stage.

L72-230.3

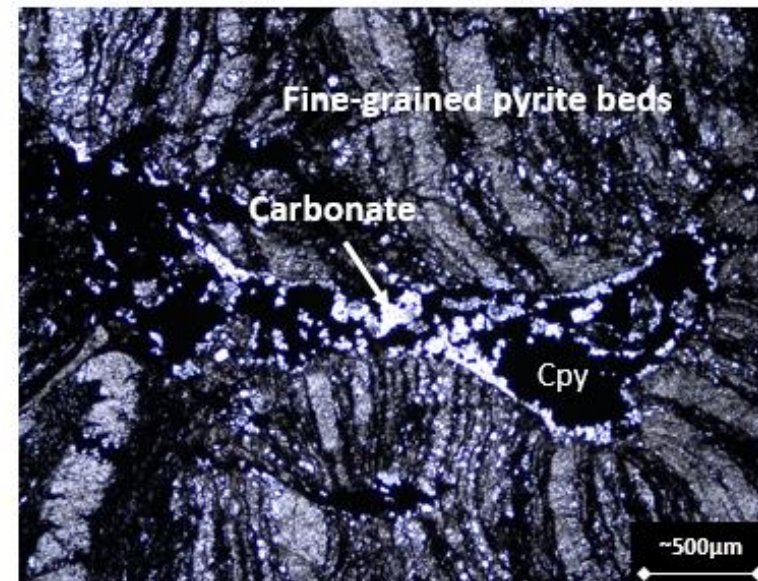


Core Sample: Fine-grained pyrite disseminated with chalcopyrite with lens of sphalerite.



Above: Reflected light image intergrown sulphide mineralization disseminated throughout fine-grained pyrite inferring a single mineralization event.

Below: Plain polarized light image displaying cross-cutting of carbonate vein hosting chalcopyrite mineralization. Fine-grained pyrite beds are slightly deformed inferring chalcopyrite vein-infill post-dates pyrite bedding.



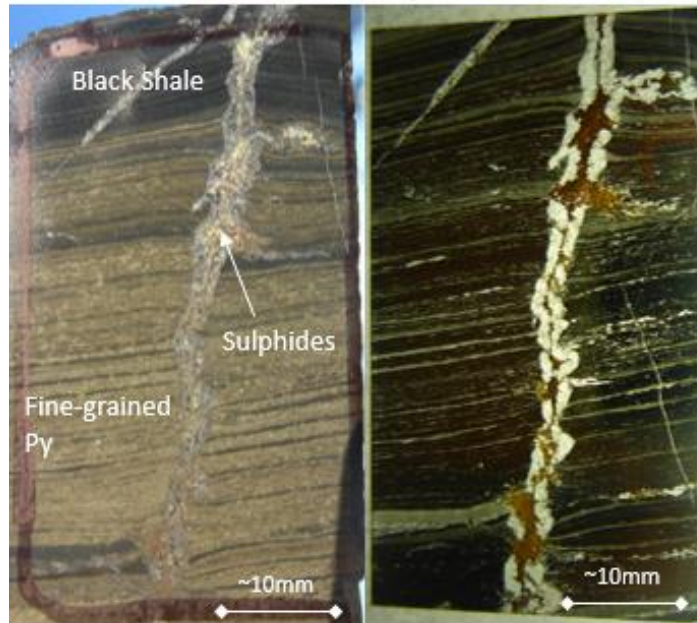
Host Rock: Massive fine-grained pyrite riddled with carbonate and vein-fill chalcopyrite with patchy disseminated black shale. Bedding of fine-grained pyrite indistinguishable.

Veins/infill: Predominantly chalcopyrite vein-infill throughout fine-grained pyrite. Possible large scale (>2cm) vein-infill of an ore lens composed of sphalerite and pyrrhotite.

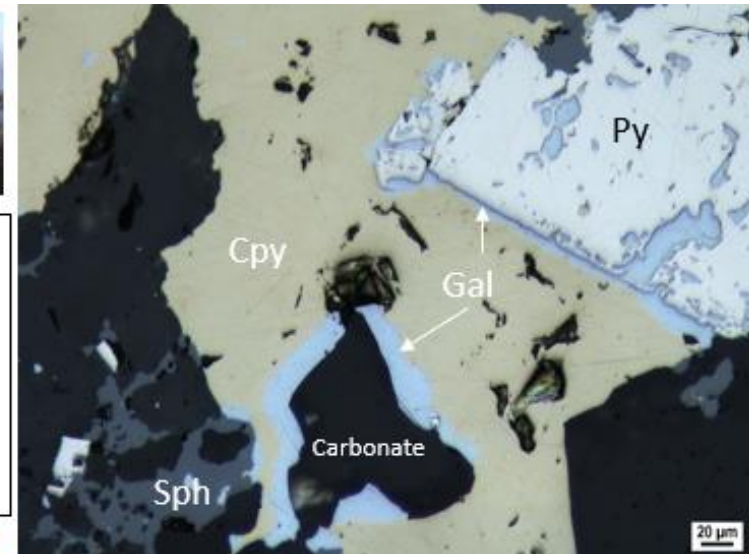
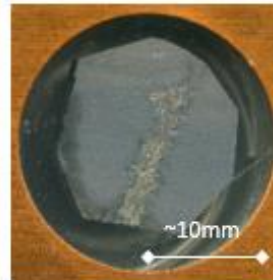
Modal Proportions: 50% pyrite, 30% carbonate, 10% sphalerite, 5% chalcopyrite, 4% pyrrhotite, 1% black shale

Summary: Massive fine-grained pyrite bedding overprinted by carbonate and chalcopyrite mineralization with a lens of sphalerite ore.

L72-264

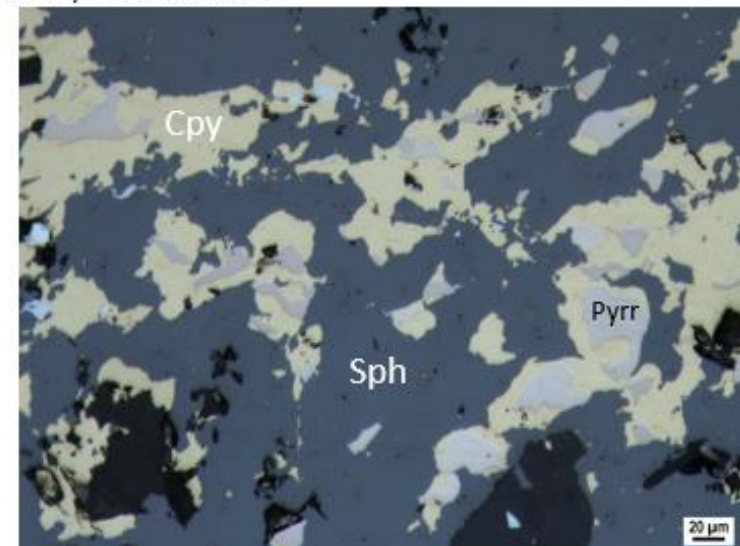


Core Sample:
Massively interbedded fine-grained pyrite and black shale with late carbonate vein hosting sulphide mineralization.



Above: Reflected light image displaying zoning of galena around carbonate, pyrite and sphalerite mineralization inferring they are associated with the same mineralization event with post-mineralization of chalcopyrite.

Below: Reflected light image displaying intergrown pyrrhotite and chalcopyrite throughout sphalerite inferring mineralization during the same hydrothermal event.



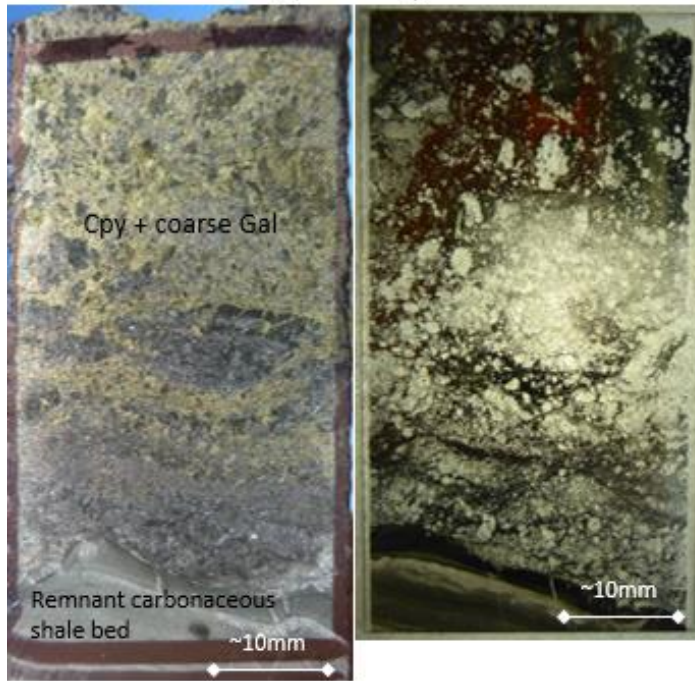
Host Rock: Interbedded black shale and fine-grained pyrite beds. Some black shale beds are carbonaceous (lighter grey).

Veins/infill: 2-5mm carbonate vein cross-cutting beds of host lithology with remnant vein material splaying onto bedding layers. Carbonate vein hosts sphalerite, chalcopyrite, pyrrhotite, galena and crystalline pyrite.

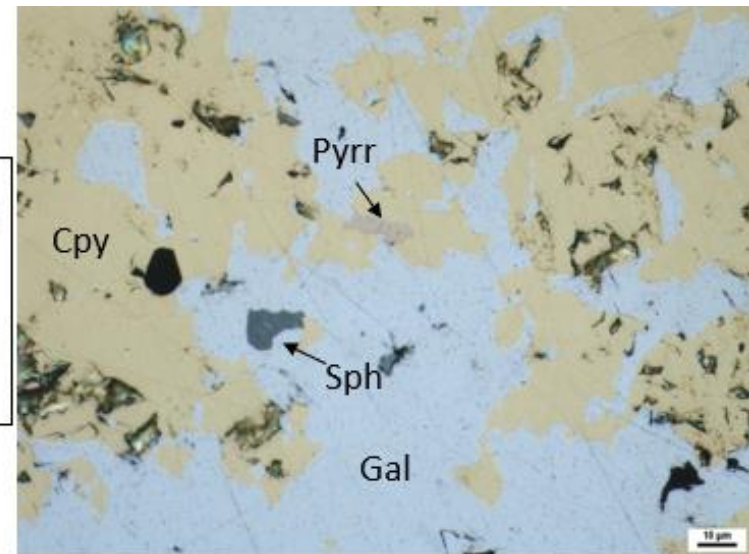
Modal Proportions: 65% pyrite, 25% black shale, 8% carbonate, 0.5% sphalerite, 1% chalcopyrite, 0.5% galena

Summary: Interbedded fine-grained pyrite and black shale with late stage carbonate veining hosting main ore-stage sulphide mineralization and associated with chalcopyrite.

L72-395.8

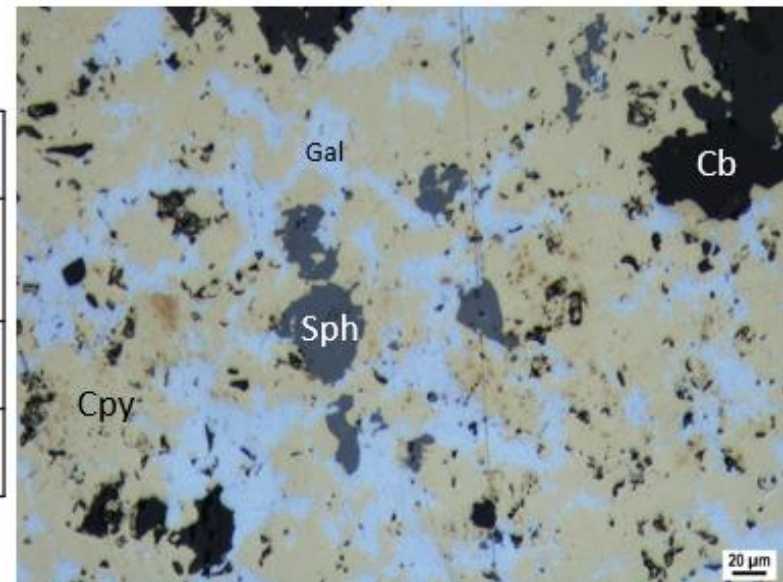


Core Sample:
Massive disseminated chalcopyrite through high-grade Pb ore neighbouring a carbonaceous shale bed.



Above: Reflected light image displaying disseminated chalcopyrite and minor associated pyrrhotite within a high-grade galena ore zone implying they were introduced during the same event.

Below: Reflected light image displaying patchy sphalerite throughout chalcopyrite and galena ore implying the same mineralization event.



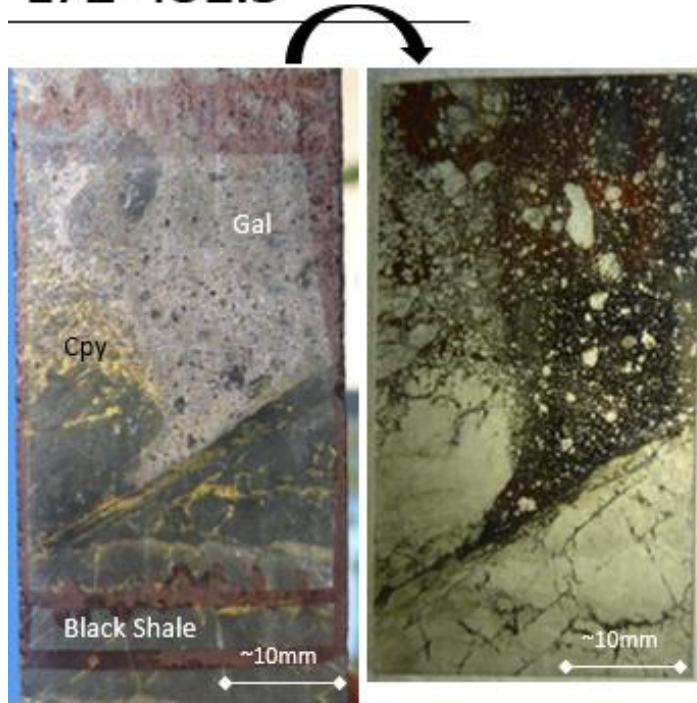
Host Rock: Carbonaceous shales beds with remnant black shale fragments disseminated throughout high Pb ore zone.

Veins/infill: Heavily deformed and brecciated black shale has been overridden by coarse galena and high-grade chalcopyrite mineralization. Carbonate veining observed near remnant shale bed.

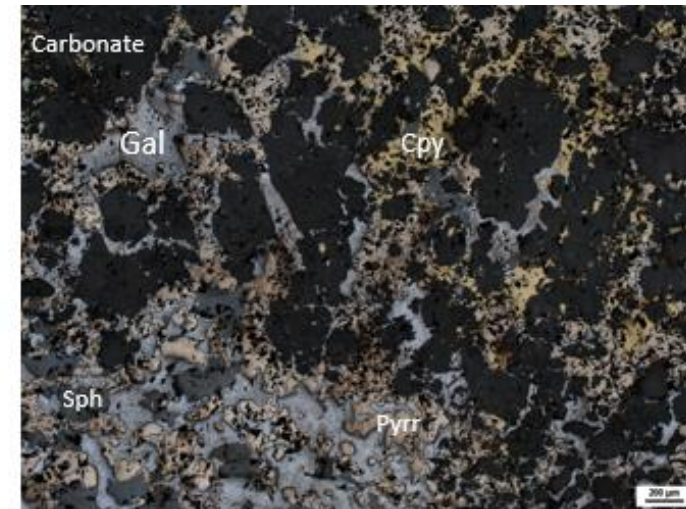
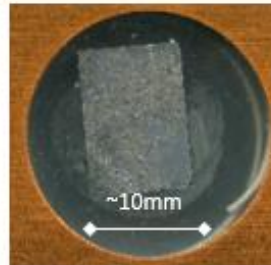
Modal Proportions: 35% chalcopyrite, 37.5% galena, 15% shale, 3% sphalerite, 10% carbonate, 0.5% pyrrhotite

Summary: Massive chalcopyrite and coarse galena zone overprinting remnant shale with minor sphalerite and pyrrhotite.

L72-431.5

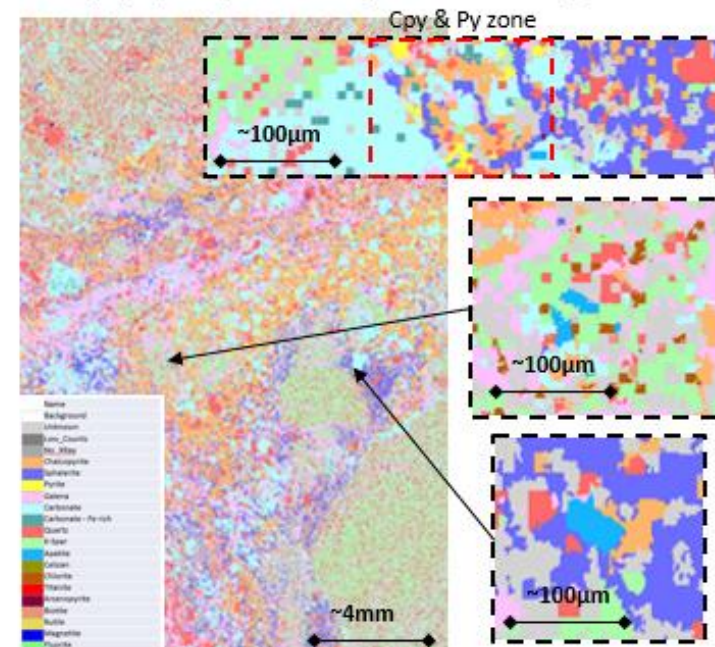


Core Sample:
Massive coarse Pb ore in contact with black shale hosting vein-infill chalcopyrite



Above: Reflected light image of later stage chalcopyrite and pyrrhotite inferred to be overprinting galena and sphalerite.

Below: MLA map displaying distribution of chalcopyrite and associated minerals. Top inset indicates association between pyrite and chalcopyrite. Middle inset displays apatite presence in galena-rich zone. Bottom inset displays apatite presence in sphalerite and chalcopyrite-rich zone.



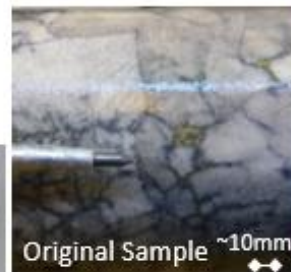
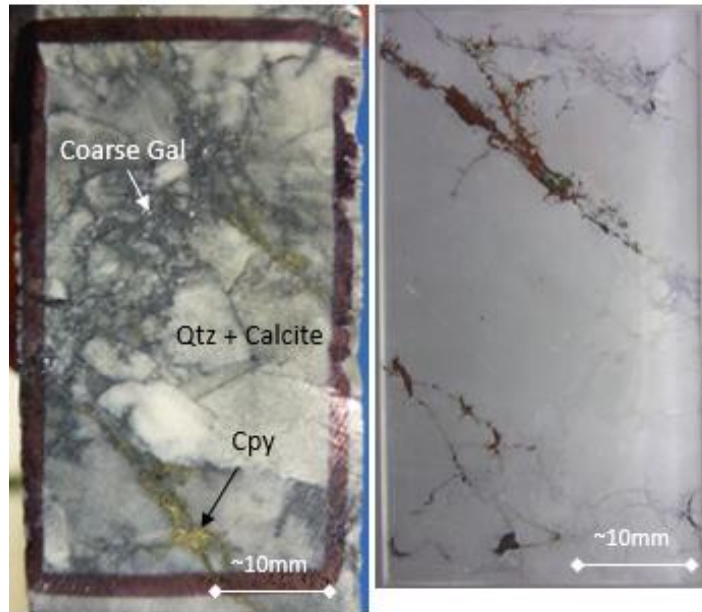
Host Rock: Black shale with coarse galena ore zone disseminated by black shale fragments. From MLA, black shale dominantly composed of quartz and K-feldspar. Black shale has deformed by galena and chalcopyrite-rich hydrothermal fluid.

Veins/infill: Chalcopyrite infill throughout black shale and coarse galena ore. Under microscope, associated sulphides include pyrrhotite and sphalerite.

Modal Proportions: 45% black shale, 35% galena, 5% chalcopyrite, 3% pyrrhotite, 2% sphalerite, 10% carbonate

Summary: Deformed black shale neighbouring high-grade Pb ore with vein-infill chalcopyrite throughout shale and disseminated chalcopyrite throughout galena ore.

L72-293.5



Core Sample: Very coarse quartz and calcite zone within vein-infill of coarse Pb ore and chalcopyrite.



Above: Cross-polarized light image displaying remnant fragments of host rock calcite and quartz within sulphide mineralization inferring a hydrothermal event post-dating calcite and quartz.

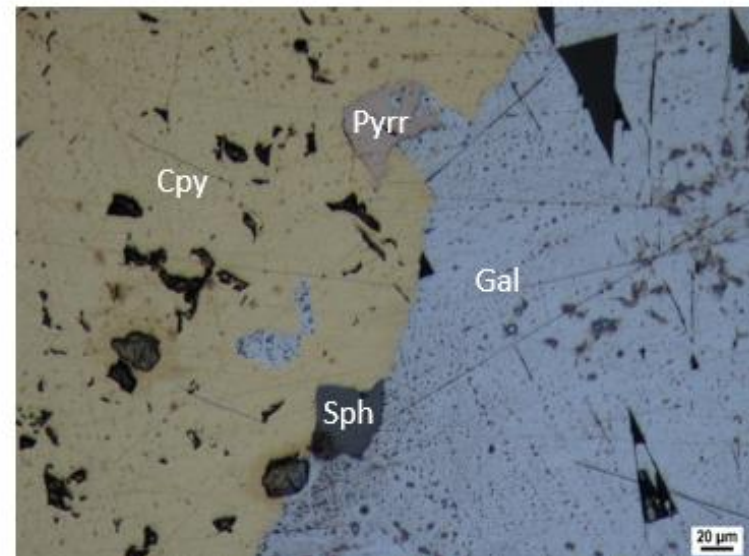
Below: Reflected light image displaying contact between chalcopyrite and galena with intergrown sphalerite and pyrrhotite inferring a single hydrothermal event or remobilization of a nearby sphalerite and pyrrhotite-rich zone.

Host Rock: Coarse crystalline calcite and quartz (2mm to 12mm) interlocking grains.

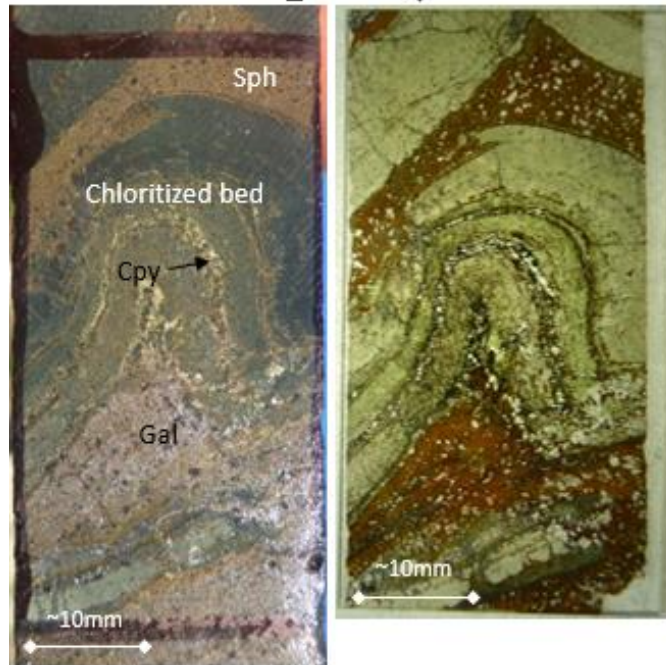
Veins/infill: Dominant chalcopyrite and coarse galena infill with minor sphalerite and pyrrhotite. Vein-infill of sulphides post-dates crystallization of calcite and quartz. Remnant calcite and quartz found within sulphide infill.

Modal Proportions: 45% calcite, 45% quartz, 7% galena, 2% chalcopyrite, 0.5% sphalerite, 0.5% pyrrhotite

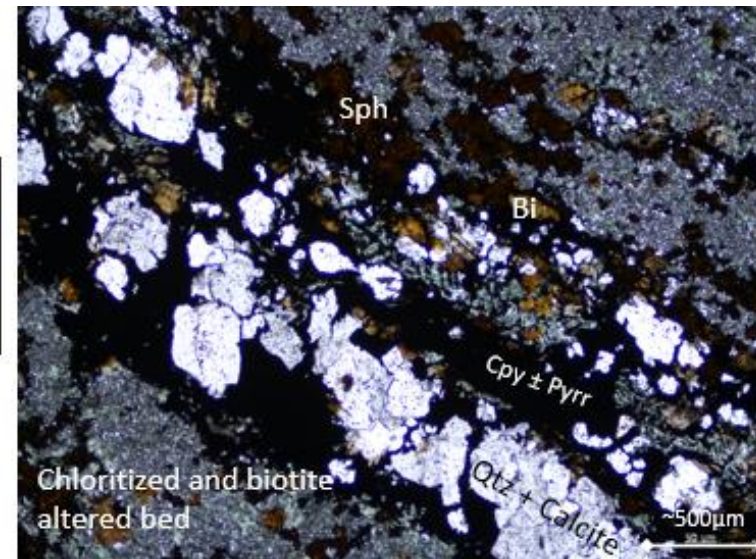
Summary: Coarse quartz and calcite with late stage galena and chalcopyrite, minor sphalerite and pyrrhotite infill.



L72-456.6



Core Sample:
Chloritized shale beds
within high-grade Pb
and Zn ore with strata-
bound chalcopyrite



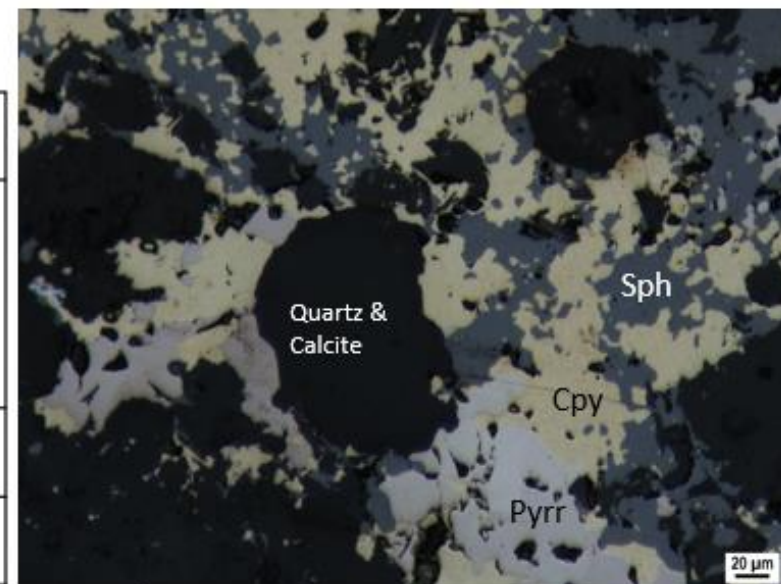
Above: Plain polarized light image of sulphide mineralization and carbonate between chloritized shale beds. Due to the presence of carbonate, sulphide mineralization could be considered vein-infill style.
Below: Reflected light image of intergrown sphalerite, chalcopyrite and pyrrhotite implying a single hydrothermal event.

Host Rock: Remnant chlorite and biotite altered shale bedding with high-grade Pb and Zn ore.

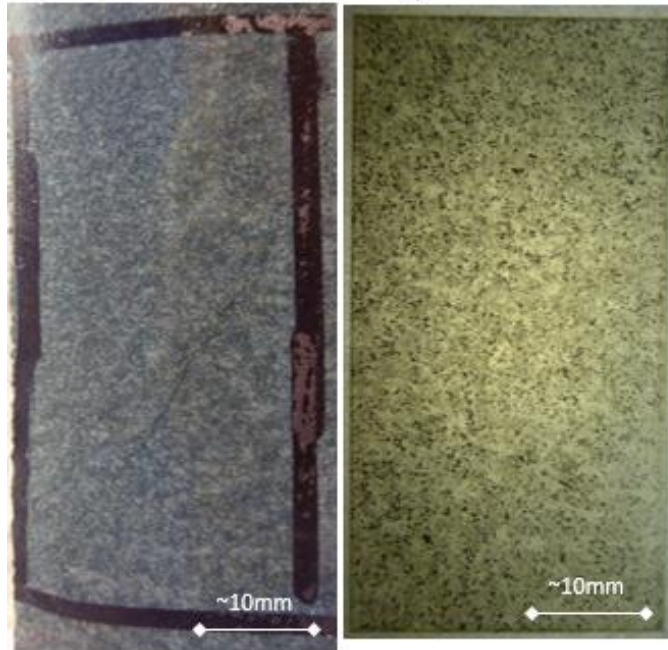
Veins/infill: Chalcopyrite observed between altered shale beds also hosts carbonate, sphalerite and pyrrhotite. Vein-infill between altered shale beds infers one hydrothermal event with a second hydrothermal event of sphalerite and galena. Hydrothermal event carrying chalcopyrite, pyrrhotite and sphalerite -> deformation of altered shale beds -> Second hydrothermal event of galena and perhaps a 2nd sphalerite.

Modal Proportions: 40% altered shale, 25% galena, 25% sphalerite, 8% carbonate, 1.5% chalcopyrite, 0.5% pyrrhotite

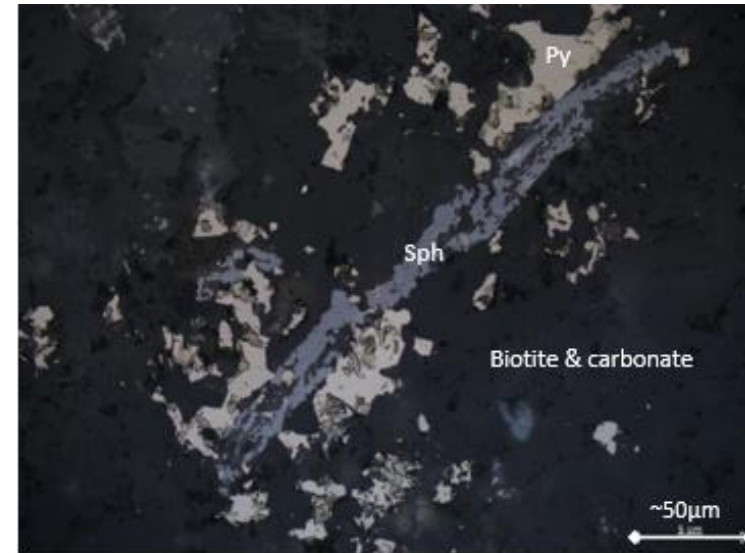
Summary: Heavily altered and deformed shale bed hosting vein-infill sulphides within high-grade sphalerite and galena ore.



L72-95.6

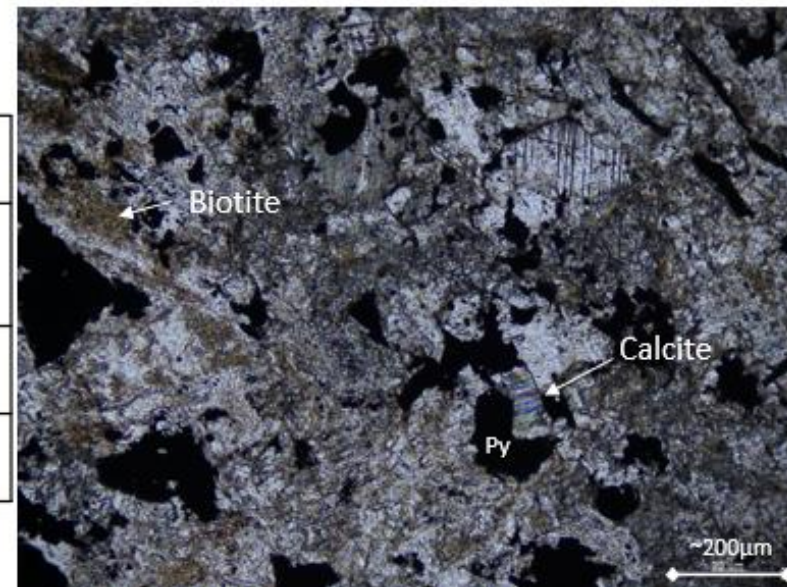


Core Sample:
Homogenous textured quartz and calcite rich rock with disseminated sulphide mineralization and minor biotite.



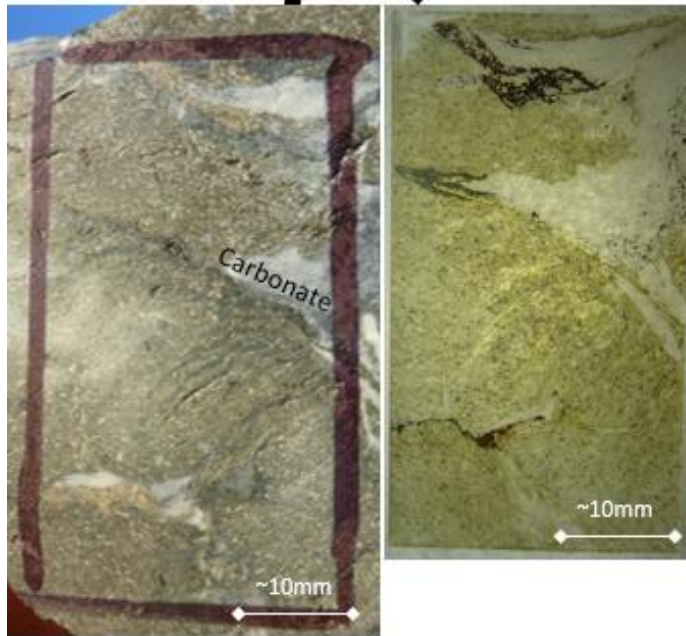
Above: Reflected light image of pyrite and sphalerite vein-infill inferring a stage of sulphide mineralization post-dating dolerite dyke intrusion.

Below: Plain polarized light image displaying minor biotite alteration which is representative across most dolerite dyke samples.

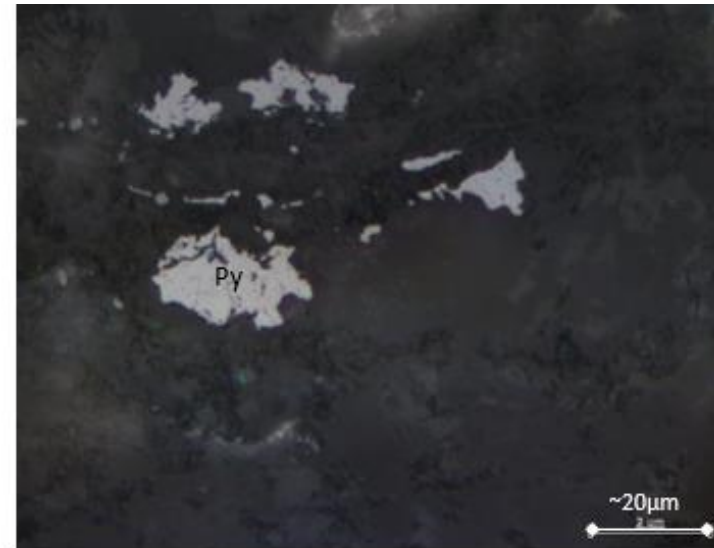


Host Rock: Mineralogy difficult to identify due to its fine-grained texture however contains crystalline calcite and minor biotite alteration.
Veins/infill: Pyrite and sphalerite mineralization observed throughout indicating a stage of ore-bearing mineralization post-dating dolerite dyke intrusion.
Modal Proportions: 45% quartz, 40% calcite, 3% biotite, 10% pyrite, 2% sphalerite
Summary: Quartz and calcite-rich rock with minor biotite alteration, disseminated pyrite and minor sphalerite mineralization.

L72-132.5

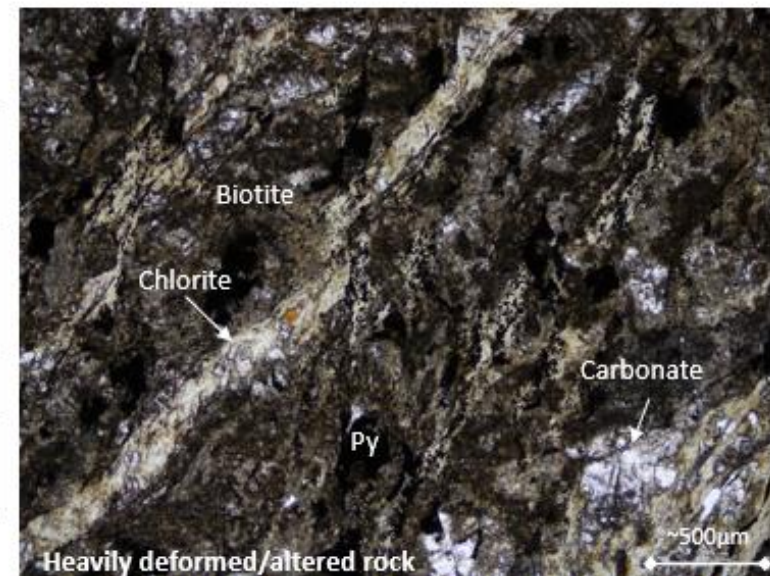


Core Sample: Heavily altered, very fine-grained rock with carbonate veining and patchy sulphide mineralization.



Above: Reflected light image of pyrite disseminated throughout the host rock inferring a stage of mineralization that post-dates dolerite dyke intrusion.

Below: Plain polarized light image of the heavily biotite altered host rock riddled with chlorite veining and carbonate.



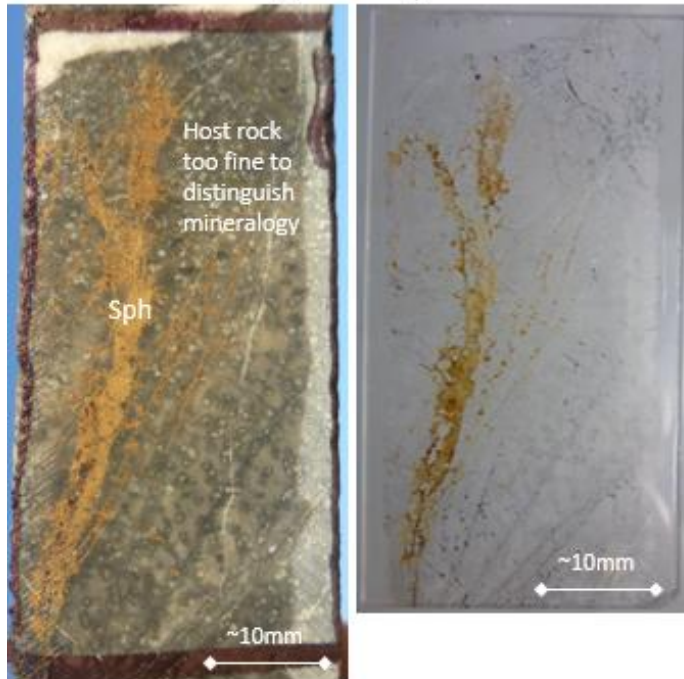
Host Rock: Biotite, chlorite and carbonate altered rock with primary mineralogy difficult to identify due to its fine-grained nature and intense alteration.

Veins/infill: Crystalline pyrite mineralization observed at the contact between carbonate veining and host rock with patchy disseminated pyrite throughout host rock. Sample dominated by carbonate and chlorite infill.

Modal Proportions: 40% carbonate, 35% biotite, 20% chlorite, 5% pyrite

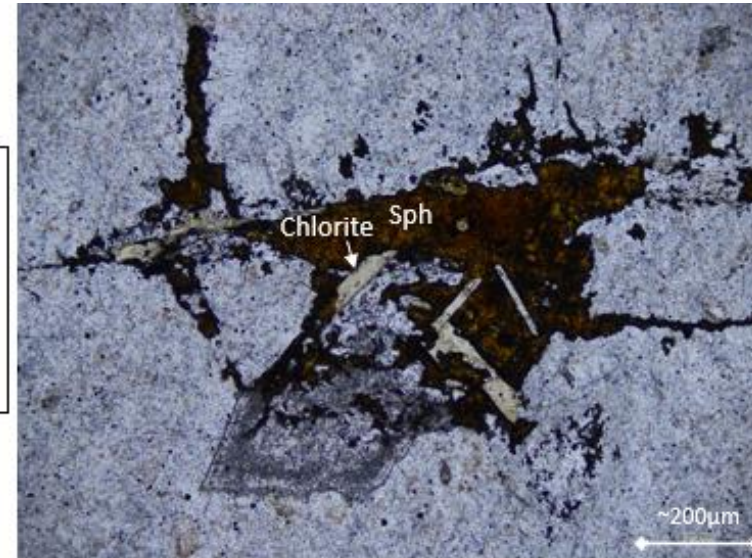
Summary: Heavily chlorite, biotite and carbonate altered rock with disseminated pyrite mineralization.

L72-179.5

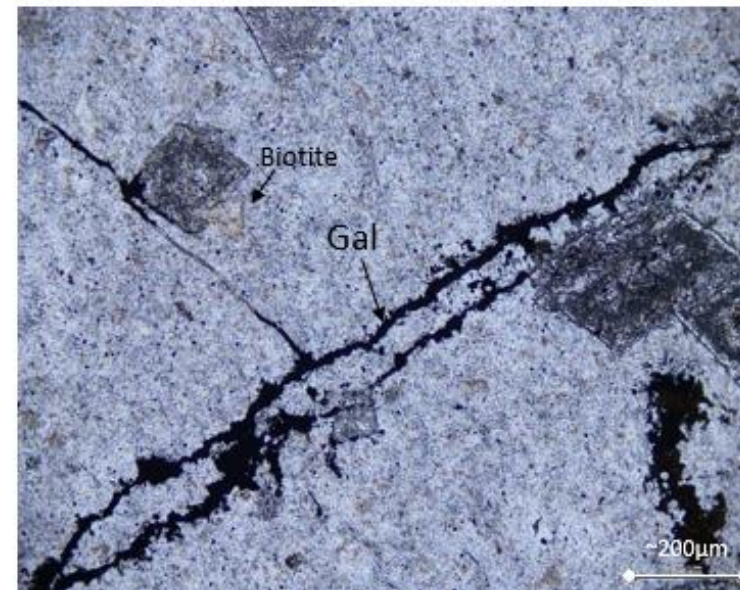


Core Sample: Very fine-grained mudstone-like host rock with late stage veining of sphalerite and minor galena mineralization.

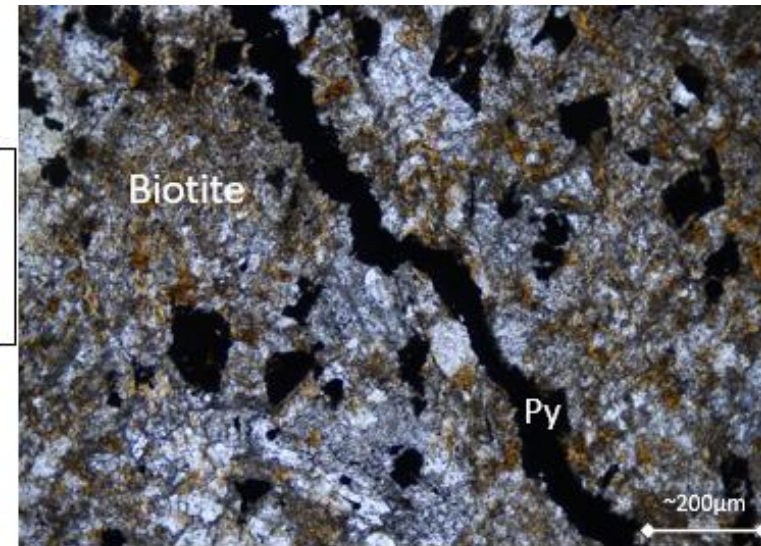
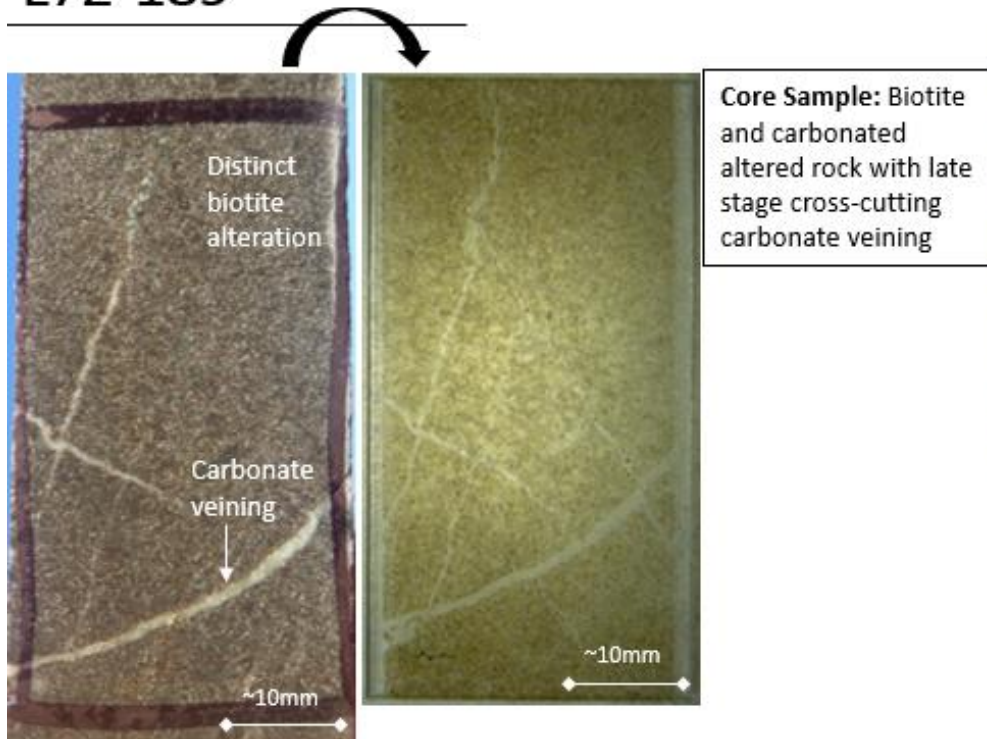
- Host Rock:** Mineralogy of host rock difficult to identify due to its very fine-grained nature. Quartz and very minor biotite alteration can be observed.
- Veins/infill:** Sphalerite and minor galena infill the veins throughout the host rock inferring a stage of ore-bearing mineralization post-dating host rock formation.
- Modal Proportions:** 80% groundmass (quartz & biotite), 15% sphalerite, 4% galena, 1% chlorite
- Summary:** Very fine-grained rock with massive sphalerite veining and minor galena infill.



Above: Plain polarized light image of sphalerite mineralization with crystalline chlorite inferring late stage mineralization of Zn ore.
Below: Plain polarized light image of galena veining throughout host rock inferring a late stage of ore-bearing mineralization.

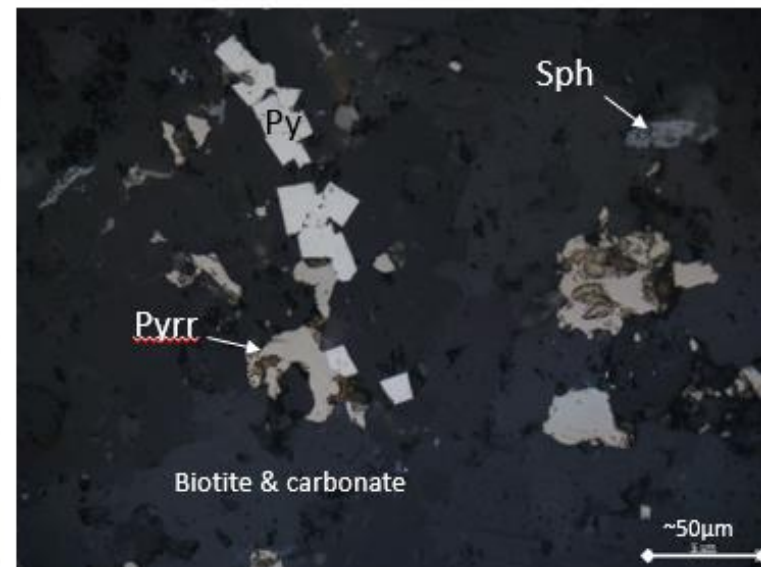


L72-189



Above: Plain polarized light image of host rock disseminated by biotite and carbonate with late stage pyrite veining inferring mineralization event post-dating dolerite dyke intrusion.

Below: Reflected light image displaying crystalline pyrite, pyrrhotite and sphalerite mineralization post-dating dolerite dyke intrusion.



Host Rock: Quartz and calcite-rich rock that has experienced significant biotite alteration.

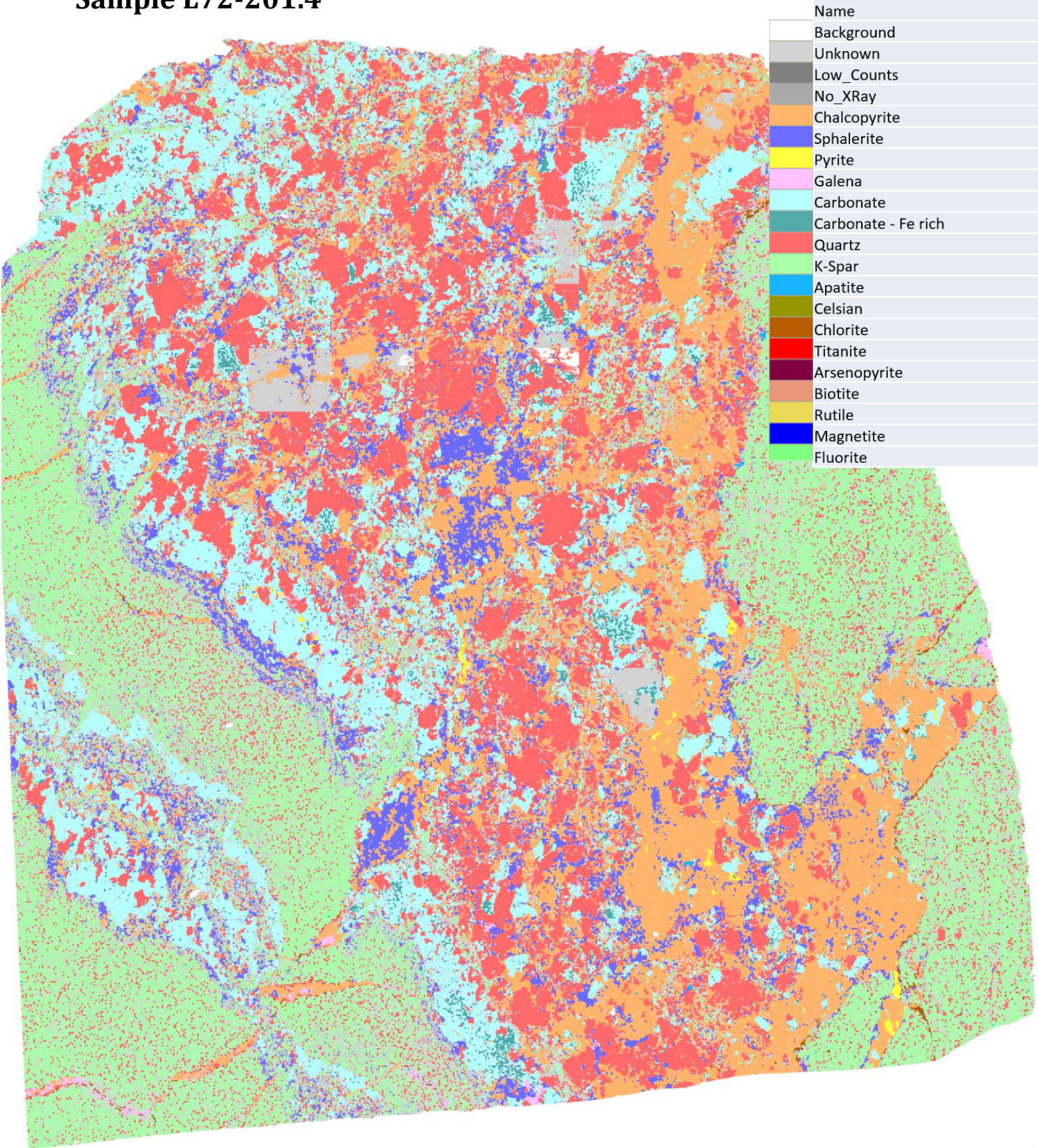
Veins/infill: Cross-cutting of carbonate veins inferring two different stages of carbonate infill. Pyrite is observed as veining and disseminated throughout host rock. Patchy pyrrhotite and sphalerite infill observed inferring post-mineralization of dolerite dyke intrusion.

Modal Proportions: 60% carbonate, 25% biotite, 10% pyrite, 4% pyrrhotite, 1% sphalerite.

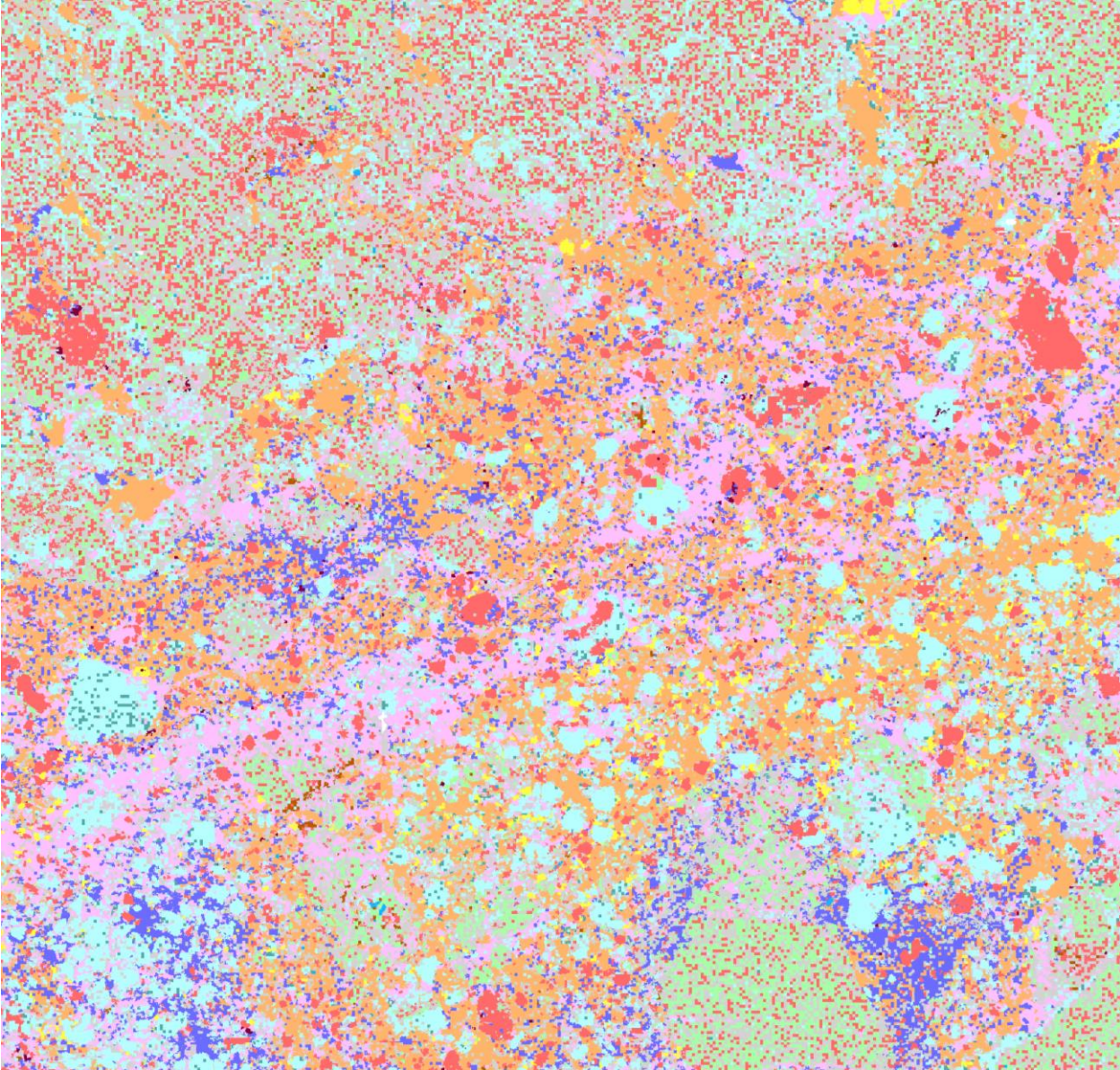
Summary: Biotite and carbonate altered rock with late stage carbonate veining and pyrite, sphalerite and pyrrhotite mineralization that post-dates dolerite dyke intrusion.

APPENDIX E: MLA MAPS

Sample L72-201.4

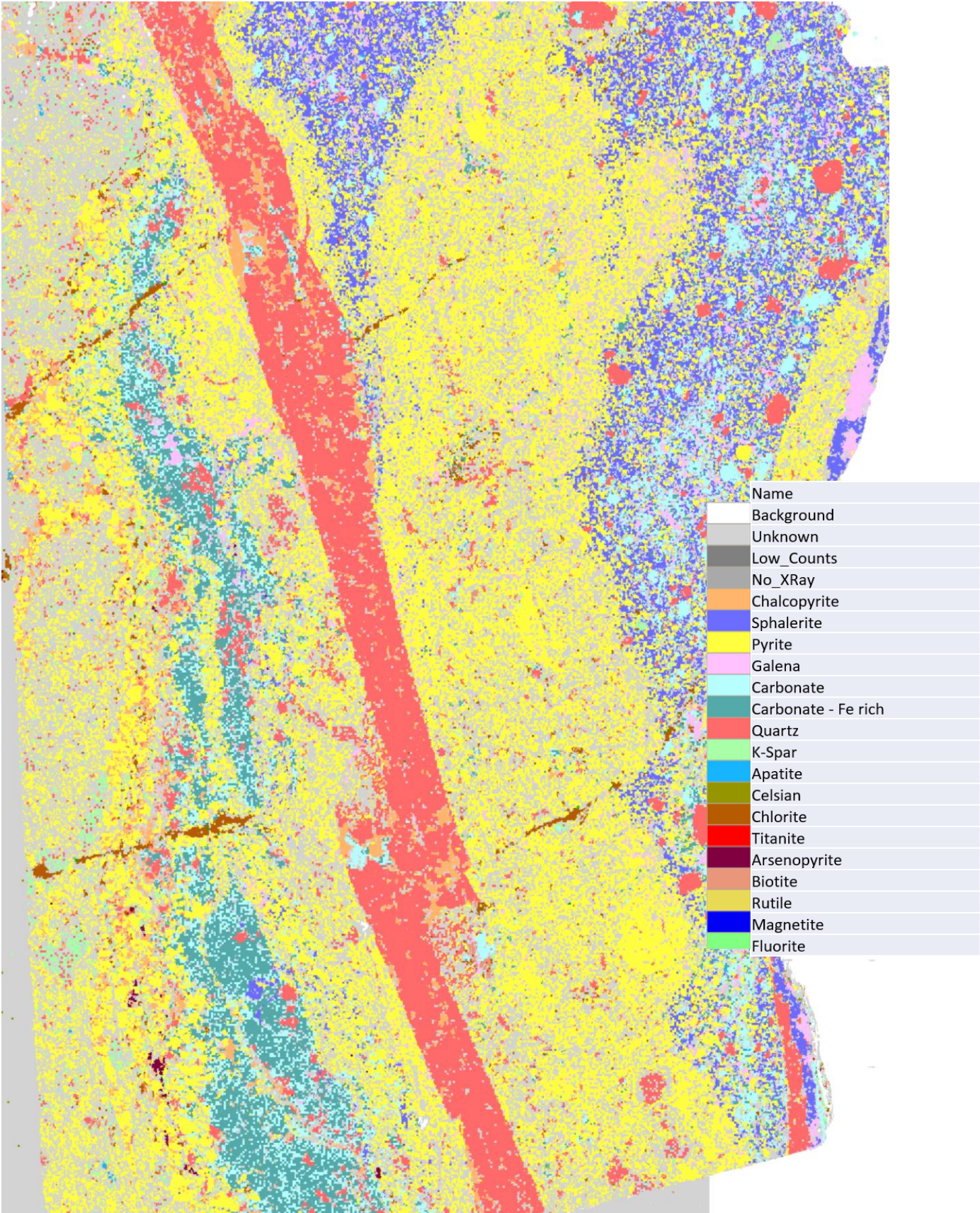


Sample L72-431.5



Name
Background
Unknown
Low_Counts
No_XRay
Chalcopyrite
Sphalerite
Pyrite
Galena
Carbonate
Carbonate - Fe rich
Quartz
K-Spar
Apatite
Celsian
Chlorite
Titanite
Arsenopyrite
Biotite
Rutile
Magnetite
Fluorite

Sample P49-17.4



APPENDIX F: ELEMENT CORRELATION TABLES

Hilton (P49) Element Correlation Coefficients (R ² Values)																				
Al	S	Mn	Fe	Co	Ni	Zn	Ga	As	Se	Ag	Cd	Ln	Sn	Sb	Te	Tl	Pb	Bi		
Al	1	0.0154	0.0098	0.0259	0.1166	0.0644	0.0951	0.5356	0.1064	0.0084	0.0463	0.002	0.0862	0.0208	0.1174	0.0353	0.2048	0.0146	0.0004	
S	0.0154	1	0.1154	0.2863	0.0283	0.0612	0.0012	0.0977	0.018	0.1332	0.0304	0.0038	0.0095	0.071	0.0087	0.0227	0.0509	0.0129	0.0497	
Mn	0.0098	0.1154	1	0.0008	0.0005	0.0035	0.0102	0.0033	0.0007	0.0028	0.0093	0.0025	0.0054	0.0179	0.0125	0.0061	0.003	0.011	0.007	LEGEND
Fe	0.0259	0.2863	0.0008	1	0.0098	0.0087	0.0004	0.0006	0.0013	0.0129	0.0221	0.0362	0.0093	0.2238	0.0208	0.0018	0.0257	0.0002	0.054	<0.2
Co	0.1166	0.0283	0.0005	0.0098	1	0.1805	0.0405	0.1143	0.2908	0.0003	0.0043	0.0162	0.003	0.0007	0.0056	0.0134	0.0081	0.0172	0.0042	>0.2
Ni	0.0644	0.0612	0.0035	0.0087	0.1805	1	0.0117	0.2697	0.0754	0.0104	0.0013	0.0056	0.0002	0.0027	0.0687	0.053	0.1035	0.0016	0.0002	>0.5
Zn	0.0951	0.0012	0.0102	0.0004	0.0405	0.0117	1	0.0003	0.1903	0.0178	0.0012	0.5624	0.0013	0.007	0.0208	0.003	0.0135	0.0797	0.0106	>0.9
Ga	0.5356	0.0977	0.0033	0.0006	0.1143	0.2697	0.0003	1	0.0055	0.0242	0.017	0.0014	0.0076	0.0001	0.0807	0.0322	0.3163	0.0143	0.0001	
As	0.1064	0.018	0.0007	0.0013	0.2908	0.0754	0.1903	0.0055	1	0.0085	0.0363	0.0038	0.0076	0.0021	0.0039	0.0273	0.0003	0.0008	0.0336	
Se	0.0084	0.1332	0.0028	0.0129	0.0003	0.0104	0.0178	0.0242	0.0085	1	0.0006	0.0119	0.0169	0.1123	0.0362	0.0511	0.0106	0.0104	0.0002	
Ag	0.0463	0.0304	0.0093	0.0221	0.0043	0.0013	0.0012	0.017	0.0363	0.0006	1	0.2134	0.5848	0.1394	0.0475	0.0527	0.0472	0.002		
Cd	0.002	0.0038	0.0025	0.0362	0.0162	0.0056	0.5624	0.0014	0.0038	0.0119	0.2134	1	0.097	0.0029	0.0154	0.0027	0.016	0.0446	0.0007	
Ln	0.0862	0.0095	0.0054	0.0093	0.003	0.0002	0.0013	0.0264	0.0076	0.0169	0.5848	0.097	1	0.413	0.0694	0.0225	0.1293	0.0145	0.0001	
Sn	0.0208	0.071	0.0179	0.2238	0.0007	0.0027	0.007	0.0001	0.0021	0.1123	0.1394	0.0029	0.413	1	0.004	0.0005	0.0445	0.0003	0.0178	
Sb	0.1174	0.0087	0.0125	0.0208	0.0056	0.0687	0.0208	0.0807	0.0039	0.0362	0.1312	0.0154	0.0694	0.004	1	0.1564	0.0987	0.2528	0.1107	
Te	0.0353	0.0227	0.0061	0.0018	0.0134	0.053	0.003	0.0322	0.0273	0.0511	0.0475	0.0005	0.0025	0.0005	0.1564	1	0.0201	0.0291	0.0058	
Tl	0.2048	0.0509	0.003	0.0237	0.0081	0.1035	0.0135	0.3163	0.0106	0.0527	0.016	0.1293	0.0445	0.0987	0.0201	0.0201	1	0.0313	0.0068	
Pb	0.0146	0.0129	0.011	0.0002	0.0172	0.0016	0.0797	0.0143	0.0008	0.0104	0.0472	0.0446	0.0145	0.0003	0.2528	0.0291	0.0313	1	0.5882	
Bi	0.0004	0.0497	0.007	0.054	0.0042	0.0002	0.0106	0.0001	0.0336	0.0002	0.002	0.0007	0.0001	0.0178	0.1107	0.0058	0.0068	0.5882	1	

George Fisher (L72) Element Correlation Coefficients (R ² Values)																				
Al	S	Mn	Fe	Co	Ni	Zn	Ga	As	Se	Ag	Cd	Ln	Sn	Sb	Te	Tl	Pb	Bi		
	1	0.0194	0.0522	0.069	0.0024	0.0202	0.0232	0.6466	0.1257	0.075	0.0003	0.0317	0.1462	0.0961	0.2991	0.0169	0.2195	0.1016	0.0796	
S	0.0194	1	0.0825	0.2947	0.048	0.0081	0.1171	0.0538	0.0001	0.0003	0.0304	0.1128	0.0085	0.0318	0.0074	0.0963	0.0021	0.0019	0.0093	
Mn	0.0522	0.0825	1	0.0003	0.0044	0.0013	0.0085	0.018	0.0001	0.0064	0.1244	0.008	0.0171	0.0072	0.0004	0.001	0.0407	0.0105	0.0113	
Fe	0.069	0.2947	0.0003	1	0.0013	0.0012	0.0012	0.0188	0.0128	0.019	0.0133	0.0036	0.0048	0.0048	0.0521	0.1251	0.0165	0.0109	0.0275	
Co	0.0024	0.048	0.0044	0.0013	1	0.0746	0.0257	0.0007	0.0057	0.0013	0.0006	0.0349	0.0839	0.0031	0.0179	0.0009	0.0006	0.0002	0.0006	
Ni	0.0202	0.0081	0.0013	0.0012	0.0746	1	0.0009	0.0404	0.0005	0.0005	0.0042	0.0005	0.0087	0.0556	0.0242	0.0085	0.0021	0.0001	0.0006	
Zn	0.0232	0.1171	0.0085	0.0012	0.0257	0.0009	1	0.0174	0.0135	0.0019	0.0545	0.3129	0.0762	0.1747	0.0457	0.0054	0.0552	0.0317	0.0882	
Ga	0.6466	0.0538	0.018	0.0188	0.0007	0.0404	0.0174	1	0.0002	0.0686	0.0004	0.0234	0.0896	0.0925	0.2652	0.1718	0.0946	0.0882		
As	0.1257	0.0001	0.0001	0.0128	0.0057	0.0005	0.0135	0.0002	1	0.0055	0.0025	0.0182	0.0068	0.003	0.0132	0.0006	0.0008	0.0001	0.0001	
Se	0.075	0.0003	0.0064	0.019	0.0013	0.0005	0.0019	0.0686	0.0055	1	0.0501	0.0004	0.0029	0.0161	0.0371	0.0524	0.0417	0.0483	0.0492	
Ag	0.0003	0.0304	0.1244	0.0133	0.0006	0.0042	0.0545	0.0004	0.0025	0.0501	1	0.0492	0.0069	0.0244	0.0249	0.0242	0.0044	0.0836	0.0827	
Cd	0.0317	0.1128	0.008	0.0036	0.0349	0.0005	0.9609	0.0234	0.0182	0.0004	0.0492	1	0.3871	0.1095	0.22	0.0573	0.0079	0.065	0.0353	
Ln	0.1462	0.0085	0.0171	0.0116	0.0839	0.0087	0.3129	0.0896	0.0068	0.0029	0.0069	0.3871	1	0.4044	0.3942	0.0025	0.0358	0.0671	0.0224	
Sn	0.0961	0.0318	0.0072	0.0048	0.0031	0.0556	0.0762	0.0925	0.003	0.0161	0.0244	0.1095	0.4044	1	0.4397	0.0024	0.0136	0.0673	0.0134	
Sb	0.2991	0.0074	0.0004	0.0521	0.0179	0.0242	0.1747	0.2652	0.0132	0.0371	0.0249	0.22	0.3942	0.4397	1	0.0113	0.1355	0.2426	0.1163	
Te	0.0169	0.0963	0.001	0.1251	0.0009	0.0085	0.0457	0.0102	0.0006	0.0524	0.0242	0.0573	0.0025	0.0024	0.0024	1	0.006	0.1054	0.1577	
Tl	0.2195	0.0021	0.0407	0.0165	0.0006	0.0021	0.0054	0.1718	0.0008	0.0417	0.0044	0.0079	0.0358	0.0136	0.1355	0.006	1	0.0282	0.0186	
Pb	0.1016	0.0019	0.0105	0.0109	0.0002	0.0001	0.0552	0.0946	0.0001	0.0483	0.0836	0.065	0.0671	0.0673	0.2426	0.1054	0.0282	1	0.7436	
Bi	0.0796	0.0093	0.0113	0.0275	0.0006	0.0006	0.0317	0.0882	0.0001	0.0492	0.0827	0.0353	0.0224	0.0134	0.1163	0.1577	0.0186	0.7436	1	

LEGEND

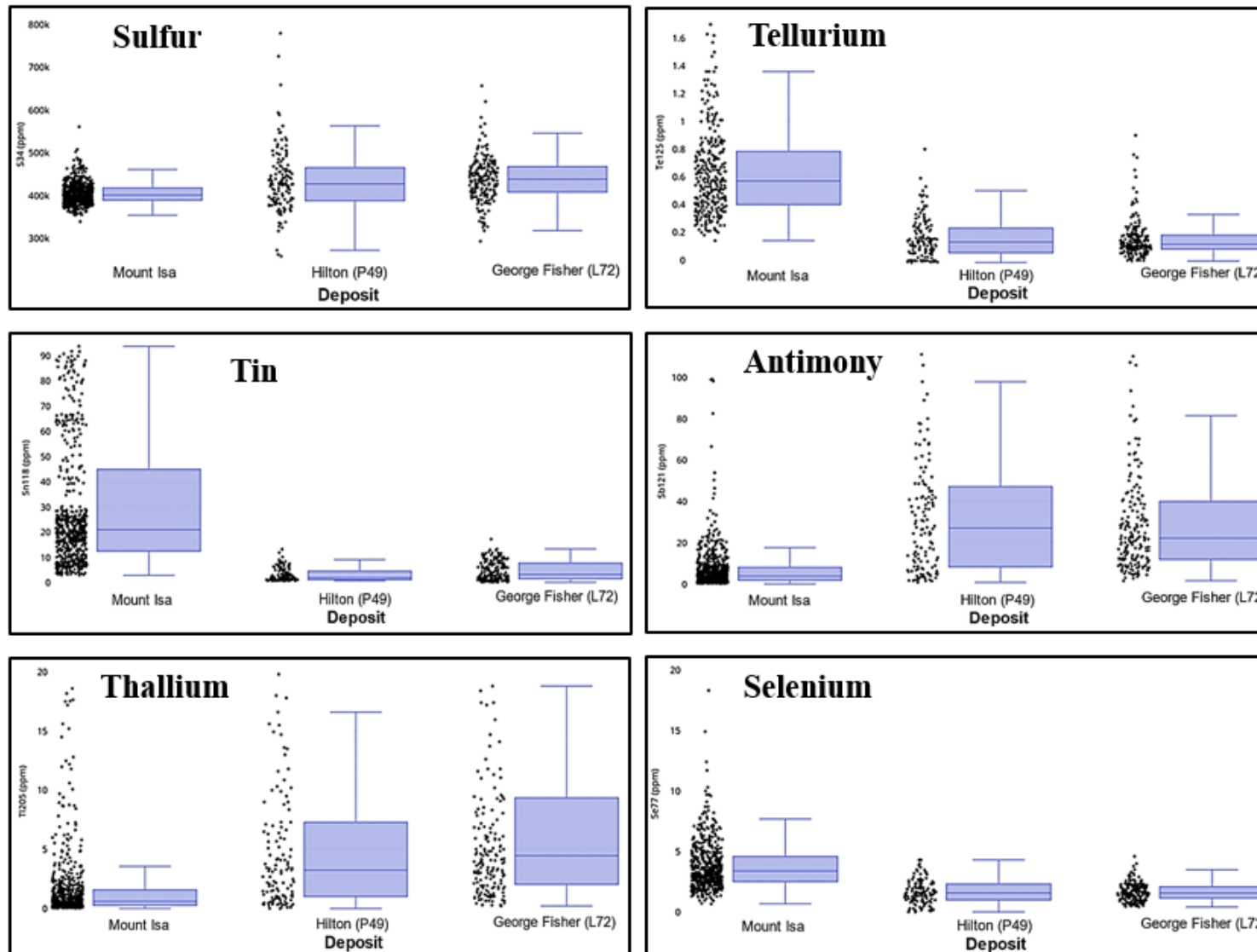
<0.2

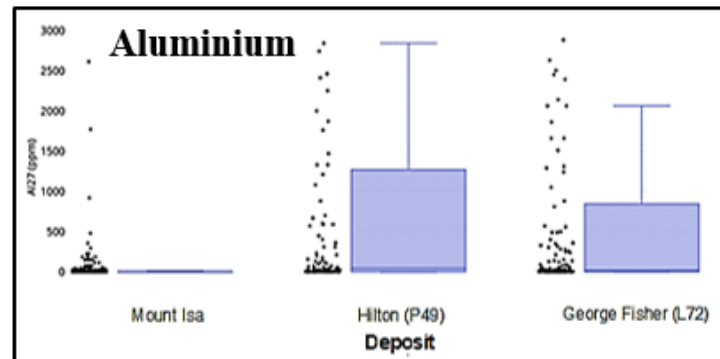
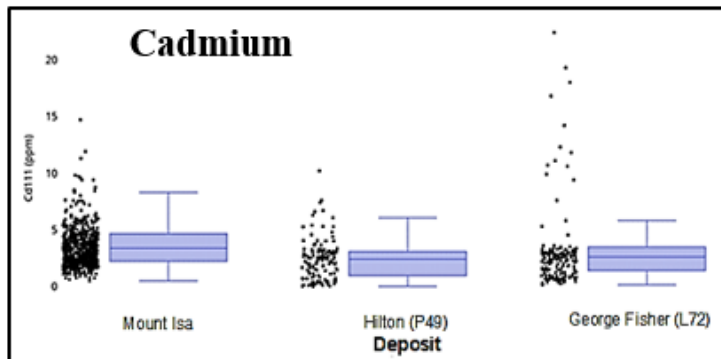
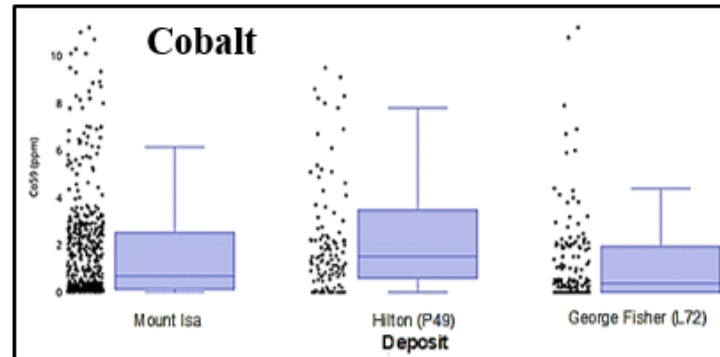
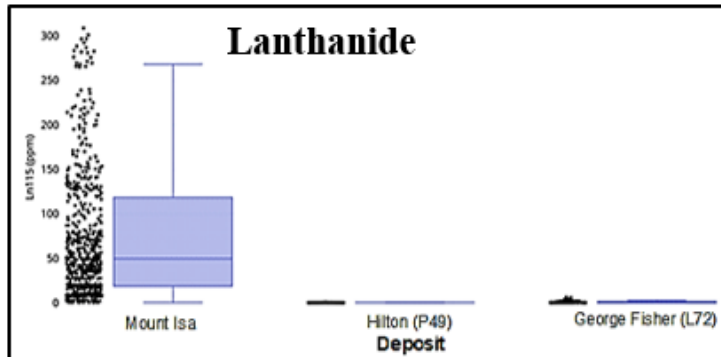
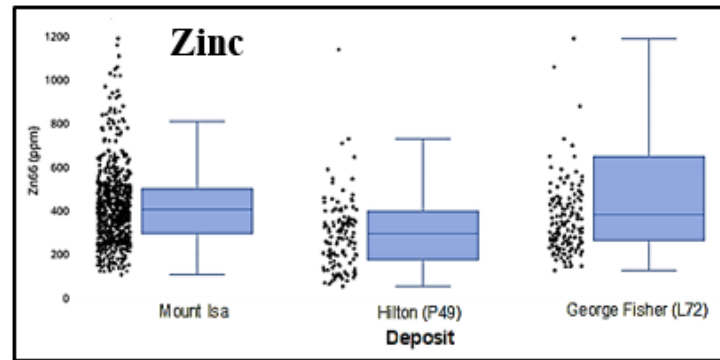
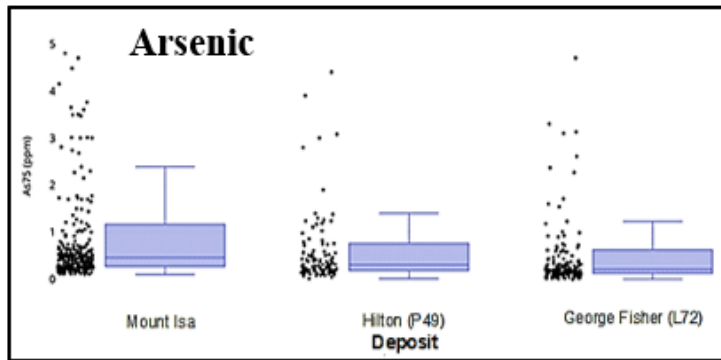
>0.2

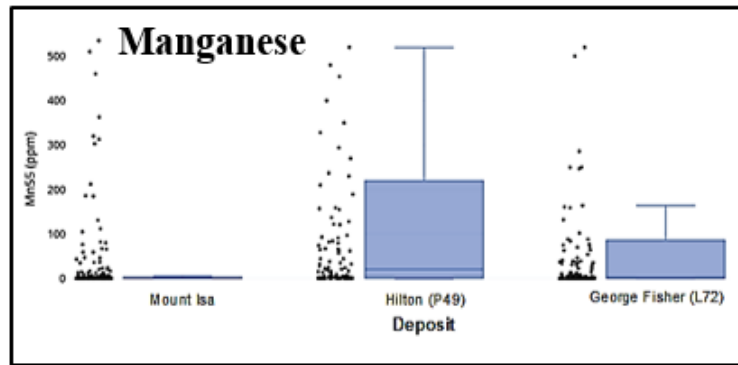
>0.5

>0.9

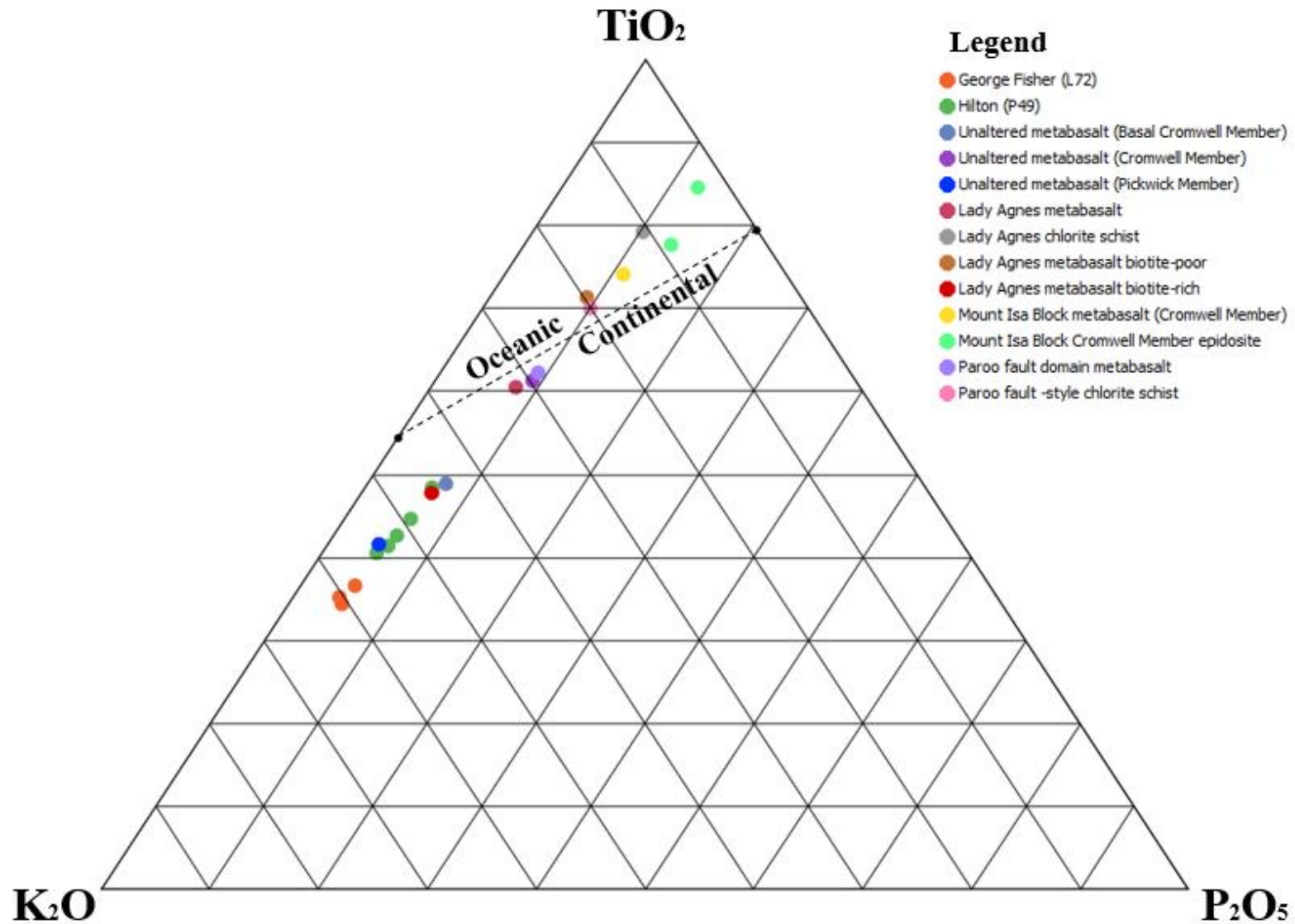
APPENDIX G: EXTENDED CHALCOPYRITE BOXPLOTS







APPENDIX H: ADDITIONAL GEOCHEMICAL PLOTS



APPENDIX I: DOLERITE DYKE WHOLE ROCK, TRACE ELEMENT AND NORMALISE VALUES

	%	%	%	%	%	%	%	%	%	%	%	%	%	%	%
SAMPLE	SiO2	Al2O3	Fe2O3	CaO	MgO	Na2O	K2O	Cr2O3	TiO2	MnO	P2O5	SrO	BaO	Total	LOI
L72-92.6	46.7	13	14.4	4.09	4.94	1.49	4.14	0.012	2.6	0.16	0.35	<0.01	0.05	98.17	6.24
L72-95.6	44.5	14	7.54	6.53	5.69	0.28	5.2	0.009	3.03	0.2	0.36	0.01	0.07	96.36	8.94
L72-132.5	39.8	12.85	15.15	4.91	7.67	0.06	2.77	0.008	2.91	0.16	0.39	<0.01	0.05	96.3	9.57
L72-189	44.1	12.2	13.55	5.91	6.02	0.08	4.51	0.007	2.56	0.24	0.36	<0.01	0.12	99.52	9.86
P49-184	44.6	12.8	12.9	6.69	7.16	0.06	3.57	0.01	2.96	0.13	0.4	0.01	0.31	99.66	8.06
P49-193	46.4	14.35	16.15	3.81	4.62	3.35	4.18	0.009	3.12	0.12	0.38	0.01	0.15	98.68	2.03
P49-196	46	13.5	16.9	4.42	5.07	3.55	3.51	0.008	2.75	0.14	0.37	0.02	0.12	98.23	1.87
P49-198A	42.3	11.6	14.3	9.14	4.57	2.46	2.16	0.007	2.31	0.19	0.29	0.01	0.08	96.94	7.52
P49-198B	50.6	14.5	15.8	1.95	5.22	3.6	3.18	0.008	2.89	0.15	0.39	0.01	0.11	100.7	2.29

SAMPLE	ppm	ppm	ppm	ppm	ppm	ppm	ppm	ppm	ppm	ppm	ppm	ppm	ppm	ppm	ppm
	Ba	Ce	Cr	Cs	Dy	Er	Eu	Ga	Gd	Hf	Ho	La	Lu	Nb	Nd
L72-92.6	406	48.4	80	32.4	6.13	3.55	1.66	22.7	6.33	5.2	1.16	20.9	0.45	16.2	28.5
L72-95.6	625	30.2	60	4.84	4.09	2.78	1.26	25.7	4.44	5.4	0.87	12.6	0.4	19.1	18.6
L72-132.5	457	102	60	3.87	7.36	3.67	3.63	21.2	10.85	5.2	1.38	51.7	0.41	17.7	52.8
L72-189	1080	55.4	60	15.2	6.89	3.4	2.63	22.4	7.82	4.9	1.19	26.1	0.44	16.6	32.1
P49-184	2670	53.4	70	0.93	4.61	2.86	1.1	20.9	5.23	5.3	0.93	24.8	0.45	18.4	30.3
P49-193	1325	57.9	60	24.6	6.6	3.77	2.67	24.9	7.41	5.8	1.31	24.9	0.52	19.3	33.8
P49-196	1065	49.9	60	22.1	6.9	3.54	2.38	25.2	7.26	5.2	1.24	21.4	0.43	17.2	29.2
P49-198A	726	42.1	50	9.16	5.97	3.48	1.7	20.4	5.83	4.6	1.17	18.8	0.42	14.9	24.9
P49-198B	914	43.5	60	16.55	5.95	3.36	1.54	25.4	6.34	5.7	1.23	18.7	0.43	18.4	25.3

SAMPLE	ppm	ppm	ppm	ppm	ppm	ppm	ppm	ppm	ppm	ppm	ppm	ppm	ppm	ppm	ppm
	Pr	Rb	Sm	Sn	Sr	Ta	Tb	Th	Tm	U	V	W	Y	Yb	Zr
L72-92.6	6.31	169.5	6.79	1	37.6	1	0.98	2.1	0.47	0.49	358	3	29.3	2.71	198
L72-95.6	4.09	106.5	4.4	2	43.9	1.2	0.62	1.84	0.35	0.57	396	2	24.1	2.3	212
L72-132.5	12.65	54.9	11.35	1	31.1	1	1.36	1.87	0.49	2.08	339	5	45.2	2.89	195
L72-189	6.99	128.5	7.93	2	32.3	1	1.13	1.87	0.5	0.52	365	4	33.6	2.75	197
P49-184	6.78	87.8	6.4	3	45	1.1	0.72	2.01	0.42	0.54	391	4	23.2	2.8	214
P49-193	7.76	161	7.58	2	92.5	1.2	1.08	2	0.56	0.56	402	2	37	3.21	217
P49-196	6.69	135	6.8	1	114	1	1.05	1.88	0.49	0.49	377	3	31.4	3.09	205
P49-198A	5.56	67.1	5.82	2	98.5	0.9	0.96	1.71	0.45	0.47	312	2	29.2	2.76	178
P49-198B	5.74	111.5	6.1	1	100	1.1	0.86	2.05	0.46	0.5	378	2	31.2	2.93	221

SAMPLE	ppm	ppm	ppm	ppm	ppm	ppm	ppm	ppm	ppm	ppm	ppm	ppm
	Ag	As	Cd	Co	Cu	Li	Mo	Ni	Pb	Sc	Tl	Zn
L72-92.6	<0.5	22	<0.5	31	28	30	1	29	9	31	150	125
L72-95.6	<0.5	<5	<0.5	16	9	70	1	17	98	34	50	21
L72-132.5	<0.5	8	<0.5	49	23	70	<1	25	205	28	40	175
L72-189	<0.5	34	1.6	29	17	40	<1	24	430	29	150	345
P49-184	0.9	<5	0.6	45	155	60	<1	40	56	31	20	162
P49-193	<0.5	21	<0.5	35	6	10	<1	21	16	35	90	112
P49-196	<0.5	17	<0.5	98	22	10	<1	39	21	31	70	151
P49-198A	<0.5	37	0.5	97	42	20	<1	41	29	27	40	136
P49-198B	<0.5	47	<0.5	51	34	20	<1	29	9	33	60	174

APPENDIX J: CHALCOPYRITE GEOCHEMICAL DATA

https://1drv.ms/x/s!Asum5_dH1NxIiFEJkBpWSddHotzh?e=SGgtaP